Hochschule für Technik und Wirtschaft Berlin
University of Applied Sciences

DLR Deutsches Zentrum für Luft- und Raumfahrt

Presentation, evaluation and validation of measurement results from operation tests of rotation and expansion performing assemblies during the commissioning of the REPA Test Rig

Bachelor-Thesis

Course of Studies: Renewable Energy Systems (B.Sc.)

Faculty: Engineering - Energy and Information

Hochschule für Technik und Wirtschaft Berlin

presented by:

Christian Schütt

Berlin, 03.04.2018

Carried out and presented at the

German Aerospace Center (DLR)

Institute of Solar Research

Supervision and Assessment:

1st Examiner: **Prof. Dr.-Ing. Volker Quaschning**

2nd Examiner: **Dipl.-Ing. Wolfgang Reinalter**

Tutor: **Dipl.-Ing. Christoph Hilgert**

Declaration of Academic Honesty / Eidesstattliche Erklärung

I hereby declare to have written the present bachelor's thesis on my own, having used no other resources and tools than the listed. All contents cited from published or nonpublished documents are indicated as such.

Hiermit erkläre ich, dass ich die vorliegende Bachelorarbeit selbständig verfasst und keine anderen als die angegebenen Hilfsmittel verwendet habe. Alle Inhalte, die wörtlich oder sinngemäß aus veröffentlichten oder nicht veröffentlichten Schriften entnommen sind, sind als solche kenntlich gemacht.

_____ _____

Place, Date Signature

Abstract

Critical parts in Parabolic Trough Collector (PTC) power plants are the flexible pipe connections, also called Rotation and Expansion Performing Assemblies (REPAs) between the absorber tubes and the feeding pipes. REPAs have to compensate tracking movements of the collector to follow the course of the sun and the heat dilatation of the absorber tube. REPAs have to withstand an operating time of 30 years under harsh weather conditions. Damages at these components lead to leakages and breakdowns of the PTC power plant. The consequences are safety risks, economic losses and environmental damages. Failure mechanisms will be investigated at the REPA test under near-operating conditions by simulating accelerated REPA life cycles.

The first part of this thesis gives thereby an overview of the state of the art in PTC power plants and the structure and function of the REPA test rig.

Furthermore, the undertaken efforts are described to contribute the commissioning of the first of four sensors for the force-measurement at test rig to measure the resulting REPA reactions. The two integrated measurement setups are presented to execute the first tests with rotation and translation movements as simulation of typical collector motions. Measurement results have been evaluated for the first tests during the commissioning of the test rig to determine the forces and moments for rotation and translation movements under different operating parameters.

The second test results are presented to define the additional influences from the pipe section between the two installed REPAs at the test rig. The impact of the traverse piping on the total measurement has been investigated. The measurement results are compared and validated with the simulation (ROHR2) model of the traverse piping. Moreover, measures are presented to decrease uncertainties by the force and moment measurement. With this first measurement results, the following future life cycle test can be evaluated more in detail and the test rig commissioning can be continued and also the installation of the force-measurement sensors.

Kurzfassung

Kritische Bauteile in Parabolrinnenkraftwerken sind die flexiblen Rohrverbinder auch als REPAs (Rotation and Expansion Performing Assemblies) bezeichnet, zwischen den Absorberrohren und den Versorgungsleitungen. Diese müssen die Nachführungsbewegungen des Kollektors zur Sonnenlaufbahn und die Wärmeausdehnung des Absorberrohrs kompensieren. REPAs müssen außerdem einer Betriebsdauer von 30 Jahren standhalten unter rauen Wetterbedingunegn. Beschädigungen an den Bauteilen führen zu Leckagen und Betriebsunterbrechungen des Parabolrinnenkraftwerks. Die Folgen sind Sicherheitrisiken, wirtschaftliche Verluste und Umweltschäden. Versagensmechanismen werden zukünftig am REPA Teststand unter betriebsnahen Bedingungen bei der Simulation beschleunigter REPA Lebenszyklen untersucht.

Der erste Teil der Thesis gibt dabei einen Überblick über den State of the Art von Parabolrinnenkraftwerken und über den Aufbau und Funktion des REPA Teststandes.

Außerdem sind die erfolgten Bestrebungen beschrieben, um die Inbetriebnahme des ersten von vier Sensoren der Kräftemessung am Teststand fortzusetzen und die resultierenden Einflüsse auf die REPAs zu messen. Zwei Messaufbauten sind präsentiert, um die ersten Tests mit Rotations- und Translationsbewegungen durchzuführen und um die typischen Kollektorbewegungen zu simulieren. Die Messergebnisse von den ersten Tests während der Inbetriebnahme wurden bewertet, um die Kräfte und Momente für Rotations- und Translationsbewegungen mit verschiedenen Betriebsparametern zu bestimmen.

Die zweiten Versuchsergebnisse sind präsentiert worden, um den zusätzlichen Einfluss von dem Rohrleitungsbereich zwischen den beiden installierten REPAs zu bestimmen. Der Einfluss der Traversenrohrleitungen auf die gesamte Messung wurde dabei untersucht. Die Messergebnisse wurden verglichen und validiert mit dem Simulationsmodell (ROHR2) für die Traversenrohrleitung. Darüber hinaus werden Maßnahmen zur Verringerung von Unsicherheiten für die Kräfte und Momenten Messung vorgestellt. Mit den ersten Messergebnissen können zukünftige Lebenszyklustests detaillierter bewertet werden und die Inbetriebnahme kann fortgesetzt werden, genauso die Einrichtung der Kräftemessungssensoren.

Contents

List of tables

List of figures

List of abbreviations

Abbreviation	Meaning
BJA	Ball Joint Assembly
BOP	Balance of Plant
CIEMAT	Centro de Investigaciones Energéticas, Medioambientales y Tecnológicas
CSP	Concentrating Solar Power
DLR	Deutsches Zentrum für Luft- und Raumfahrt (German Aerospace Center)
DNI	Direct Normal Irradiation
EJ	Expansion Joint
GUI	Graphical User Interface
HCE	Heat Collector Element
HCES	Heat Collector Element Support
HTF	Heat Transfer Fluid
IC	Intercept Factor
LCOE	Levelized Cost of Energy
LV	LabVIEW
OPC	Open-Platform-Communication-Server
PLC	Programmable Logic Controller
PSA	Plataforma Solar de Almería
PTC	Parabolic Trough Collectors
REPA	Rotation and Expansion Performing Assembly
RFHA	Rotary Flex Hose Assembly
SCA	Solar Collector Assemblies
SCADA	Supervisory Control and Data Acquisition
SCE	Solar Collector Element
SJ	Swivel Joint
ST	Solar Tower
TES	Thermal Energy Storage

Glossary

Symbol	*Unit*	*Description*
α	K^{-1}	**Coefficient of linear expansion**: Coefficient of linear expansion is a factor for the expansion of a substance from its initial length per rise in temperature of one kelvin [1].
φ	°	**Rotation angle**: The angle for the rotation movement of the traverse along the rotation axis, measured by a sensor. Range from {-20°; 180°}, stow position φ_{STOW} = -20°, vertical position φ_{VER} = 90°, φ_{END} = 120° end position
ϑ	°	**Translation angle**: Angle between the drive pylon arms and a defined surface to measure the heat dilation movement. Range from [0°; 45°], maximum translation angle, hot position ϑ_{HOT} = 2°, minimum translation angle, cold position ϑ_{COLD} = 22°
ϑ_{HTF}	°C	**HTF temperature**: Describes the temperature of the heat transfer fluid in the pipe system. Range from {Ambient temperature; 450°C}
$\dot{V}_{HTF}$	m³/h	**HTF volume flow**: Volume of HTF which passes the pipe system in a unit of time. Range from {6 m³/h; 60 m³/h}
p_{HTF}	bar	**HTF pressure**: Pressure of the HTF in the pipe system {Ambient pressure; 40 bar}.
L	m	**SCA length**: Length of the absorber tube in a solar collector assembly.
$\Delta\vartheta$	K	**Temperature difference HTF**: Temperature difference between the hot pipe in operation and a cold pipe by none operation.
ΔL	m	**Heat dilation absorber tube**: Length of the absorber tube in hot condition minus the absorber tube length in cold condition.
ϑ_{amb}	°C	**Ambient temperature**: This temperature was not measured and is set to 20 °C.

ϑ_{dyn}	°C	**Dynamometer temperature:** Temperature within the dynamometer. Currently not measured but PT1000 mean temperature is representative for the test facility. A lower temperature can be expected as measured by ϑ_{PT1000}.
ϑ_{PT1000}	°C	**PT1000 mean temperature**: Average temperature of two PT1000 resistance thermometer installed in a metal plate on top of the sensor head. These thermometers are not representing the real temperature in the dynamometer. An integrated thermocouple is normally needed. Maximum of the K6D175 is 70°C and the allowed maximum temperature is set to 80 °C. A greater temperature changes the zero-signal [2].
ϑ_{Pipe}	°C	**Mean temperature pipe:** Average temperature of four PT100 thermometers installed in the traverse pipe section as shown in **Figure 19**. {Ambient temperature; 400°C}

1 Introduction

For a further reduction of greenhouse gas emissions and to keep global warming to a minimum level, it is indispensable to reach the agreed climate targets of the Paris Convention in 2015. For keeping the rise of the global average temperature less than 2 °C, compared to the pre-industrial level, it is necessary to use every technology of renewable energies in order to replace conventional power plants in the long-term. Therefore the aim in Europe is a reduction of greenhouse gas emissions by 40% (compared to 1990 levels) and a 27% share for renewable energy until 2030 [3].

Concentrating Solar Power (CSP) is one of the key technologies to reach these abovementioned targets. Currently, Solar Tower (ST) power plants and Parabolic Trough Collector (PTC) power plants are the most promising technologies in the CSP sector because of comparatively low costs of energy production. In PTC power plants for example, it is possible to store the generated excess energy with Thermal Energy Storage (TES) in molten salt storage tanks. This specific advantage allows an electricity supply in times with less sunlight or during the night [4]. In combination with other renewables, this could be one technology to bridge energy shortages by disadvantageous conditions for wind and photovoltaic power plants with less solar irradiation and wind.

For a reliable electrical supply using PTC power plants, every component in a solar field has to withstand 30 years of operation under harsh weather conditions. The most stressed parts in such a solar field of a power plant are the flexible pipe connections between the fixed supply pipes and the absorber tubes of the PTCs, named Rotation and Expansion Performing Assemblies (REPA). Failures in these parts may lead to leakages and could even cause fires and the release of Heat Transfer Fluid (HTF) to the environment. Repairs and additional maintenance of the REPAs during operation cause a stop of the whole system and a drain of the HTF. In conclusion, potential damages at these REPAs increase the maintenance costs of PTC power plants significantly. This is why the REPAs failure mechanisms must be understood precisely.

The content of this work gives an understanding of the loads, which react on the REPAs. These loads are investigated by the help of the REPA test rig at the Plataforma Solar de Almería (PSA) in Spain. This test facility is able to simulate the forces and moments, which react on the REPAs during a life cycle of a PTC power plant. The research results are done by the evaluation and validation of measurement results during the commissioning of the REPA test rig.

After finishing the commissioning of the REPA test rig, complete life cycles of the REPAs can be simulated. The subsequent tests will provide the results and knowledge for the improvement of REPA design and the adjacent components.

1.1 Fundamentals CSP

The utilization of the sun's energy has a long history and began hundreds of years ago in China and Greece to create fire with mirrors and glasses. Inventions of electrical machines in the middle of the 19th century created the demand of electricity for the 20th century. This energy demand has been met by conventional power plants over decades. A rethink started in the 1980s as a reaction of oil crises in 1973 and 1979 [5]. The first research projects to produce electricity by means of CSP Technology started at this time. The first cornerstone was laid for the development of commercial CSP power plants to provide large amounts of electrical energy. After more than three decades of research and building of solar-thermal power plants, there are basically four main concepts for CSP systems. All the outlined CSP systems given below are shown in **Figure 1**.

Parabolic trough collectors: In PTC power plants parabolic mirrors are aligned along the longitudinal axis to a large complex, which concentrates the sunlight in a focal line. These collector rows can be several hundred meters long and are one-axis tracked to the sunlight. The tubular receiver conducts the HTF, which is supplied by the solar field piping and the transported heat is coupled in a Clausius-Rankine process to produce electrical energy [4].

Solar tower: A solar tower system consists of several hundred or even more mirrors, reflecting the light to the receiver on top of the tower. Every heliostat holds a number of mirrors and is individually two-axe tracked by a computer to follow the course of the sun during a day. In common receivers the tubes to transport the heat transfer fluid (HTF) are made of steel and uncoated or black painted [5]. In most applications the energy of the HTF is used to drive a general steam turbine which is connected to a generator.

Linear Fresnel Systems: This system utilizes the same basic mirror system as used in parabolic trough collectors. The mirrors are only one-axially slightly curved and glued to a support structure. An additional concentrator is sometimes used on top for further focusing.

Dish/engine systems: Mirrors of dish/engine systems have to depict a high reflectance and accurate parabolic shape to concentrate the sunlight on the receiver [5]. The reflective layer is made of silvered glass and is attached to a metal frame work. A two-axis tracking system is required to collect the direct solar radiation. Every dish has an own receiver in the focal point, which is equipped with a Stirling engine, that is normally energized with HTF out of the receiver.

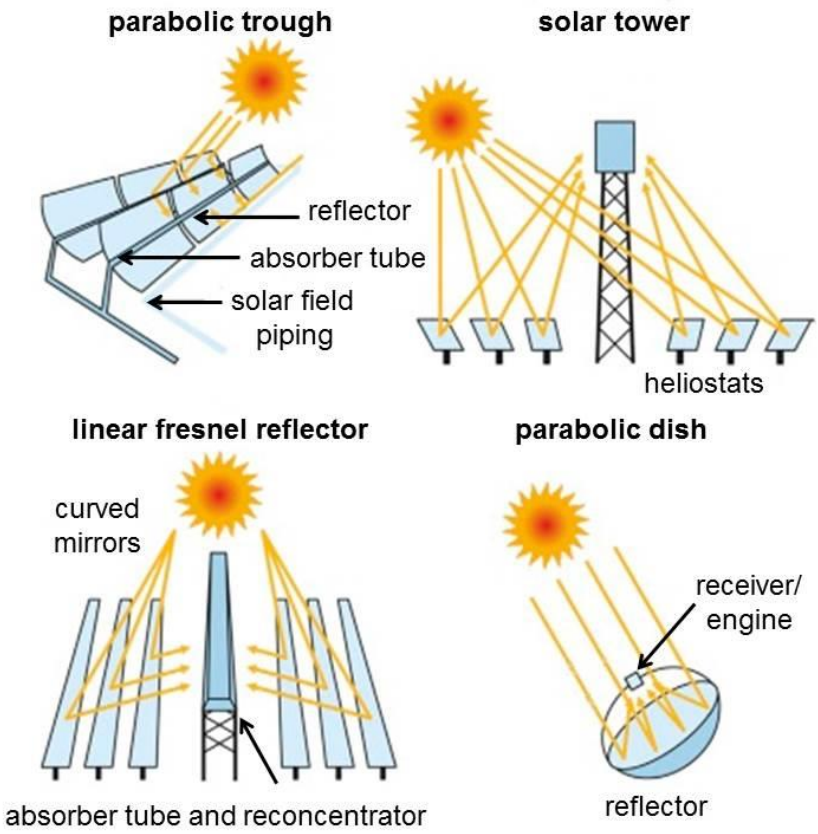

Figure 1: Four main concepts of CSP systems[6], left column: line concentrators, right column: point concentrators.

The basic condition for all these concentrator systems is a high annual yield of direct solar irradiation. Under an economic view, solar-thermal power plants have to be planned in large dimensions to minimize the Levelized Costs of Energy (LCOE) and to build them cost-competitive to conventional power plants. Consequently, it is necessary to build these plants in countries with a high irradiation, for example in desert-like regions. A minimum annual threshold of 2,000 kWh/m² of direct normal irradiation (DNI) must be guaranteed to make their operation economic [7]. The following **Figure 2** displays the distribution of DNI in a world map.

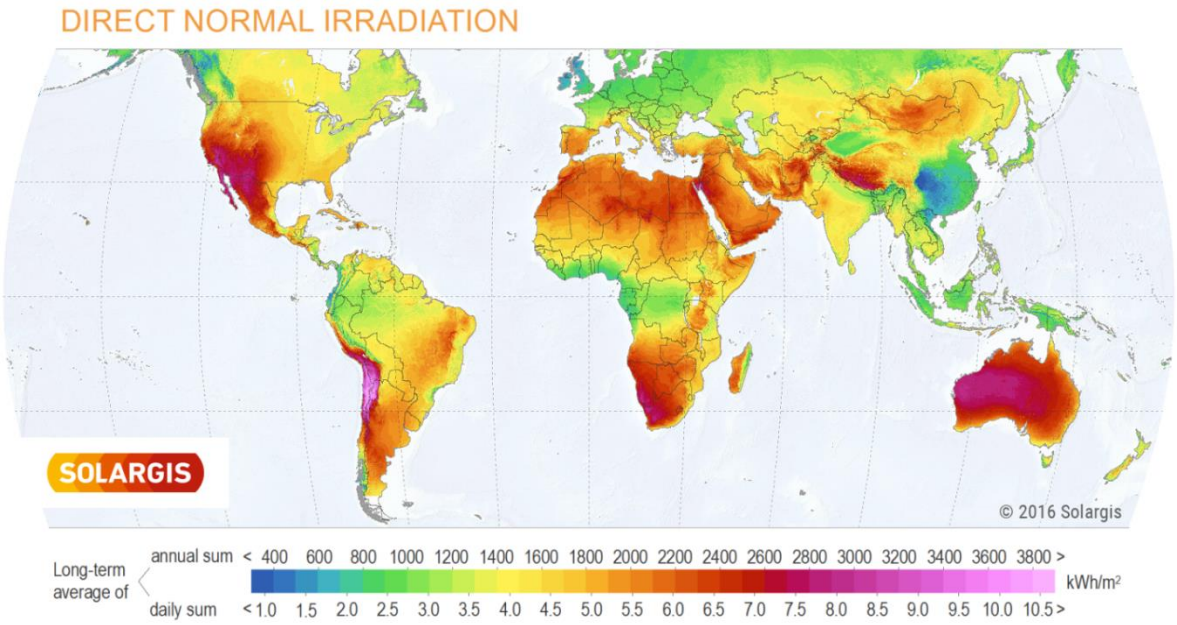

Figure 2: World map with annual and daily totals of DNI in kWh/m² on a horizontal plate [8]

As shown in the graphic above, the dark orange colored areas deliver the minimum irradiation to build CSP power plants. The red and purple zones provide perfect condition for this kind of technology. Furthermore, big parts of Australia, Africa, South and Central America are suitable for the operation of economic CSP power plants. The global potential for CSP technology is calculated with 3,000,000 TWh/y. Compared to this, the worldwide electricity consumption amounts to 18,000 TWh/y [9]. This number clearly shows the high potential of CSP in the desert to supply the whole world with electrical energy from concentrated sunlight. Nevertheless, CSP is less used compared to the installed capacity of other renewable energies. One reason for this is the relatively high cost for the most CSP technologies. Just parabolic trough collectors are already able to produce electricity for an acceptable price per kWh, which is comparable to conventional power plants. 4,900 MW of CSP power for electricity generation was installed in the year 2015 [5]. More in detail 4,115 MW, belonging to parabolic trough collectors, 497 MW to central receivers and 179 MW to Fresnel systems [5]. Hence, currently the most common technology of CSP are PTC power plants. The focus of solar research has to be on the most promising and economical technology in order to allow a faster expansion on the market. The following chapter describes how current PTC systems work and where the potential for improvements is.

1.2 State of the art PTC

The exploitation of the suns energy by concentrating the solar irradiation in PTC started at the beginning of the 20th century. The first PTC power plant was built in a small farming village Al Meadi in Egypt in the year 1913 to drive a 45 kW steam engine for pumping Nil water. The next important point in the history of this technology were the oil crises in the 1970s. Thus an independent electricity production away from fossil energy sources moved more in the focus.

Between 1984 and 1991 the American and Israeli company LUZ built 9 pilot power plants in the Mojave Desert, California. They started to breakthrough by building the PTC stations in series. In total they installed 354 MW power for the southern California grid. The plants were also able to work with fossil fuel in order to produce electricity independent from weather conditions [10].

For a longer period of time, there were no bigger advances in the installation of PTC power plants. In 2007, Nevada Solar One was built in Eldorado Valley, Nevada and they finished the plant with 75 MW_{el}. After this, Solar Millenium and ACS Cobra planned and built Europe's first PTC power plant near Guadix, Spain. The PTC power plant Andasol 1 provides electricity since 2009 and the system is able to store the energy in tanks by the help of molten salt. Extensions of the plant followed in form of Andasol 2 and 3 [10].

1.2.1 General concept of PTC power plants

In general, PTC power plants are similar to conventional power plants, they also use steam in a Rankine cycle to generate electricity. The system can be divided into four mayor blocks: solar field (with HTF and receiver system), storage part, power block and Balance of Plant (BOP) [5]. The main component of a PTC power plant is shown in **Figure 3.**

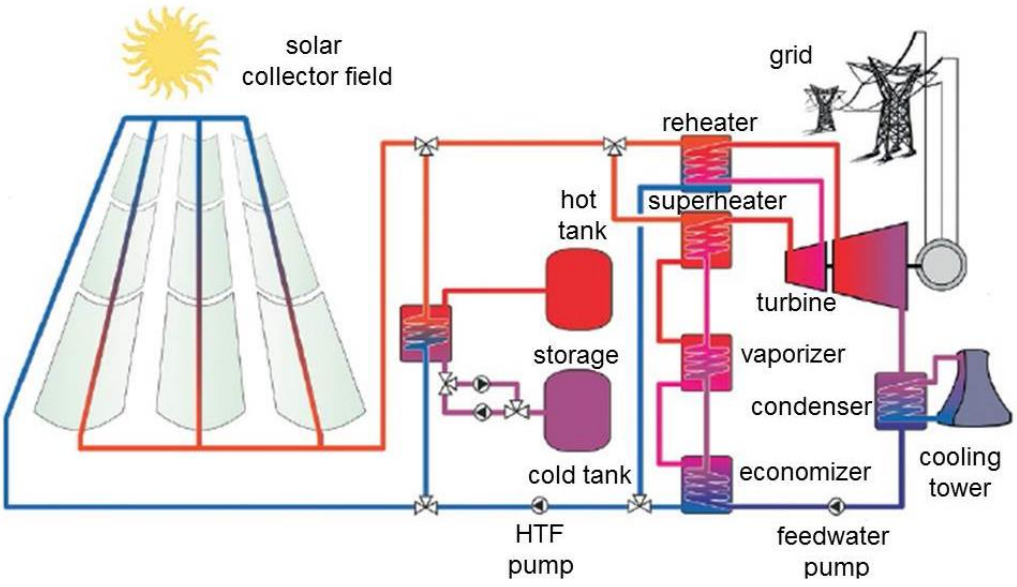

Figure 3: Scheme of PTC power plant with Thermal Energy Storage (TES) and thermal oil as HTF [5]

The requirements for every power block differ significantly. The solar field is the most critical part of the whole plant, because the components are exposed to rough environmental influences in the desert. This section consists fundamentally of parabolic mirrors, receiver tubes, collector support structure, tracking, HTF, flexible pipe connectors, valves and foundation.

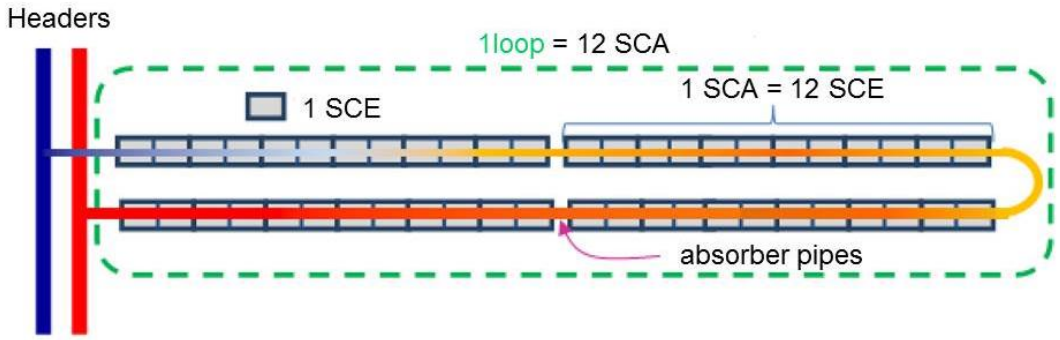

Figure 4: U-shaped loop of a PTC solar field [11]

Solar fields can be subdivided in to subunits, like single loops with normally four Solar Collector Assemblies (SCA), as shown in **Figure 4**. These assemblies are connected in series and supplied with HTF of middle temperatures (typically 300 °C) from the colder header. Furthermore, the rotation movement is done by a hydraulic drive unit located in the drive pylon in the center of each SCA. SCAs can be subdivided in typically twelve Solar Collector Elements (SCE). One of them is depicted in **Figure 5**.

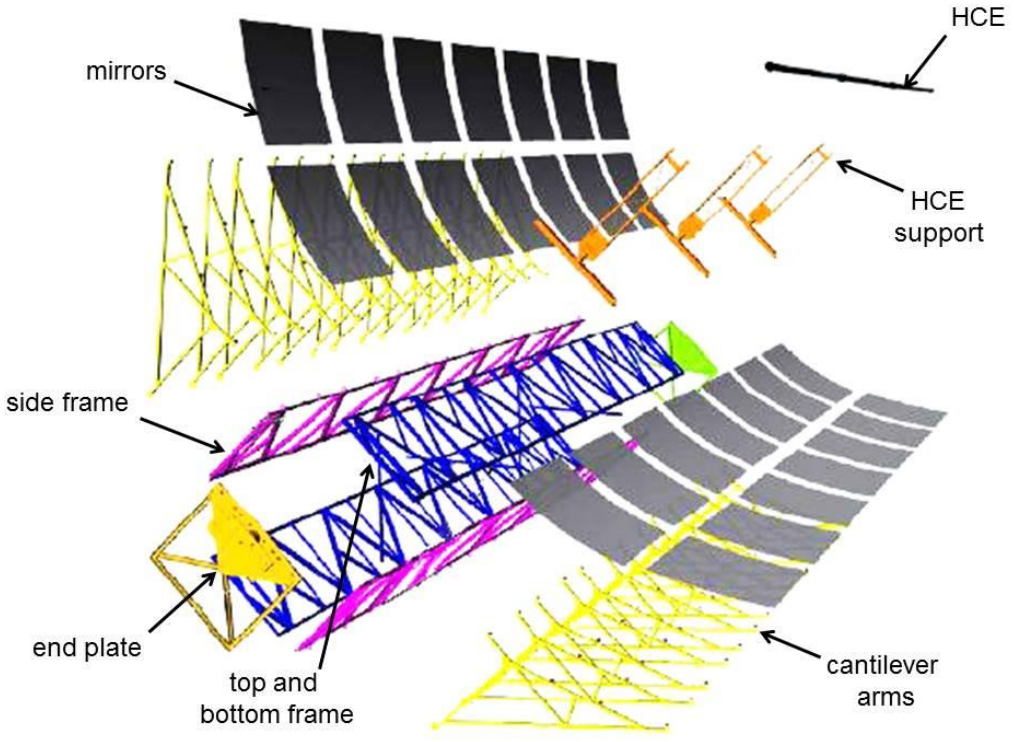

Figure 5: Exploded view of a SCE from a PTC power plant by example of EuroTrough collector [12]

As the smallest sub-assembly, this SCE is build out of a rigid steel space frame structure called torque box. On both sides are cantilever arms, which are connected to the mirror elements. On one hand the framework must be stable and rigid to resist strong wind and on the other hand the connection to the parabola must be very precise to decrease deformations of the mirrors. A significant step for building a PTC power plant is to check the geometry of the attachment points by the help of photogrammetry. Every larger uncertainty has a big influence on the shape of the mirror and can lead to stresses in the material and changes of the focal line. Furthermore, the mirrors have to be shaped accurately and the surface should offer a maximum reflectance. The Intercept Factor (IC) describes the effect of deviations in geometrical concentrator conditions on the optical performance. The factor consists of the ratio of solar irradiation, which is reaching the receiver tube and irradiation, which is reflected from the concentrator surface. Basically, the IC is essentially determined by [5]:

Mirror shape deviations: Slope deviations from an optimum design of the mirrors independent from structure tolerances and gravity loads

Receiver tube position: Misalignment of the absorber away from the focal line of the collectors

Tracking deviations: Deviation of the focal plane and the position of the sun caused by torsion of the mirror support structure

The state of the art in mirror design is that the parabola consists of two differently shaped mirror facets. One facet is used for the inner parabola and the other one for the outer parabola. By using four varying mirrors for the whole parabola, the irradiation is reflected in one focal line, where the absorber tube is located. In conclusion the characteristic LUZ and EUROTROUGH design consists of four mirror elements for shaping one partial segment of the parabola [5]. In implementation most collectors are north-south orientated. An east-west orientation decreases the annual yield to 80%, but it has the possibility to achieve a more constant monthly yield during the year [13].

1.2.2 Absorber tube

One of the high thermal stressed parts is the receiver tube, which absorbs the solar radiation and transmits the solar energy to the HTF. These tubes are moveable mounted to the Heat Collector Element Support (HCES) and have a fixed point located at the drive pylon. The thermal expansion of the tube appears away from these connection points. The temperature in the Heat Collecting Elements (HCE) of the power plant can easily reach 400 °C. Occurring temperature differences are causing a large linear expansion of the absorber tube which has then to be compensated by the flexible pipe connectors.

Another effect that takes place in the absorber tubes is that the used materials expand in different dimensions. This effect is based on varying linear coefficients of expansion α. These are many times higher for steel as for quartz glass. Consequently, the metal absorber tube, shown in **Figure 6,** expands more than the quartz glass, which causes high stresses to the tube. Therefore the thermal expansion is compensated by two bellows at the ends of the tube. Additionally, the surface of the absorber tube has a selective coating to optimize the absorptance and to decrease heat losses. The space between the absorber tube and the glass enveloped tube is evacuated to decrease heat losses to the environment. Moreover the glass is also very insensitive against abrasion and has a high transmittance.

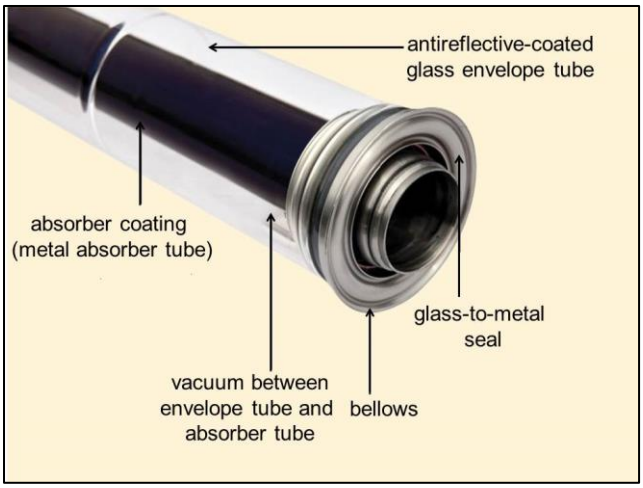

Figure 6: Components of a common receiver tube for PTC [14]

1.2.3 Heat transfer fluids

Furthermore, there are various types of HTFs in use, especially in research facilities and prototypes. HTFs can be subdivided in steam/water, molten salt and synthetic high temperature oils. However the most approved ones in commercial power plants are heat transfer oils with a temperature limit around 400 °C. The most used and approved HTF oils are Syltherm 800, Therminol VP-1, Dowtherm Q, Helisol 5A [15] [16]. These HTFs can distinguish into oils based on Biphenyl / Diphenyl oxide (BP/DPO) like Dowtherm A and Therminol VP-1. The other classification can be made in HTFs based on silicone oils as HELISOL® 5A and Syltherm 800 [15] [16].

Table 1: Operating Temperature range of common HTF oils [15] [16]

HTF oil	Freezing point [°C]	Maximum temperature [°C]
Syltherm 800	-40	398
Therminol VP-1	12	397
Dowtherm Q	-35	360
HELISOL® 5A	-65	425

The maximum operating temperature for the HTFs in PTC power plants is also one important limiting factor for the efficiency. Operating the oils at high temperatures leads to chemical instability and the aging process happens much faster as on lower temperature set points. Also the gas phase occurs more heavily and has to be separated from the oil in order to reduce heat losses. Hydrogen is one of the critical

gases released by this reaction, because it is able to diffuse through the pipe in the vacuum which causes an increase of heat losses to the environment. A so-called getter material is included in the construction to absorb the hydrogen.

1.2.4 Molten salt systems

Ambition goes also to the use of molten salt as HTF. A reason therefor is that a heat exchanger between the collector loops and the storage tanks can be omitted as shown in **Figure 7.** This fact simplifies the plant significantly and saves costs. Another advantage is that the useable temperature level can be increased up to 565 °C and the power block efficiencies rises up to 45%. A disadvantage is the melting point of the molten salt, so the fluid has to be maintained at a temperature higher than 140 °C during the night or less sunny days, otherwise the pipes get blocked by solidified oil. Another detriment is the corrosive property of molten salt. The reaction with the receiver tube and other components which have a direct contact with the HTF has to be monitored during operation [17].

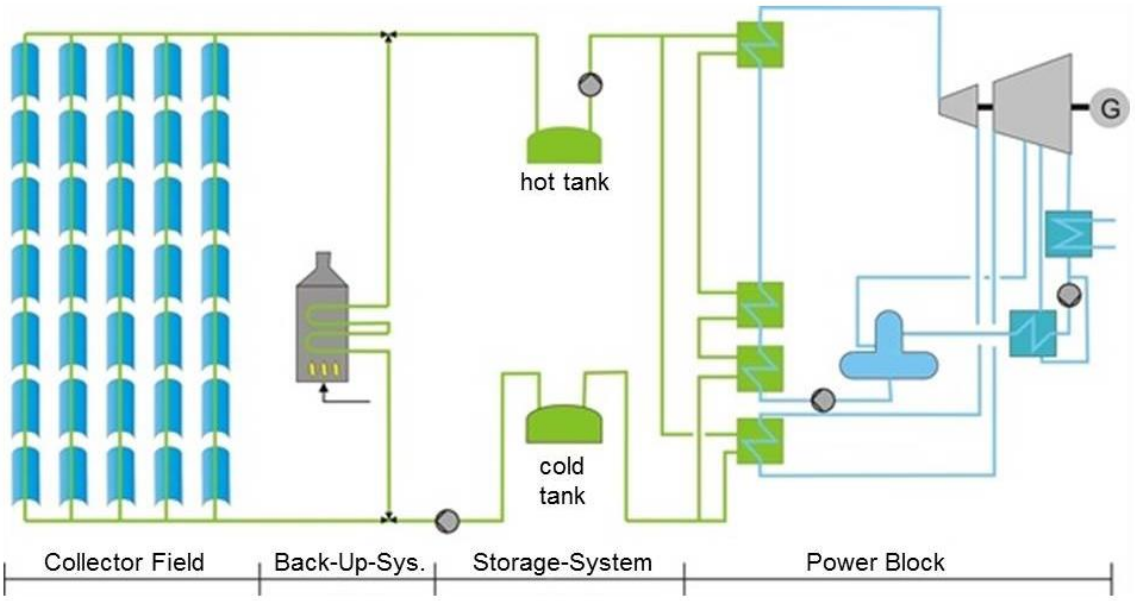

Figure 7: Scheme of a PTC power plant with TES molten salt as HTF (blue: water/steam, green: molten salt) [17]

1.2.5 Tracking system

In order to reach a maximum power yield during the day it is necessary to track the collectors in the optimal position to the sun. For this task a 90° position of the parabola to the sun is needed. Weather conditions can change really fast, so all the collector lines must be able to react rapidly to this circumstance to reach a maximum yield or in some situations prevent the oil and the absorber from overheating. These movements are usually made by hydraulic driven pistons in very small and precise steps. Another possibility is the direct actuation via electrical motors. The drive systems are controlled

in different ways. One is to calculate the elevation of the sun and position the collectors by the help of a position sensor. The other way is to use a sensor that determines the position of the collector to the elevation of the sun. Moreover, a combination of both systems is possible [14].

1.3 Ball Joint Assemblies and Rotary Flex Hose Assemblies

All these tracking movements along the longitudinal axis for the heat expansion of the receiver tube have to be compensated by flexible receiver connections also called REPAs. These assembly parts are linking the fixed piping with the receiver tube. Their main task is to compensate the occurring forces in order to prevent damages to the structure. Another important point is that they have to be leak-tight to avoid environmental contaminations. Currently there are two main concepts on the market, Ball Joint Assembly (BJA) and the other one is called Rotary Flex Hose Assembly (RFHA), sown in **Figure 8**.

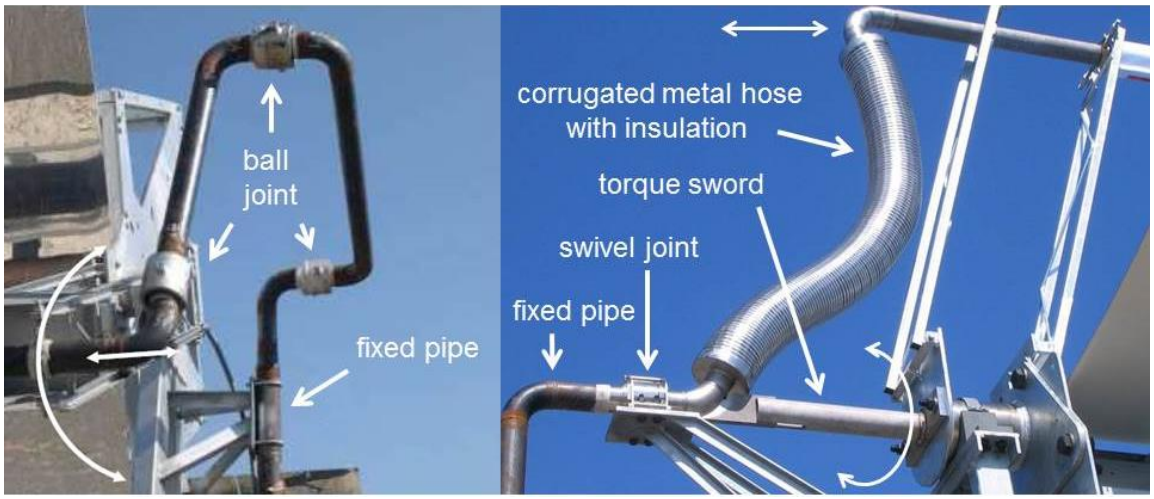

Figure 8: Left: Ball Joint Assembly (uninsulated). Right: Rotary Flex Hose Assembly [5]

BJAs basically consist of three single ball joints. Each of them allowing rotation movements and their specific arrangement enables the assembly to absorb tracking motions and linear expansion.

Inside these joints an inner and outer compression sealing is holding the ball-shaped head from one pipe side as shown in **Figure 9**. To prevent leakages and reduce friction, the gap between these two metal seals is filled with reinforced graphite and which is called injectable sealant. The refilling of these seals is necessary during the operation of a power plant and is refilled via the injector port. Normally this maintenance task can be done by a pressurized pipe system.

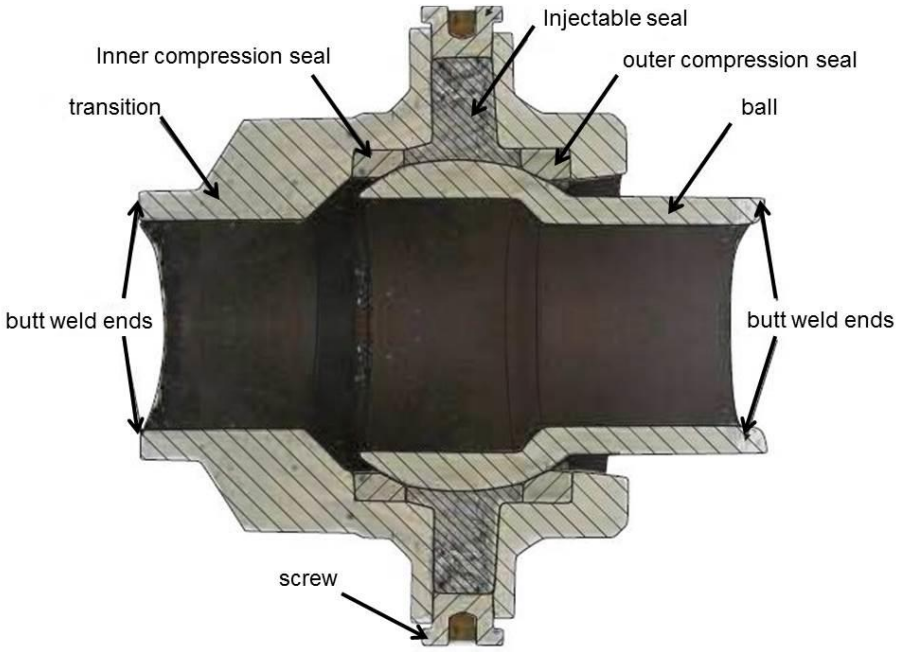

Figure 9: Sectional view BJA [18]

The other design RFHA utilizes a different principle as the rotation movement of the collector is compensated by a swivel joint (SJ). A corrugated metal hose is the connection between the fixed piping and the receiver tube and the translation is regulated by the flexibility of the hose. Furthermore, a direct connection to the bottom part of the flexible hose and the swivel joint is realized by the torque sword to rotate the assembly and to minimize stresses by not pulling through the receiver tube connection.

REPAs are one of the critical parts in a PTC power plant, because they are subjected to rotation and translation movements, environmental influences, high pressure and HTF temperatures of 400 °C. Therefore, life cycle tests are necessary and have been executed for example by the company Senior Flexonics GmbH in form of test rigs for RFHAs. One of the special performance test benches was built for RotationFlex© Single and Double systems. In the facility two sensors measure the reaction forces of the RotationFlex© system during the life cycle test. The swivel joints are filled with HTF and the test rig operates at a maximum temperature of 550 °C and 40 bar pressure while the flexible hoses are filled with water of ambient temperature and 40 bars. An issue is that by simulating the daily collector tracking in the form of rotation and translation movements, there is no circulating of the HTF possible. However, a separate test rig for durability tests was built to execute tests just for the flexible hoses under realistic operation conditions and circulating HTF by temperatures of 450 °C and 40 bar pressure [5].

Abengoa Solar constructed and operates a test rig for REPAs with molten salt as HTF. The operation conditions are set to a maximum temperature of 500 °C and a pressure up to 40 bar. A rotation and linear movement is possible and also the detection of

torque, force, pressure and temperature. 30 years of operation are simulated or 11.000 cycles without any leakages [5] [19].

Table 2: Owerview of REPA test rigs with main parameters [19]

	REPA	HTF	P_{max} [bar]	T_{max} [°C]	Cycles
ATS	BJ	-	-	-	-
Hyspan	BJ	DOWTHERM A	<30	393	11.000
IRAtec	SJ	Therminol VP-1	6	345	15.000
DLR/CIEMAT	RFHA	Slytherm 800	20	300	321
Abengoa Solar	RFHA/BJA	Solar Salt	25	550	11.000
Senior Flexonics	RFHA	Water/ Therminol VP-1	40	550	ca. 11.000

In conclusion, there are six test rigs for single components of REPAs, which investigate the influence of HTF pressure and temperature to those. The test benches of Abengoa Solar and Senior Flexonics GmbH are able to simulate the same operation parameters (temperature, pressure) of common PTC power plants. They also detect forces and torque from rotation and translation movements, but some important influencing input factors are not considered. A closed circulating loop with HTF oils is necessary to simulate the volume flow of PTC power plants. Another missing impact is a rotation motion generated by a drive pylon in order to have a comparable tracking motion of common SCAs.

1.4 REPA test rig

At the Plataforma Solar de Almería in Spain, a unique test rig was built in order to execute life time tests for REPAs under real operation conditions of PTC power plants. This undertaking has been done in cooperation with the Centro de Investigaciones Energéticas, Medioambientales y Tecnológicas (CIEMAT).

The HTF circulates with the same flow volume as in common PTC power plants. Also an oil temperature of 450 °C and a pressure of 40 bars are realized to study durability and damage mechanisms of the flexible pipe connectors. The daily collector movement can be executed in a range of 210°, which is equal to normal collector tracking. Moreover, collectors with a focal length of 1,5 up to 2,3 m can be represented by the kinematic unit. Between 10.000 -11.000 cycles are necessary to simulate 30 years of solar operation in a real power plant. Furthermore, a translation movement is possible to depict thermal expansion of the absorber tube. Real outdoor conditions are not completely replicated, because the electronic parts and measurement devices must be protected from weather influences. Therefore, a half open roofing was built. After the commissioning, the accelerated aging test should perform 15.000 cycles in two months, which corresponds to 1,5 times the lifetime. Another advantage of the test rig is the possibility to investigate two REPAs at the same time, for example two BJAs or two

RFHAs. But a combination of two different types of REPAs is not intended. These tests should deliver more knowledge about the long term performance of single components and different kinds of REPAs. Criteria resulting from potential life cycle test should improve the production of REPAs in the future to avoid damages and down time of power plants. A second assignment is the detection of oil aging during fixed operation hours. A new generation of heat transfer oils will be tested by taking samples and analyzing them (for example Therminol VP-1, HELISOL® and Syltherm 800). The target here is to prove more environmental friendly oils, but there is also the possibility to investigate common oils [5].

1.4.1 Design of the main assemblies

Figure 10 gives an overview of the REPA test rig's main components. The main task in this life cycle test facility is to generate the rotation and translation movements on the REPAs in a precise way. The whole construction is divided in two mayor sub-units in order to protect the power cabinet, control cabinet and operating staff from possible HTF leakages because of high pressure and temperature. On the left side the **Main Assembly** is located, which contains the kinematic unit and the traverse to simulate typical motions. The other sub-unit is the **HTF-cycle** to generate typical pressures and HTF-temperatures of common power plants. Also the Supervisory Control and Data Acquisition (SCADA)-system is sited here to collect all sensor outputs and to ensure the correct function of the kinematic unit.

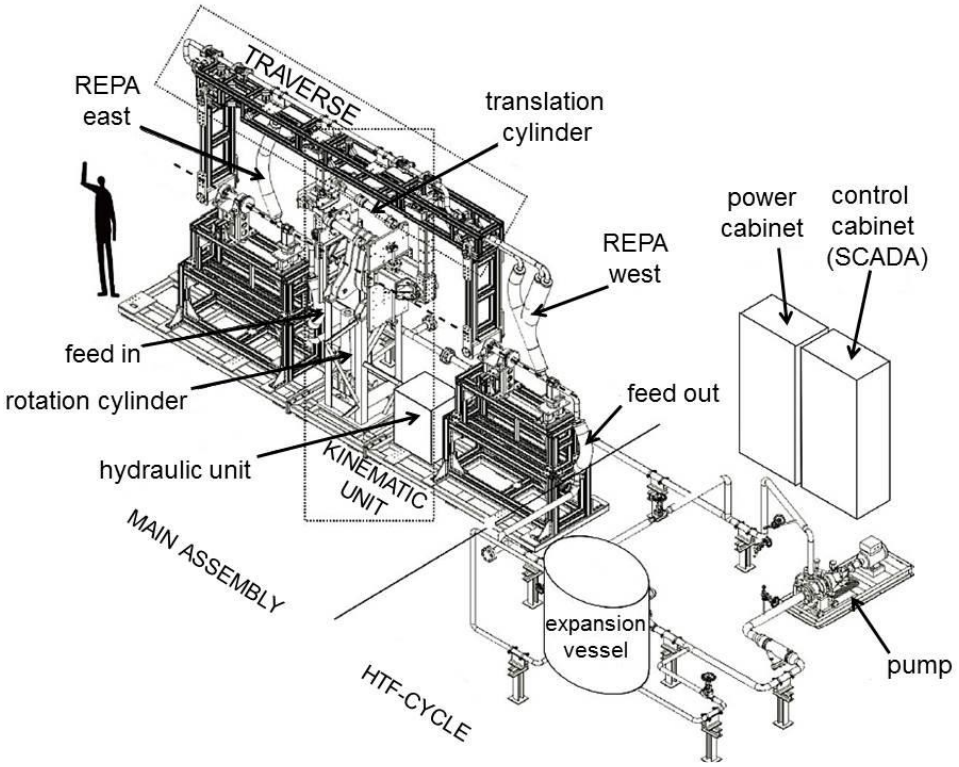

Figure 10: REPA test rig scheme with all main components (without roofing and dividing wall). A more detailed view on specific installed parts can be found in appendix 7.3

The **Kinematic Unit** is composed of two rotation cylinders for the movement around the rotation axis and two translation cylinders push the table arms to simulate the thermal expansion of the receiver tubes. A hydraulic unit houses a servo motor to drive the hydraulic pump and move the actuators in exact steps. By turning the table arms, a rotary feedthrough turns the lower part of the REPAs and the swivel joint. Another important detail is that the kinematic unit can be adapted in order to represent different focal lengths of different collector designs. The traverse is the connector between the two flexible hoses and is attached to two drive pylon arms. The west dynamometer is installed to measure the resulting torque and forces.

To operate under a defined pressure, a magnetic coupled pump has been installed and six electric band heaters with 3500 W power, each heats the HTF temperature up to 450 °C. An expansion vessel compensates the thermal expansion of the heat transfer fluid with the help of nitrogen to hold the pressure at a configured level. Additionally, a bypass isolates the main assembly and the pump quickly in case of leakages.

Mainly, the **SCADA-System** is separated into five basic areas: the Observe System /Check Safety, the “Operate HTF cycle”, the Operate Kinematics Unit and the Data Acquisition and Human-Machine Interface. The SCADA subsystems are the Open-Platform-Communication-Server (OPC), LabVIEW (LV) and the Programmable Logic Controller (PLC). The Graphical User Interface (GUI) has been programmed in LabVIEW to represent the important parameters and to control the operating interface of the OPC-Server, which is the connection between LV and PLC. Furthermore, the operation of single components, for example the cylinders, is carried out by the PLC.

After finishing the installation of all described subunits, a photogrammetric setup has been provided to ensure the correct position of the traverse to the rotation axis. This measurement allows a corresponding mounting position of the REPAs with minimum tolerance. Another necessary step was the programming for regulation of the mechanical parts and to develop a control interface, which allows the operation and monitoring. To execute these life cycle tests, the commissioning of the test rig begun. In order to do this, two RFHA REPAs of the manufacturer Senior Flexonics GmbH have been installed to represent a typical Eurothrough system.

1.4.2 REPA test rig settings and operation range

In order to find representative parameters for the REPA test rig in form of HTF temperatures, rotation angle and translation angle for the heat dilatation of the absorber tube, the operating conditions of Eurotrough power plants can be used. In these PTC power plants, comparable conditions are 30 bar HTF pressure and 239 °C HTF temperatures for the inlet of the loop and 20 bar and 393 °C after passing the loop. The daily rotation angle φ equates 215° of the complete SCA to follow the sun during a day. The rotation motion of a Eurotrough collector is depict in **Figure 11,** for example of a RFHA REPA. The normal procedure in an actual power plant is that REPAs rotate

slowly from φ = 0° to φ = 181° to follow the sun and after this, they move back in a stow position, where they are left during the night at φ = -34°.

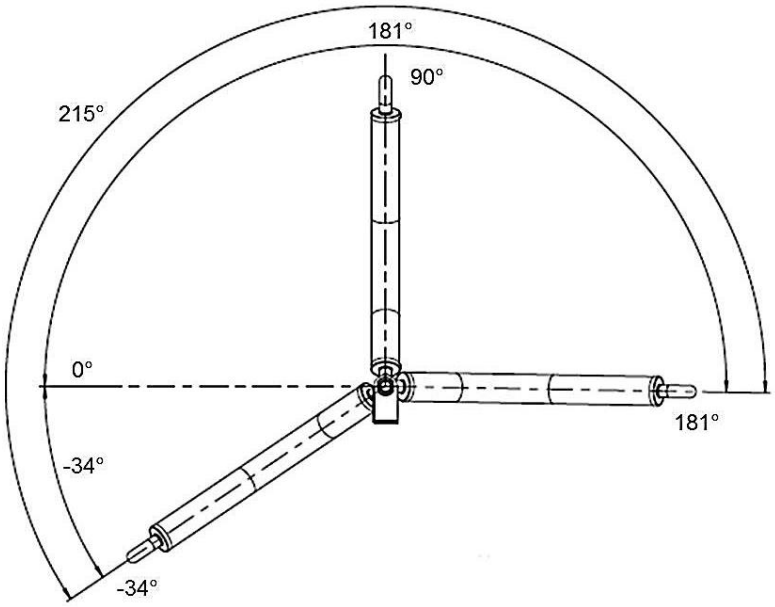

Figure 11: Rotation movement of a RFHA REPA in a usual Eurothrough system. Maximum daily position is φ = 181° for the collector and stow position is here φ = -34°.

A translation angle ϑ of 20° in total, represents the thermal expansion of the absorber tube in all working conditions of a commercial Eurothrough. **Figure 12** points out the different heat dilation lengths in three operation conditions.

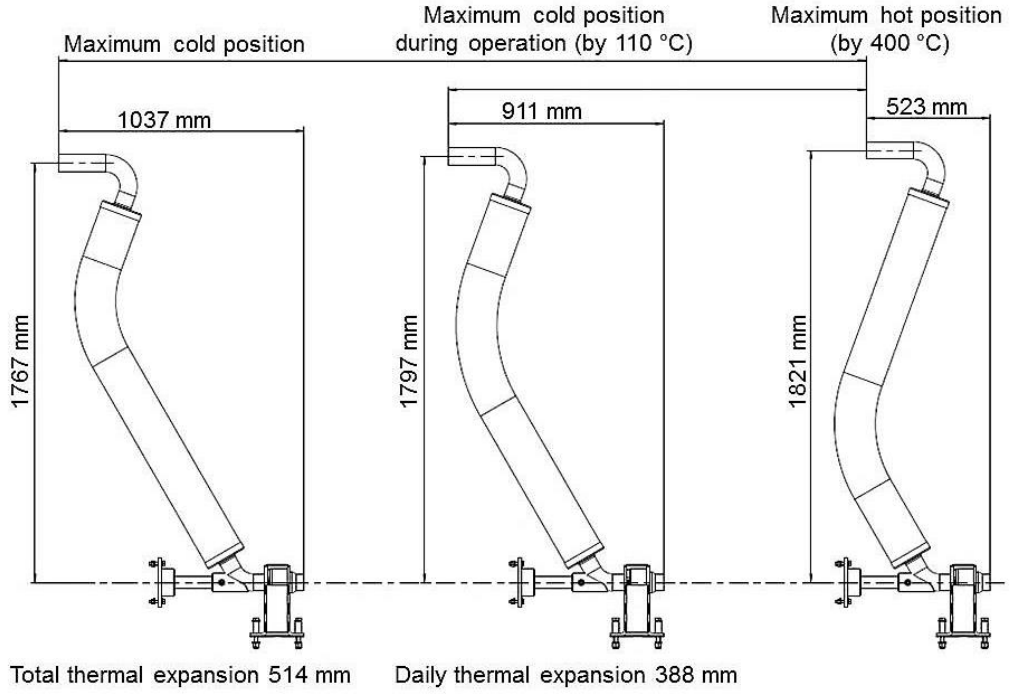

Figure 12: Currently installed RFAHs in the REPA test rig and their position during typical operating conditions. Technical drawing for a Single RotationFlex©- System DN 65 Eurothrough company Senior Flexonics.

The cold position occurs just in an operative power plant after HTF is cooled down completely. The daily heat dilation for this example amounts to 388 mm between the maximum cold position during operation and maximum hot operation by 400 °C, so this length is representative for daily stresses to the REPAs. The general heat dilation of an absorber tube can be calculated by the following **equation 1.1** [13]:

$$\Delta L = \alpha \cdot L \cdot \Delta\vartheta \qquad \text{(Eq. 1.1)}$$

α = coefficient of linear thermal expansion (material dependent)
L = Length of SCA
$\Delta\vartheta$ = Temperature difference between cold and hot absorber tube
ΔL = Heat dilation of the absorber tube

The traverse at REPA test rig can be moved in a much bigger angle up to ϑ = 45 ° to simulate different types and dimensions of PTC power plants. Moreover, the whole facility is developed to withstand a HTF design temperatures of 500 °C. To reach the maximum operation temperature of 450 °C, a 120 mm thermal isolation for the piping system is needed. The volume flow $\dot{V}_{\mathrm{HTF}}$ can be controlled by the pump in a range of 6 to 60 m³/h and the HTF pressure p_{HTF} is regulated by a nitrogen cushion inside the expansion vessel up to 40 bar. At the moment HELISOL© 5A is used for the commissioning of the test rig, but in the future different HTFs will be used for REPA life cycle tests.

2 REPA measurement setup

In order to know the ageing impacts to the REPAs and to prevent malfunctions during a life cycle of a PTC power plant, it is necessary to measure and understand the forces, which react to the flexible pipe connections. Therefore, two different measurement setups were needed and have been integrated to the test rig for collecting these data during every operation condition and to allow a better understanding of REPA impacts. The first test has been done with **installed REPAs and HELISOL© 5A as HTF** and the second test was executed **without REPAs and air as HTF**. For the understanding of both tests, the integration of the forces measurement is explained and depicted in the **chapter 2.1** and also the REPA integration.

2.1 REPA test rig, REPA integration / force measurement

To investigate all resulting forces and torque interacting on both REPAs, it is inevitable to understand all reactions in the traverse first. The target is to know all forces and moments, caused by thermal dilatation and rotation of the traverse pipe section. Those are unwanted influences, measured by the dynamometer. In later tests, after commissioning the additional forces and moments caused by the traverse, should be subtracted from the total measurement in order to know only the influences on the REPAs. Important influencing factors are fixed bearings and the heat expansion of the traverse piping, which is mostly absorbed by compensators. In order to detect this dilatation, a separate test without REPAs and air as HTF is needed. This test has been performed in the past with air as HTF before the traverse was installed at the kinematic unit. This previous test and the results of it forms the basis to compare the following tests and to build up the measurement setup. The next step to more realistic operation conditions is to replicate this test with the integrated traverse and typical rotation movements of PTC in common power plants. The test results should give a calculation base for the influence of the pipe temperature and heat dilation on the rotation movements for the test with REPAs and circulating HTF.

As written in **chapter 1.3,** different manufactures executed life cycle tests for REPAs in various types of test rigs. Senior Flexonics GmbH carried out force and torque measurements at the Rotationflex Single System to understand the influence of rotation and translation movements. The basic knowledge of these tests was decisive for the force and torque measurement at the REPA test facility. Inspired by this, the target is to install four dynamometers for the complete measurement during REPA life cycle test. Two of four sensors will be attached directly to the traverse piping next to the flexible hoses and two others will be bolted under the swivel joints.

A detailed view of the dynamometer positions is depicted in **Figure 13.** The location of the sensors in the traverse is called ‘top-west’ and ‘top-east’ position and the ones under the swivel are located at the ‘bottom-west’ and ‘bottom-east’ position. At the moment just one dynamometer is installed in the ‘top-west’ position and the others are

replaced by mechanical dummies with the same design sizes. The reason for this is to assess the functionality of the dynamometer before installing three more sensors of the same kind. Moreover, the first sensor is a K6D175 dynamometer from the manufacture ME-Messsysteme. More detailed information on sensor specifications is written down in **Appendix 7.4**. The utilized sensor has the measuring range of 10 kN to detect forces in x, y and z-direction, also torque around these axes can be determined until 1 kNm.

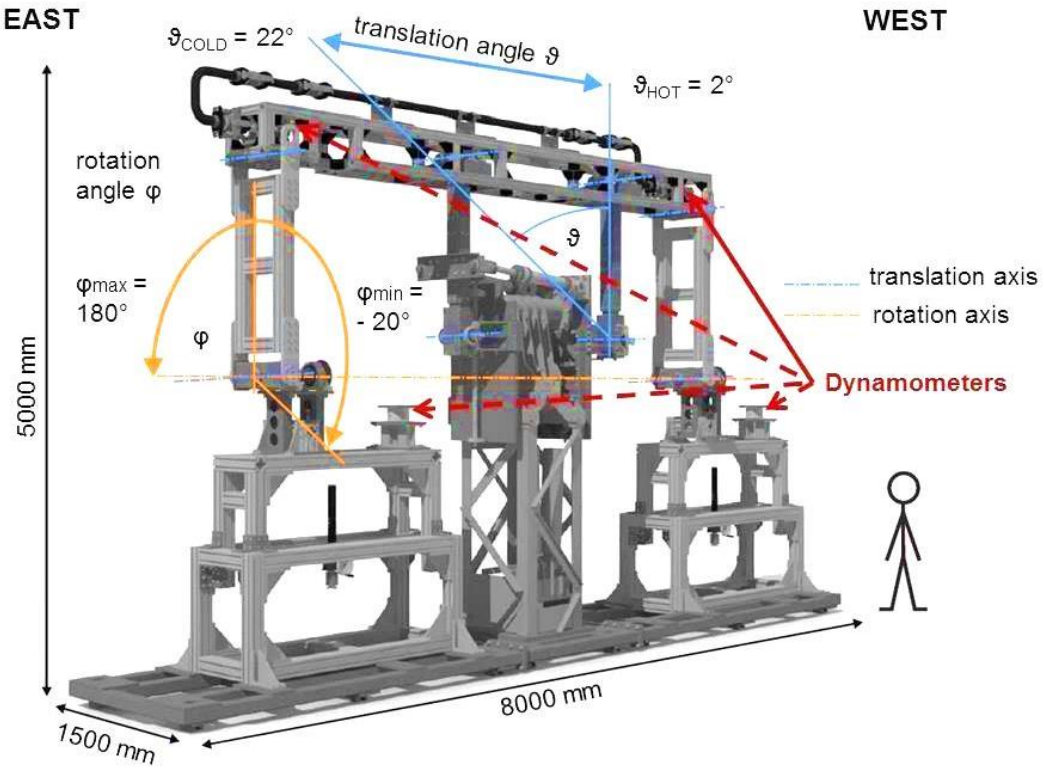

Figure 13: Mounting position for dynamometers at REPA test facility in traverse and kinematic unit (dashed arrows are planned dynamometer positions) [5]. Also shown are the ranges for rotation and translation movements as configured in the PLC.

The measurement principle is based on strain gauges. They have the characteristic to change their electrical resistance by minimum deformations. The strain gauges are attached to the sensor head by the help of special glue in order to detect every resulting movement. A voltage signal is induced into the sensor and a coupled measuring amplifier converts this input into a force and torque value by the help of a calibration matrix. The data logging is done by a computer with the help of “GSV-multichannel software”, the output here as a text file is used as data base. After the commissioning, the sensor data should be coupled directly with the PLC in order to minimize the number of data sources.

Furthermore, it is essentially to have a closer look at the traverse piping installation in order to understand the measured forces and torque. Basically, the traverse can be separated from the plane of the location bearing, as shown in **Figure 14** . These fixed bearing distribute the heat dilatation in east and west direction of the traverse and a

floating bearing on each side permits the longitudinal expansion. The dynamometer itself also works as a floating bearing. To prevent high stresses in the pipe, angular expansion joints have been installed, but just on the west side of the traverse in order to scrutinize the correct function before the installation on the east side. The others will be integrated after commissioning of the first sensor and reliable test results. Two single hinged expansion joints enable the pipe to compensate elongations in a vertical direction and the gimbal hinged expansion joint can be also moved horizontally. Another compensator is the bended pipe on both ends, in form of a u-bend and s-bend. The idea is to equalize most of the forces and torque, which react on the installed dynamometer in order to measure just the impact of the rotation and translation movements, which are introduced by the REPA under testing.

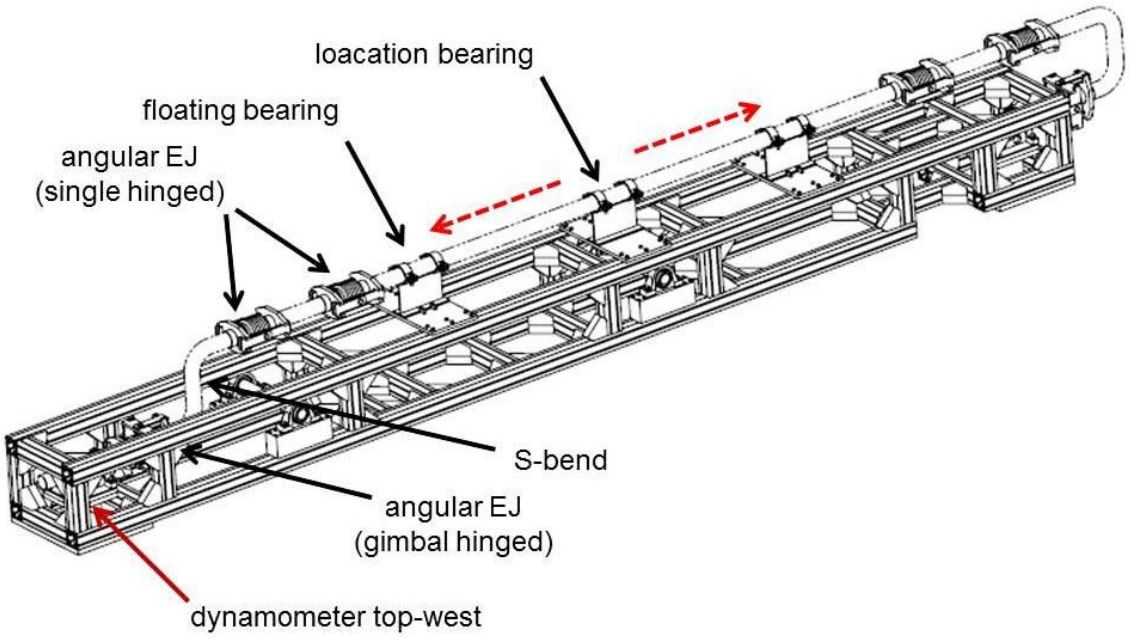

Figure 14: Drawing of the traverse piping system with bearings and angular expansion joints (EJ). Left and right side are similar in the number of expansion joints and bearings. Red arrows show the direction of thermal dilatation of the pipe.

The first floating bearing after the location bearing guides the pipe to the dynamometer support and the linear expansion, caused by the heat dilatation, is stopped at the fixed bearing at the end of the support. An illustration of the pipe support and the bearings is given in **Figure 15.**

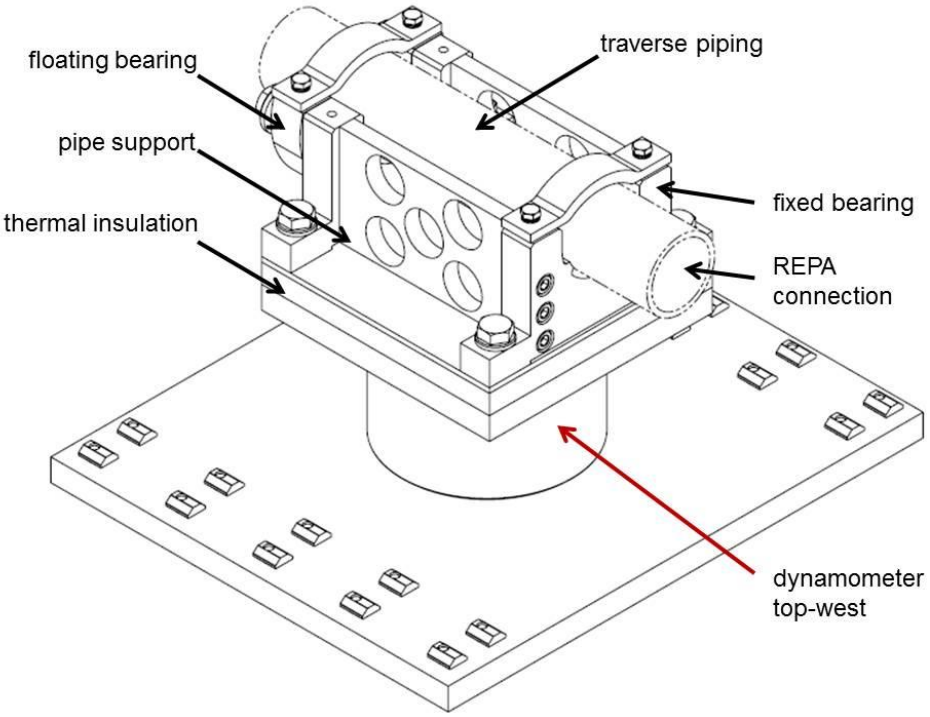

Figure 15: Cutout of dynamometer integration in the traverse with support and bearings.

In order to protect the dynamometer from overheating, a thermal insulation layer minimizes the heat transfer from the pipe to the sensor. In conclusion, the forces from the REPA and traverse pipe converge at this point, where the floating bearing is located. The force measured by the dynamometer can be combined to F_{dyn} and contains the moments resulting from the fixed and floating bearing of the pipe support. The following **equations 2.1 – 2.6** explain the correlations between all forces, which have to be included in to the approach [19]:

$$F_{\mathrm{dyn}} = F_{\mathrm{fix}} + F_{\mathrm{float}} \qquad \text{(Eq. 2.1)}$$

The measured force F_{dyn} consists of two separate elements, one is from the REPAs F_{REPA} and the other is from traverse pipe system $F_{traverse}$.

$$F_{\mathrm{dyn}} = F_{\mathrm{traverse}} + F_{\mathrm{REPA}} \qquad \text{(Eq. 2.2)}$$

Also the simulation model Rohr2 F_{ROHR2} represents the influence of $F_{traverse}$.

$$F_{\mathrm{Rohr2}} = F_{\mathrm{traverse}} \qquad \text{(Eq. 2.3)}$$

With this in mind, the forces and moments which really have an effect to the REPAs, are those without the force of the traverse piping system.

$$F_{\mathrm{REPA}} = F_{\mathrm{dyn}} - F_{\mathrm{Rohr2}} \qquad \text{(Eq. 2.4)}$$

To calculate the resulting moments, it is necessary to include levers. The reason for this is that the ideal positions of REPA, bearings and dynamometer are not equal.

$$M_{\mathrm{ROHR2}} = M_{\mathrm{fix}} + M_{\mathrm{float}} + F_{\mathrm{fix}} \cdot h_{\mathrm{fix}} + F_{\mathrm{float}} \cdot h_{\mathrm{float}} \qquad \text{(Eq. 2.5)}$$

$$M_{\mathrm{REPA}} = M_{\mathrm{dyn}} - M_{\mathrm{ROHR2}} - F_{\mathrm{REPA}} \cdot h_{\mathrm{REPA}} + F_{\mathrm{ROHR2}} \cdot h_{\mathrm{ROHR2}} \qquad \text{(Eq. 2.6)}$$

To have a better understanding of the resulting levers, **Figure 16** visualizes the relationships.

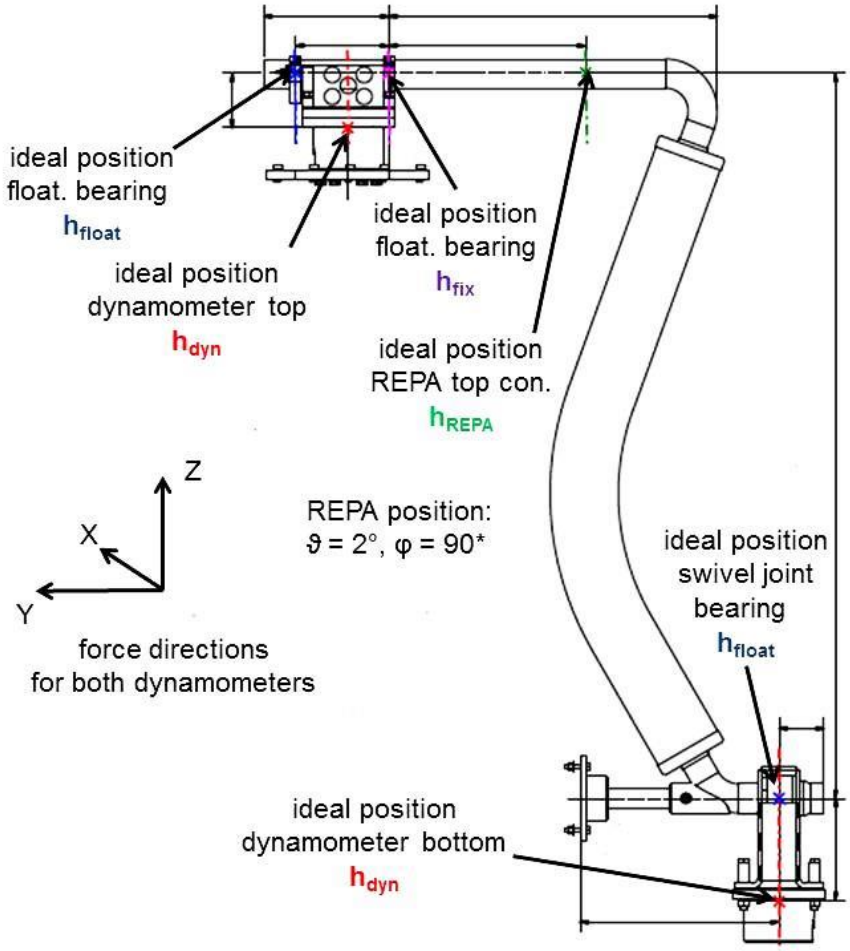

Figure 16: Technical drawing of REPA and dynamometers [2]

2.2 Measurement setup with installed REPAs and HELISOL© 5A as HTF

The aims of the first measurements during the commissioning of the REPA test rig are to fulfill the following expectations:

Rotation movement impact: Conclusions about the measurement range of forces and moments and the specific course during each rotation.

HTF temperature impact: Influence of different HTF temperatures on the specific course of forces and moments for rotation and translation motions and on the entire measurement.

Translation movement impact: Conclusions about the measurement range of forces and moments and the specific course during each translation movement.

Volume flow impact: Influence of different volume flows on the entire measurement during rotation movements.

Pressure impact: Influence of different pressures on the entire measurement during rotation movements.

Dynamometer reliability: Insight about a rising dynamometer temperature on the measurement. The extent of sensor drift and settling time on the total measurement and the correct function during long-term measurements.

Sensor measurement range: Examination of the suitability of the dynamometer with regard to the measurement range.

All the named impacts are extensively investigated with the same measurement set up as for later REPA life cycle but with one installed dynamometer. Explicit findings can be proved with data of these measurements and the results are visualized in the following chapter 4. But all measurement results of this setup include the impact of traverse pipe section. This important fact must be taken into account by the consideration of the measurements and the results.

In order to prove the expectations, a specific measurement setup was needed to execute the measurements with a dynamometer. Basically, the experimental setup consists of two separate partial measurements. One is a permanent data collection of the REPA test rig. The data acquisition is done by the PLC by recording the output of every sensor installed at the test facility apart from the dynamometer. The PLC output consists of 114 signals measured during the operation of the test rig. But the important sensors for this consideration measure the volume flow of the HTF, the HTF temperature, HTF pressure, rotation and translation position. A list of the sensors and their installation position is shown in **Appendix 7.3.**

The second partial measurement is done by the first dynamometer, installed in the traverse independently of the PLC recording. The measurement chain for the dynamometer is visualized in **Figure 17**. The K6D175 sensor in the first picture is connected with a data cable in to the amplifier GSV-1A16USB and the transformed measuring signal goes to the validation software GSV-Multichannel, installed on a laptop.

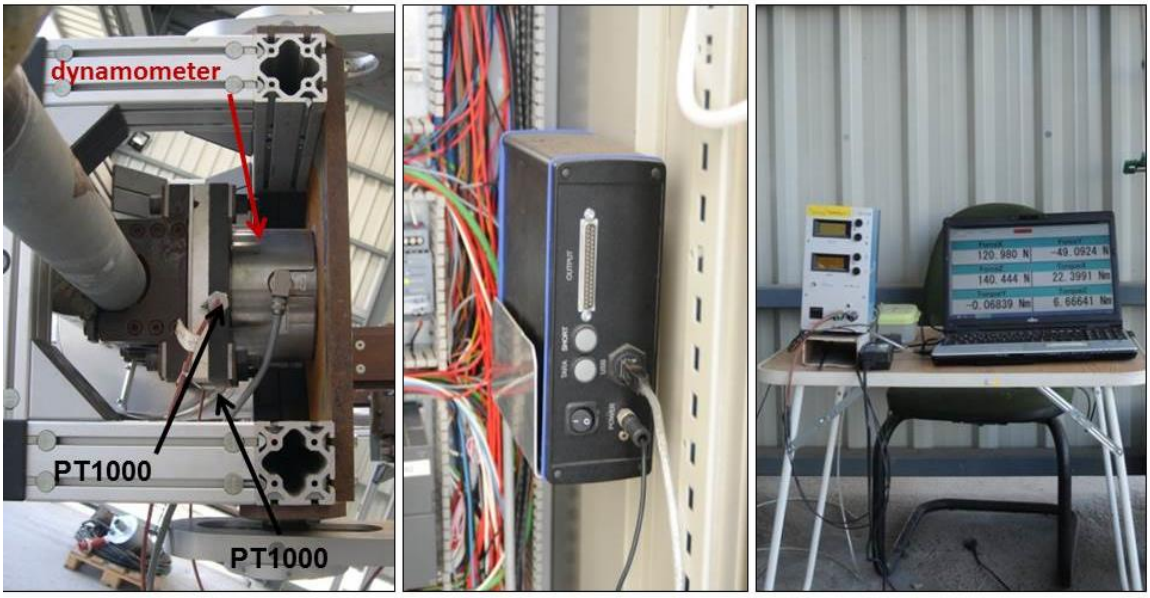

Figure 17: Measurement chain of the test facility. Left: dynamometer in installed position with two Pt1000, Middle: Amplifier GSV-1A16USB located in the cable cabinet, Right: Laptop with the software GSV-multichannel coupled to the amplifier.

2.3 Measurement setup without REPAs and air as HTF

The second measurement setup has been developed in order to investigate the traverse as a separate assembly. This intermediate step is necessary to understand all influences on the forces and moments reacting to the REPAs in later life cycle tests. The setup has been installed to know the following correlations:

Heat dilatation impact: Determination of forces and moments resulting from thermal expansion of the traverse pipe section in west direction.

Rotation movement impact: Determination of forces and moments during rotation movement of the traverse pipe section.

Pipe temperature impact: Determination of the influence on forces and moments of different pipe temperatures measured during rotation movements of the traverse pipe section.

In order to find the outlined impacts to the traverse without REPAs, another measurement setup has been installed. Therefore, the HTF pipe system has been

drained and the REPAs have been removed. After this step the traverse can be investigated independently from the rest of the test facility. Rotation and translation movements can be done without a connection to the HTF pipe system and the operation remains the same with the normal REPA control interface. The installation of a heater station was the next step to finish the measurement setup. With the help of this station, the traverse pipe can be heaten up by a separate heat source away from the major test rig to a temperature of 400 °C. This is realized by a blower and an air heater, installed on an item structure as shown in **Figure 18**.

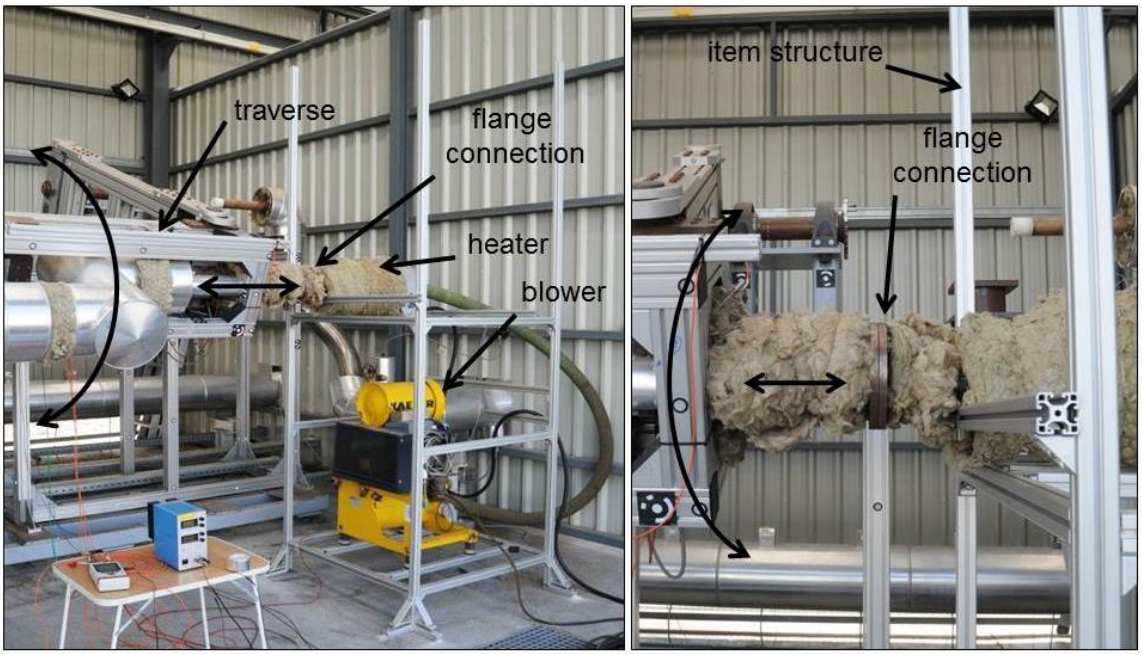

Figure 18: Measurement set up for traverse test without REPAs. Left: The blower is connected by a hose with the heater and a hopper, all mounted on an "Item"-structure. Right: Heater and pipe section connection is done by driving the traverse in translation direction in an end position, where both flanges have a seating surface.

One important design detail for the measurement setup is the connection of the heater with the traverse pipe section. Hence, two metal flanges have been welded at the end of each pipe. By moving the traverse in translation direction "west", the contact of each component can be achieved and the flanges have a seating surface. This kind of connection has the advantages that no lock or screw connection is needed to attach the two pipe ends and to heat up the complete pipe section. As a result of this, no personal has to touch hot parts in order to connect the two pipe ends for example with a kind of lock. Another benefit is that the heat source has a fixed and save position in the "Item"-structure. No hoses are permanent connected to the traverse during rotation movements and neither is a directly installed heater at the traverse pipe end needed. This measurement setup achieves a minimum risk of injuries for the operating person.

After heating the pipe up for several hours, the rotation and translation movements can be executed. To perform a complete rotation motion, the pipe end of the traverse has to

be moved back in “east” direction for disconnecting the two flanges. After this step, a rotation motion can be executed. A result of this is a time range of roughly four or five minutes, where the pipe system is cooling down during the testing procedure. This cooling period has an unwanted impact on the forces and moment measurement during the rotation. After this, another temperature step up to 400 °C can be performed by connecting the assembly with a translation motion until the two flanges have a seating surface again.

Moreover, a heat-loss estimation has been done to make sure that the temperature of the pipe does not decrease to fast during the movements. The result of this calculation is that a temperature loss of ≈ 2 K/min can be expected without any heat supply to the pipe. The entire calculation can be found in **Appendix 7.2.**

Another detail of this test setup is the measurement of the pipe temperature in the traverse section. To measure this representative temperature, four PT100 resistance thermometers have been installed under the insulation, directly attached to the metal surface of the pipe. The average of these four sensor outputs is also called ϑ_{pipe} in the following contemplation. The exact positions of all temperature sensors are illustrated in **Figure 19**.

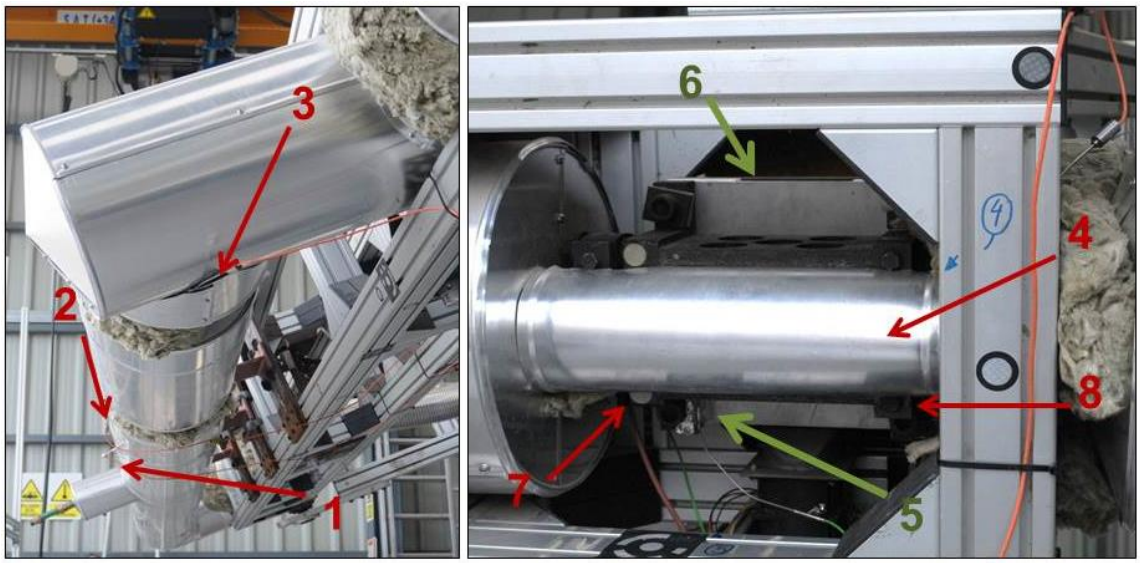

Figure 19: Overview of all temperature sensors in the traverse pipe section (left) and dynamometer bearing (right). 1-4: Four PT100 for pipe temperatures; 5 and 6: Type K thermocouples, 5 for temperature at the floating bearing, 6 for dynamometer temperature; 7 and 8 PT 1000 for temperature in the bearing support metal plate (logged in PLC). (1=TempBearing1, 2=TempEJ1, 3=TempEJ2, 4=TempSup, 5=TempFloat, 6=TempDyn)

One of two Type K thermocouples measures the temperature directly at the floating bearing of the pipe support and the other one is directly installed on the housing surface of the dynamometer to detect the heat conversion from the pipe. All the named sensors are just installed for the measurement setup **without REPAs and air as HTF** to investigate the heat dilatation, rotation and pipe temperature impact. The two PT1000 are permanent measurement equipment for the REPA life cycle test.

3 Simulation – ROHR2

3.1 Setup of the model

Before the traverse pipe section was installed at the kinematic unit, it could be considered as a separate pipe system in order to understand the influence of varying pressure and temperature on the dynamometer in this section of the test rig. As described in **Eq.2.2 -2.4,** it is indispensable to understand the forces and moments, which result from the thermal expansion of the traverse pipe section. The Rohr2-model was developed with the aim to simulate the reacting forces and moments on the dynamometer at specific operation conditions. For this thesis the dilatation of the pipe section was simulated for different temperatures and pressures with the integrated expansion joint design. The simulation software ROHR2 of *Sigma Ingenieurgesellschaft* is used to determine the static behavior of the traverse pipe section. Despite of the expansion joints, small bearing reactions cannot be eliminated completely. The model simulation has been executed for many different HTF temperatures and pressures and these conditions can be defined as load cases. Those represent typical operation conditions of a PTC power plant, simulated with the traverse pipe section for different types of HTFs. Furthermore, the medium in the pipe can be represented by the use of the specific density based on data tables for each temperature. The influence of the mass flow cannot be implemented in the model.

During the development and installation of the complete test rig, different ROHR2-model versions have been generated to simulate the traverse behavior for the specific requirements in each construction phase. Four versions were the results until the commissioning started. A summarized overview of every model is depicted in **Table 3**. The first one, *Traverse_40*, represents the traverse pipe section in dimensions and geometry as planned. Later, a thermal insulation has been added. The underlying model for the validation experiment with the separate traverse was *Traverse_999,* created without insulation in order to have a better comparability with the used setup. This model has been improved with realistic dimensions by use of the photogrammetry measurements and changes in the initial compensator design. The outputs are the models *Traverse_100* without insulation and *Traverse_200* with insulation for the later test rig operation. *Traverse_100* was the final compared model used in the past measurement experiment [2].

Table 3: ROHR2 base model overview [2]

Base model	Geometry	Insulation	Compensators	Purpose
Traverse_40	planned dimensions	as planned	none	inital model
Traverse_999	planned dimensions	none	none	inital model
Traverse_100	photogrammetry	none	updated values	validation exp.
Traverse_200	photogrammetry	as built	updated values	test rig operation

In order to compare the results from tests without REPAs and with air as HTF, the ROHR2-model is needed. The heat dilatation impact and the impact of different pipe temperatures on the rotation movements must be compared with this model. These specific conditions can be simulated and illustrated.

The ROHR2-model does not allow dynamic modelling, thus the traverse tube model is executed in several rotation positions, varying temperatures and pressures. With these results, an interpolation for intermediate angle steps has been done to fill the missing steps. A data base with 60 load cases represents the reactions in every degree step for a full rotation. These sub-models contain five different pressure points for each of twelve different temperatures. Databases for more fluids can be added by defining a reference load case with a maximum stress scenario for the highest values for ϑ_{HTF}, p_{HTF} and density [19]. To calculate the forces and moments at the dynamometer bearing, the **equation 2.6** is used and the input of the simulated load cases. A "Matlab" program offsets the ROHR2 results to create plots and make the evaluation comparable. This routine is currently defined for the HTF Helisol© and for air. By the use of linear interpolation, each combination of pressure, temperature and density is possible to obtain the required results.

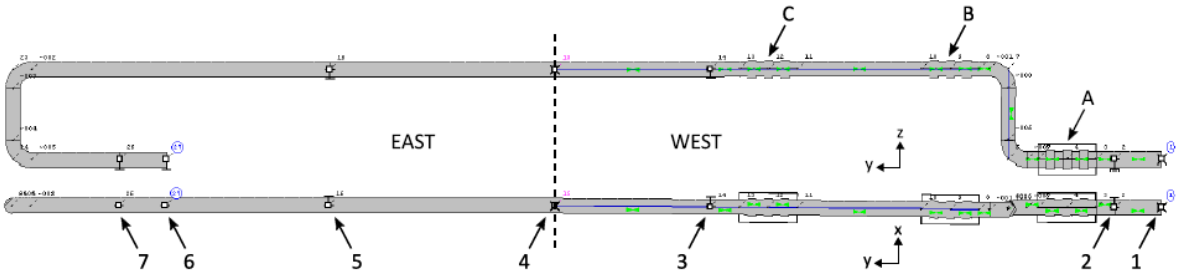

Figure 20: Side and top view of the traverse pipe section in ROHR2 as simulated with the model *traverse_100*. B and C are single hinged compensators and A is gimbal hinged. 1 and 4 are fixed bearings and 2,3,5,6,7 are floating bearings [19].

Figure 20 shows the *Traverse_100* model in ROHR2 and indicates where compensators and bearings are located. Only the west part of the pipe has a direct impact on the installed dynamometer, because of to the fixed bearing (number four) in the middle of the traverse. Heat dilatation just appears to the west or east direction starting from the separation line in the center, so each side can be regarded separately. Bearing one is the second fixed bearing before the REPA. Two single and one gimbal hinged angular expansion joints compensate the thermal expansion between these rigid points. These compensators work as springs, which stay in a neutral position if no force or torque is introduced.

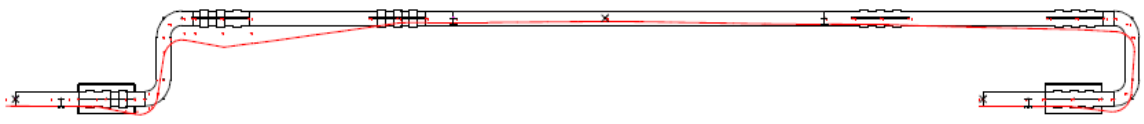

Figure 21: Profile of the traverse pipe section with superimposed bending line under pre-tensioning conditions. The red line shows the pipe position in cold conditions [20].

To reach a neutral position of the pipe section at a design point of 350 °C, different pre-tensioning condition for the compensators are necessary. In order to reach this, the pipe sections have been reduced by the length of the thermal heat dilation for each part. The resulting pipe line is clarified in **Figure 21** by the help of the red line. One effect is that the expansion joints are deflected at cold conditions.

The ROHR2-model is designed with the consideration that the pipe temperatures in a PTC power plant loop differ between 300 - 400 °C. The inlet temperature can be set to 300 °C by using Therminol VP-1 at the collector pipe inlet. After passing through the absorber tube, a temperature of 400 °C is reached. The design point here is 350 °C in order to represent a mean temperature in the middle of the absorber tube. Pressure losses occur during the passing of this part of the loop, because of friction to the pipe walls. Based on the rising temperature, a decrease of the HTF density is the result [19].

3.2 Model results

This sub-chapter comprises the main plot results and statements of the ROHR2-model simulation for the assessment of the tests without REPAs and air as HTF. The *Traverse_200* model is used, because the older ones are not representative anymore for the installed traverse. Also, the insulation and real installation dimensions measured by photogrammetry are considered in this type of simulation model.

Previous investigations have proven that the expansion joints in the pipe section work as assumed. The heat dilatation can be compensated partially. Small deviations are detected during the first traverse test with ‘open’ pipe section. The design point has not been reached completely, but just an average pipe temperature of around 320 - 340 °C [2].

The simulation of the*Traverse_200* model in view of the rotation angle response, is done for air and Helisol© with the same pressure and temperature for each medium. The gravity influence is nearly the same in each case by a pressure of 1 bar. In conclusion, the weight impact of the HTF is nearly negligible in this special case.

As shown in **Figure 22,** forces and moments have a nearly symmetrical course considered from the zero degree position of the traverse. This has been expected, because the traverse moves symmetrical apart from minimum tolerances. The set temperature of the model has direct influence on the Fy and Fz forces only, the Fx component is unaffected. Mz is unaffected by the temperature as well. However, Mx shows a significant deviation and My differs less. The force Fy deceases by the rising temperature to 400 °C. A reason for this is the pre-tension of the pipe section in cold condition. By reaching the design point of the traverse, the force in y-direction decreases as shown in **Figure 21**.

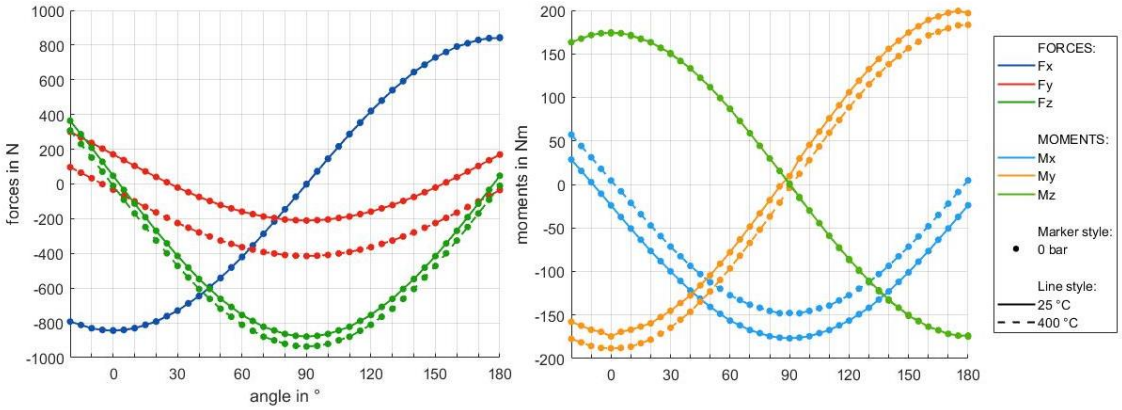

Figure 22: ROHR2 plot for the *Traverse_200* model, forces and moments over the rotation angle at two different HTF temperatures. Left: forces over rotation angle, Right: moments over rotation angle. Heat transfer medium is air; in this case the pressure is set to 1 bar.

As represented in **Figure 23,** Fz represents the direct weight force of the pipe section. A positive value for Fz is depicted in stow position (φ = -20°) of the traverse. This value is a result of the overextended traverse position. The weight force of the pipe pulls the sensor head in a positive Fz direction and in a negative Fx direction. The highest weight is pressing on the sensor by an angle of φ = 90° with a negative Fz force as consequence. Fx is influenced by the weight force as well. As expected this force becomes zero in top position and has a negative maximum in stow and positive maximum in end position. Mz has the same course as Fx, this is caused by the curved pipe section, which reacts as lever to Fx. This moment has the opposite positive value in the φ = 180° position. Mx behaves proportional to Fy.

Figure 23: Picture of the kinematic unit and the traverse pipe section in stow position with force directions as measured by the dynamometer.

In conclusion, the forces and moments Fx, Fy, Mx, My are affected by a rising temperature taking into account the rotation movement.

The following **Figure 24** shows the temperature response separately for the forces and moments at a rotation angle of φ = -20°. This angle equals the stow position of the real traverse at the REPA test rig and the result is later used as a reference. As expected, the same forces and moments Fx, Fy, Mx, My, as shown in **Figure 22,** have a direct temperature influence on the *Traverse_200* model.

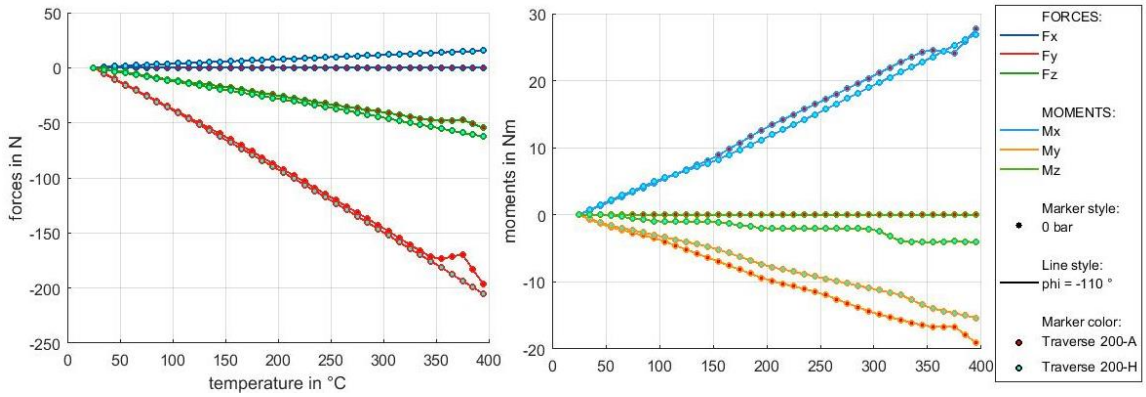

Figure 24: ROHR2 plot for the *Traverse_200* model, forces and moments over ϑ_{HTF}. Heat transfer medium is air, in this case the pressure is set to 1 bar. Left: forces over HTF temperature, Right: moments over HTF temperature.

The heat transfer medium has an impact on the forces at ambient pressure. Notable is the changing line of Fy and Fz by 350 °C for air. The graphs for Helisol© has a linear course of forces.

4 Presentation and evaluation of measurement results

This chapter contains the summarized measurement results of both tests which include the two measurement setups. One is constructed with **installed REPAs and HELISOL© 5A as HTF** and one **without REPAs and air as HTF**. The evaluation is done with the focus on the specific expectations and impacts of each test as formulated in chapter 2.2 and 2.3. The results from the tests during the commissioning of the complete test rig are those with **installed REPAs and HELISOL© 5A as HTF**. The evaluation of the first results from this tests has to be considered as an overview of the total reactions on REPAs. A distinction of forces and moments from the traverse and REPAs reacting on the sensor is not possible at this point of time in the investigation.

The test results from the setup **without REPAs and air as HTF** provide the necessary information to differentiate between the forces and moments from the traverse and REPA. Thereby, the forces and moments resulting from the traverse are determined by the evaluation of these outcomes.

In order to understand the composition of the results from both tests, the measurement execution is described.

4.1 Measurement execution

4.1.1 Measurement execution with installed REPAs and HELISOL© 5A as HTF

The tests with installed REPAs have been done during the commissioning of the REPA test rig. This temporal sequence of both tests (first: test with installed REPAs and HELISOL© 5A as HTF, second: test without REPAs and air as HTF**)** is based on the fact, that the installed REPAs have an operation temperature of 400 °C. The test facility is designed for ϑ_{HTF} = 450 °C during operation. Therefore, the REPAs have to be replaced to fulfill the planed operation temperatures of 450 °C after the first test until 400 °C.

One important point in this research is that the performance of the tests for both measurement setups is reproducible. To fulfill this requirement, a test procedure has been used for the rotation and translation movements for the defined temperatures from 200 °C until 400 °C. The temperature points are 200, 250, 300, 325, 350, 375 and 400 °C. They represent typical HTF temperatures of loops in PTC power plants during operation.

Table 4 contains the first six operation steps of the test procedure for the investigation of the rotation and translation motion impact on the dynamometer. The following sequence is executed in order to approximate a typical operation or cycle of a PTC. The approximation consists in a continuous motion, whereas the real collector moves in steps of φ = -20° until φ = 180° and then goes back to the initial position. These steps representing typical tracking motions of a PTC from the stow position to the end position

and back during an operation day. After one rotation motion, a movement in translation position from ϑ = 2° (hot position) until ϑ = 22,2° (cold position) and back to the initial position is executed to simulate the daily expansion of a real absorber tube.

Table 4: Test procedure for measurement setup with REPAs for one HTF temperature point

Step	Operation task	Rotation angle	Translation angle
1	Traverse in rotation stow position	φ = -20°	ϑ = 2°
2	Traverse in translation hot position	φ = -20°	ϑ = 2°
3	Traverse in rotation end position	φ = 180°	ϑ = 2°
4	Traverse in rotation stow position	φ = -20°	ϑ = 2°
5	Traverse in translation cold position	φ = -20°	ϑ = 22,2°
6	Traverse in translation hot position	φ = -20°	ϑ = 2°

At first, the traverse has to be moved in the initial position. That is performed with the steps one and two. The rotation and translation movements of the traverse are done by following steps 3-6. The last four positions are repeated with different temperatures until 400 °C.

4.1.2 Measurement execution without REPAs and air as HTF

After the commissioning and the first test with HELISOL© 5A, the next measurement setup has been installed as described in **chapter 2.3** without REPAs and air as HTF to measure the forces and moments reacting on the dynamometer generated by the traverse pipe section.

The test procedure for the investigation of the rotation impact is shown in **Table 5** for one single temperature point. The measurement points here are 200, 250, 300, 325, 350, 375 and 400 °C like in the test before. The main difference for the rotation motion is that the traverse has to be moved back from the heater (ϑ = 4°) to start with the rotation movement. A separation of the flange connection is needed otherwise the pipe ends would impede the rotation movement, because of overlaying flange surfaces (at ϑ = 2°). Due to the fact of the missing REPAs, the translation movement has a negligible influence on the dynamometer measurement and was not further investigated. The translation motion only serves as a closing movement in this kind of measurement setup.

Table 5: Test procedure for measurement setup without REPAs for one temperature step

Step	Operation task	Rotation angle	Translation angle
1	Traverse in rotation stow position	φ = -20°	ϑ = 2°
2	Traverse in translation hot position	φ = -20°	ϑ = 2°
3	Traverse in rotation end position	φ = -20°	ϑ = 4°
4	Traverse in rotation stow position	φ = 180°	ϑ = 4°
5	Traverse in translation cold position	φ = -20°	ϑ = 4°
6	Traverse in translation hot position	φ = -20°	ϑ = 2°

For the investigation of the heat dilatation impact, the traverse piping was heated up to 400 °C and was cooled down by the help of the blower in order to accelerate the cooling process until ambient pipe temperature.

4.2 Test results with installed REPAs and HELISOL© 5A as HTF

4.2.1 Rotation movement impact

After moving the REPAs and the traverse at different temperature points from 200 °C until 400 °C with the same procedure, the first conclusion is, that forces and moments have the same graphs apart from small deviations.

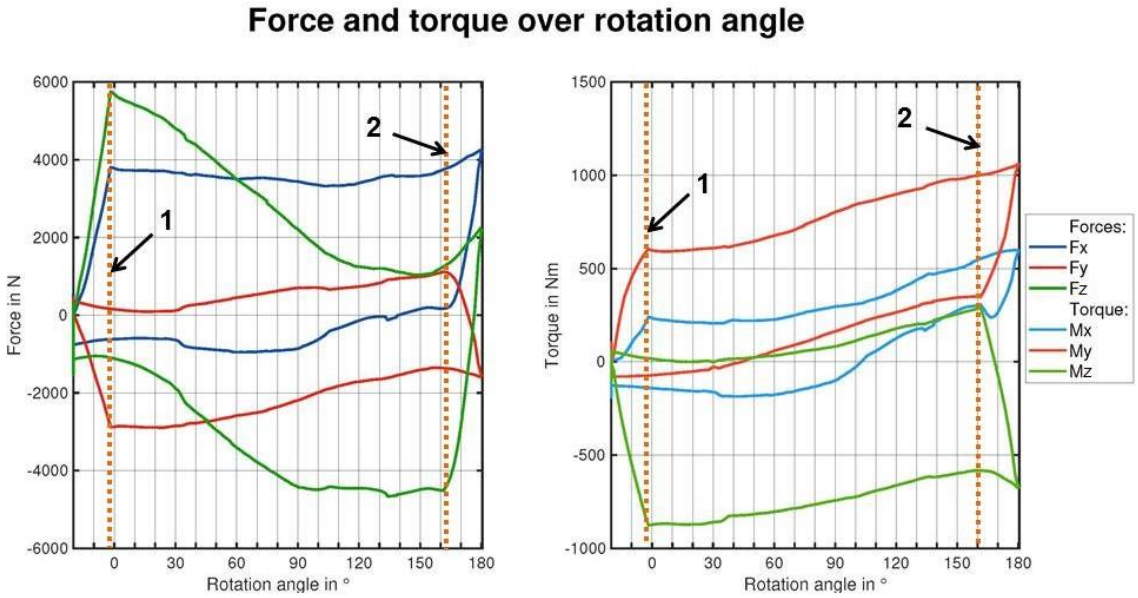

Figure 25: Forces and moments for a full rotation movement by ϑ_{HTF} = 200 °C and p_{HTF} = 16 bar

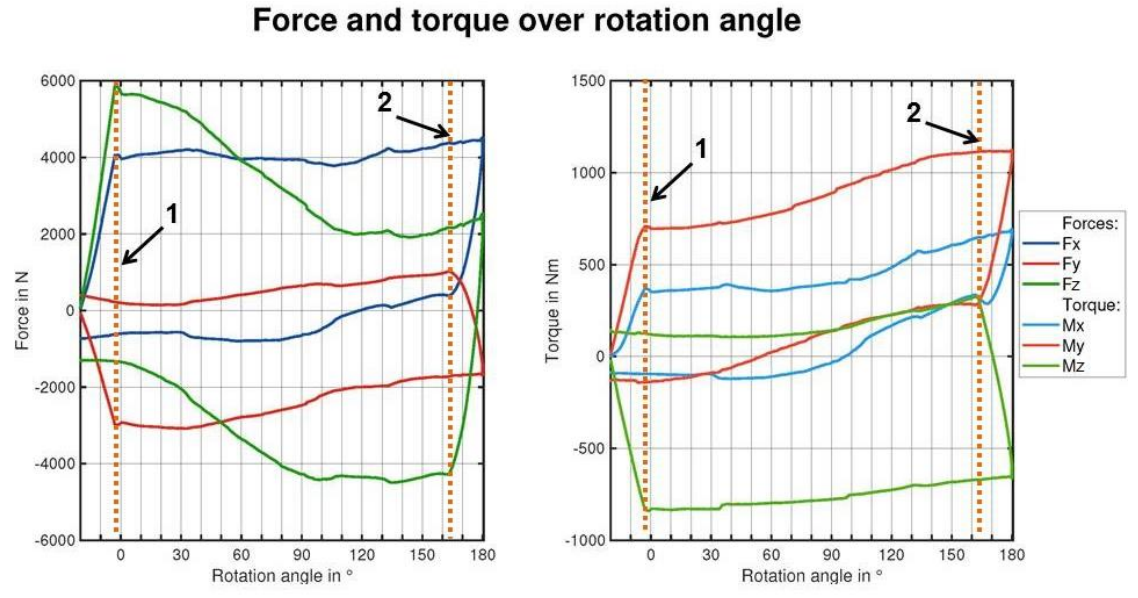

Figure 26: Forces and moments for a full rotation movement by ϑ_{HTF} = 400 °C and p_{HTF} = 19 bar

The rotation and translation movements generate the same sequences as expected. **Figure 25** and **Figure 26** show the specific course of moments and forces during a full rotation movement by two different temperatures. The temperature influence has been removed by offset compensation of the dynamometer in order to make the plots comparable.

One important result is that different HTF temperatures have no visible influence on the courses of forces and moments. That means that the traverse and the REPAs move without influencing friction caused by heat dilatation. Critical components for example, are swivel joints and bearings which could cause friction and unexpected forces and moments. On the other hand, the torque sword works against this impact by inducing a rotation movement to the REPAs. By considering the measurements limit of 10 kN/ 1 kNm the moment My is above the manufacture specifications. The temperature influence on the end values is not included by these two different plots. The real range can be expected with higher end values for moments and forces. This means a dynamometer with a bigger measurement range is necessary to detect all resulting forces from the REPA.

Noticeable is the increase of Fx, Fy and Fz at the beginning (marked as line **1** in both pictures) of the movement. This effect occurs again after moving the traverse from the end position (φ = 180°) to the stow position (φ = -20°) in opposite direction as a decrease of all forces. This specific course of the forces is caused by the weight force of the hose. Another reason is space in the tracking for the bottom part of the REPA. The rotation movement of the kinematic unit is transmitted by the torque sword and the swivel joint to the flex hose. More in detail, a tapped transmits the torque to a rod which is connected to the REPA. The connection between tapped and rod is not directly linked. This results in deviations of the angles at the top and bottom of the REPA. The REPA swivel joint follows the traverse staggered at the beginning of the movement until the weight of the REPA is in motion.

The rotation movement has an effect on Fz, after the high peak (marked as line **2** in both pictures). At the beginning, the graph declines rapidly until the end position (φ = 180°). This can be explained by the changing weight force of the mounted pipe section. For example, in a vertical position at 90° for the scale in **Figure 25** and **Figure 26,** the weight of the complete pipe results on the sensor head and this leads to an opposite negative Fz force, this minimizes the Fz value significant. The force directions measured by the sensor are shown in **Figure 23**. By driving the traverse from the end position (φ = 180°) to the stow position (φ = -20°), the opposite effect occurs. The angle deviation between traverse and sword leads to high negative values for all forces at the beginning of the movement. After passing the vertical position at 90° back to the stow position (φ = -20°), the weight impact on the sensor is reduced and this leads to less negative value for Fz.

Fx is primary influenced by the lateral weight force of the pipe section. The course of this force has a slightly change by moving the traverse from the end position (φ = 180°) to the stow position (φ = -20°). In this case the weight force is changing Fx from a positive direction to a negative direction as expected. As a result, the value for Fx decreases from the end position (φ = 180°) back to the stow position (φ = -20°), because of the sidewise force Fg on each side.

Reactions of the system along the longitudinal axis are detected as Fy. Apart from the influence of the breakaway torque as described before, small changes in the course arise in a full rotation cycle. Possible reasons here are small deviations of the translation position during a rotation movement. A reason for this could be air in the hydraulic fluid of the translation cylinders. Minimal lateral movements of the traverse are visible during a full rotation. Furthermore, the weight force has a minimal influence on the Fy force.

By inclusion of all forces and moments from stow position (φ = -20°) to end position (φ = 180°) and the movement back to the initial position, a nearly symmetrical course is illustrated.

A breakaway torque leads to the highest increase or decrease of the forces at the beginning of each sub-movement (lines 1 and 2 in **Figure 25** and **Figure 26**). The forces Fy and Fx depend on the changing weight force of the REPAs and the installed pipe section in the traverse. The largest moments react as My and Mz and these are based on the weight of the west REPA. The lever for the toque here is the small pipe section behind the dynamometer support with the fixed bearing. Impacts such as the deviations in the tracking of the REPA and the changing weight force of the flexible hose by a rotation attack here at the end of the west traverse pipe. A detailed insight of the installation position of the west REPA is depicted in **Figure 16**. Mz and My can be reduced by minimizing their lever. One opportunity is to decrease the length of the pipe section between the fixed bearing and the REPA connection. Another opportunity is to locate the fixed bearing of the pipe support closer to the REPA connection.

4.2.2 Translation movement impact

In order to understand all reactions in a REPA life cycle, it is also necessary to have a detailed look on the translation movement impact, which represents the heat dilatation of the absorber tube**. Figure 27** shows a section of the procedure for the translation movement directly after a rotation movement by ϑ_{HTF} = 400 °C and a constant pressure of p_{HTF} = 19 bar. A general difference to **Figure 25** and **Figure 26** is that the course of forces and moments did not start at nearly zero, because no offset compensation has been done between rotation and translation movements. In this plot both measured values are ending near the zero line. Apart from that, the translation movements have been done by different temperatures (250 °C until 400 °C) combined with the rotation movement. The course by different temperature points is nearly the same like in the

results of the rotation respond. Mechanical influences, which have an influence on the dynamometer, did not increase during a heating up of the HTF.

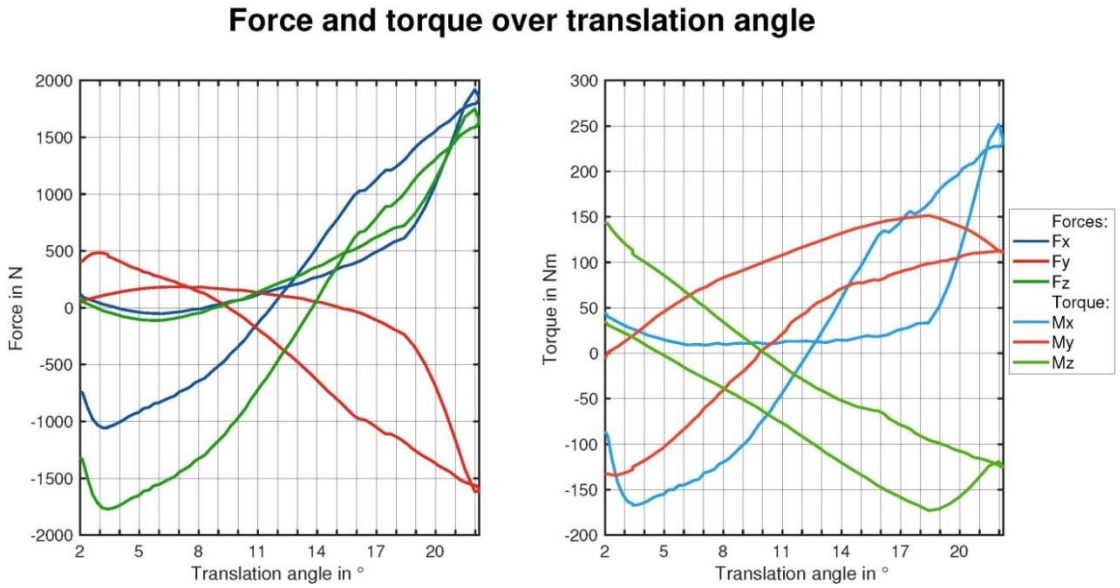

Figure 27 Forces and moments over a full translation movement during test procedure by ϑ_{HTF} = 400 °C and p_{HTF} = 19 bar

By moving the traverse from the hot position (ϑ_{HOT} = 2°) to the cold position (ϑ_{COLD} = 22°) and back to the initial position, a significant change in the course of forces and moments can be recognized. Fy decreases to a negative value, while the movement is done in the opposite direction. The weight of the REPAs generates a negative Fy counterforce contrary to the direction of motion. By moving the traverse in the cold position (ϑ_{COLD} = 22°), a positive force in Fx and Fz direction can be determined in every translation movement. By a movement in initial position, Fx and Fz decrease back to nearly zero. These two forces correlate with inertia and the weight of the flexible hose. The hose in the REPA (west position) is stretched by a movement in ϑ_{COLD} = 22° and compressed by ϑ_{HOT} = 2°. The opposite effect must occur at the REPA in the east position by later test. The measurement with a second dynamometer in the west position must show the contrary course of Fz, Fy and probably in Fx direction. The flexibility of the hose has relevant influence on the forces and the resulting moments. The interaction of both REPAs to the traverse and to the dynamometer has a possible impact to the measurement. Finally, only a fraction of the measurement range has been used to detect the moments and forces during the investigation of the translation respond. In order to know more about the origin of the moments, single tests for separate translation movements have to be repeated.

4.2.3 Volume flow impact by rotation and translation movements

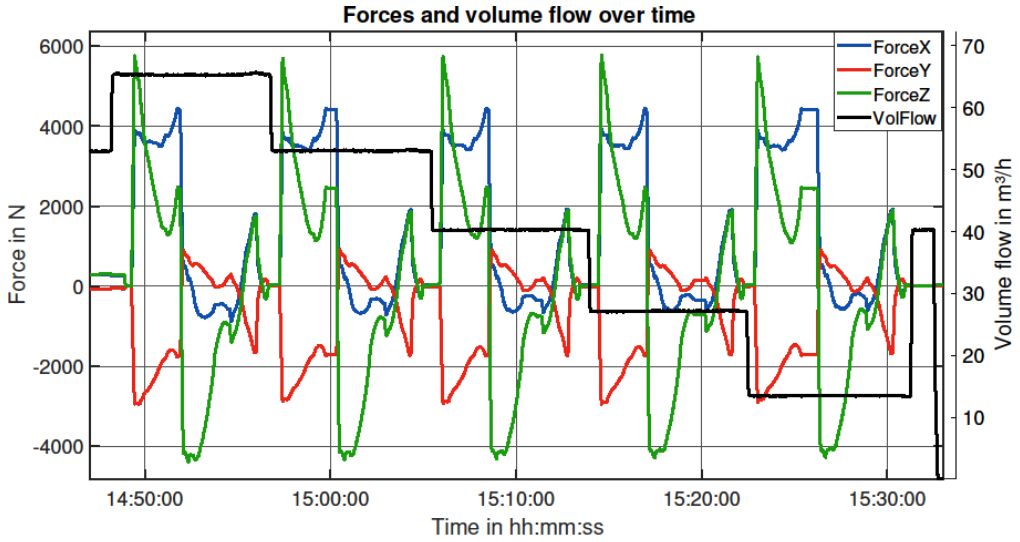

Figure 28: Forces for rotation and translation movement by different volume flows at ϑ_{HTF}= 300 °C and p_{HTF} = 17 bar

In **Figure 28** five rotation and translation movements have been measured by varying volume flow at a nearly constant pressure and oil temperature. The movements are done one after another by single steps in the test procedure shown as it is shown in **Table 4**. The volume flow has been reduced by 20% for each rotation and translation movement. Not every motion cycle has exactly the same course, but the value peaks are nearly the same. The most visible deviations come from manual controlling of every action. Time lags between each step lead to a cut-off of single graphs. No offset compensation has been done between these five cycles. One important result is that the impact of the volume flow on forces during rotation and translation movements is approaching zero.

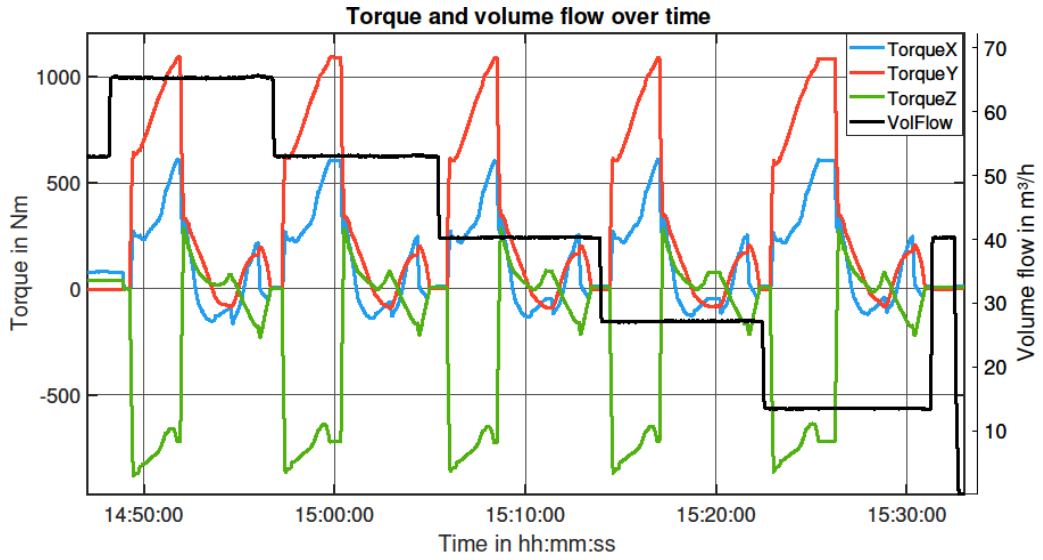

Figure 29: Moments for rotation and translation movement by different volume flows at ϑ_{HTF}= 300 °C and p_{HTF} = 17 bar

The course of moments in **Figure 29** indicates the similar value peaks for each cycle at the different volume flows. The same procedure has been used as for **Figure 28** to generate this plot. Again, the influence of the volume flow has a low impact on the course on the torque during rotation and translation motions. Another observation by this plot is that every rotation movement has one positive peak for the y torque, which exceeds the construction limits of the dynamometer of 1 kNm.

4.2.4 Dynamometer reliability and measurement range

In order to examine the correct function of the dynamometer and the influence of measurement uncertainties, different sub-tests have been made. First of all, single rotation and translation movements with cold HTF has been proceeded to get an understanding of the reactions on the dynamometer. Broken data cables and defect connectors lead to wrong measurements or bigger uncertainties. These reasons should be excluded before the life cycle tests start in full extent. The directions of forces and moments have been proofed manually by pushing the pipe section in the corresponding direction in order to check the resulting values on the display. One issue for the complete test was the already installed dynamometer. Doing separate test for example with precisely defined weights in order to have a comparative value for the displayed values was not possible. Ideal conditions would have been an unloaded sensor before every measurement. That was not the case for both tests. The sensor has preloads in every initial position, which originate from the screwing with the traverse structure and also from the position in relation to the gravity force. These preloads have been removed temporarily by a manual offset compensation before every movement. The next specific behavior of the sensor was a settling time after switching on the amplifier. These effects have to be taken in to account before recording a measurement. In **Figure 30** a long-term test is depicted in order to have an impression of the sensor drift after starting the measurement. The peak values of forces and moments correspond to nearly 2% of the measurement range. But a decrease of the ambient temperature happened during the measured time and this has a clear impact on the measured values. In conclusion, the drift generates a not negligible uncertainty on the end values of each measurement.

After a series of attempts of rotation and translation movements by different system parameters, the dynamometer worked reliable. The impact of the settling time can be minimized and the influence of the sensor drift has to be taken into account by a measurement uncertainty calculation for the measurements. But in general, the dynamometer is suitable for the planned application. A potential issue is the measurement range of the dynamometer. The range for moment measurements is widely exhausted or even exceeded. Probably the measured values for forces and moments will increase for tests with a complete consideration of the temperature influence up to ϑ_{HTF}= 450 °C and under higher pressure. One possibility is to install a K6D175 dynamometer with a larger measurement range. The manufacture ME

Messsysteme offers the sensor with a bigger measurement range of 20 kN/ 2 kNm, but with the same sensor design dimensions.

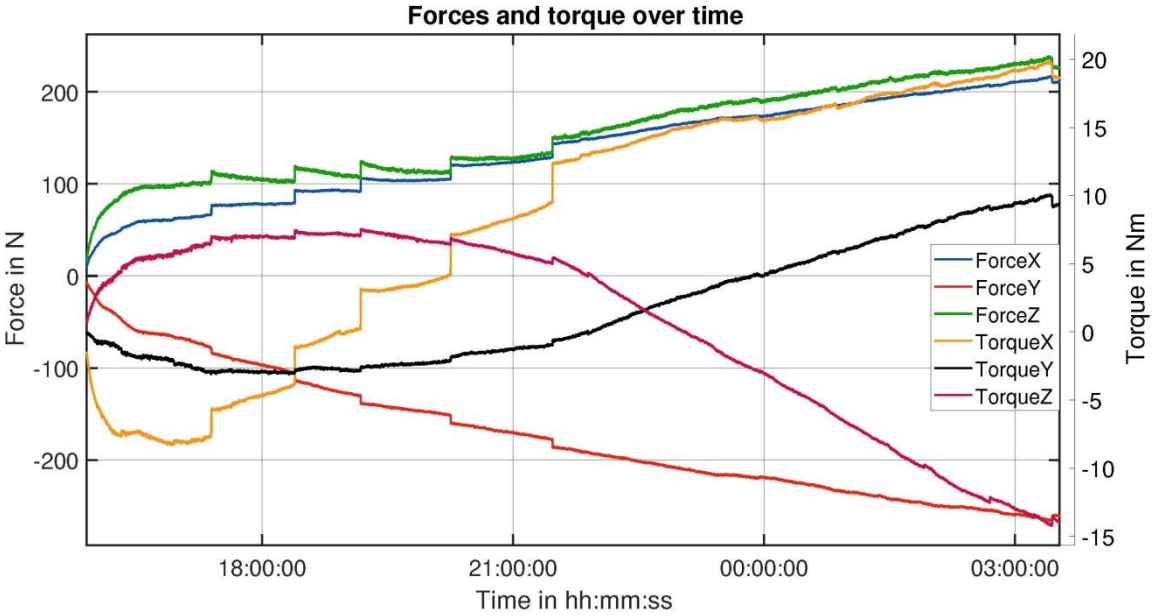

Figure 30: Sensor drift measurement of forces and moments as long-term test

More information about the different sensor variants are in **Appendix 7.4**. One big advantage is that a simple replacement of the sensor and the same amplifier and software that were used before is possible. This larger range will cause measurement uncertainties because just a minimum of the range for the forces will be used after replacing the sensor. The sensor is then oversized for both forces and moments. It is definitely necessary to measure every resulting force and moment. The dynamometer in the top-east and top-west position in the traverse will measure in the same dimension apart from small deviations. But the two dynamometers under the swivel joint of each REPA are unknown for the dimensions of forces and moments. If the currently installed sensor has a sufficient measurement range (10 kN/1 kNm) a dynamometer with a bigger range (20 kN/ 2 kNm) can be installed under the position of the swivel joint. It is advantageous to have a second senor with a bigger measurement range for the commissioning of the dynamometer in the bottom-east and bottom-west position. The problem with the inappropriate measurement range could appear by the measurements of both bottom dynamometers. Another possibility to prevent an overload of the moments resulting on the dynamometer is to reduce the pipe length after the fixed bearing of the sensor support until the REPA connection (**Figure 16**). By shorten the lever of the acting forces a decrease of the moments can be expected and the installed dynamometer works in the measurement range of 10 kN/1 kNm. But after installing new REPAs for ϑ_{HTF}= 450 °C in later test a change of every end value will be the result. A new test is necessary with the prospective REPAs to make a clear decision for the right measurement range of the sensors.

4.3 Test results without REPAs and air as HTF

4.3.1 Heat dilatation impact

In order to evaluate the life cycle tests for REPAs under operating conditions of a PTC power plant it is necessary to know the influence of the traverse pipe section on the dynamometer under different conditions. Therefore many attempts have been made to understand the reacting forces and moments by heating up the pipe section. One problem here was the flange connection during the heat up process. Both pipe sections with the flanges expend strongly to each other because of the heater temperatures up to 550 °C. Both flanges surfaces press against each other after a short time of heating. This leads to additional forces and moments measured by the dynamometer. An open connection of heater and traverse was necessary to minimize the interfering influence. The gap between the two components leads to high temperature losses and a longer heating period.

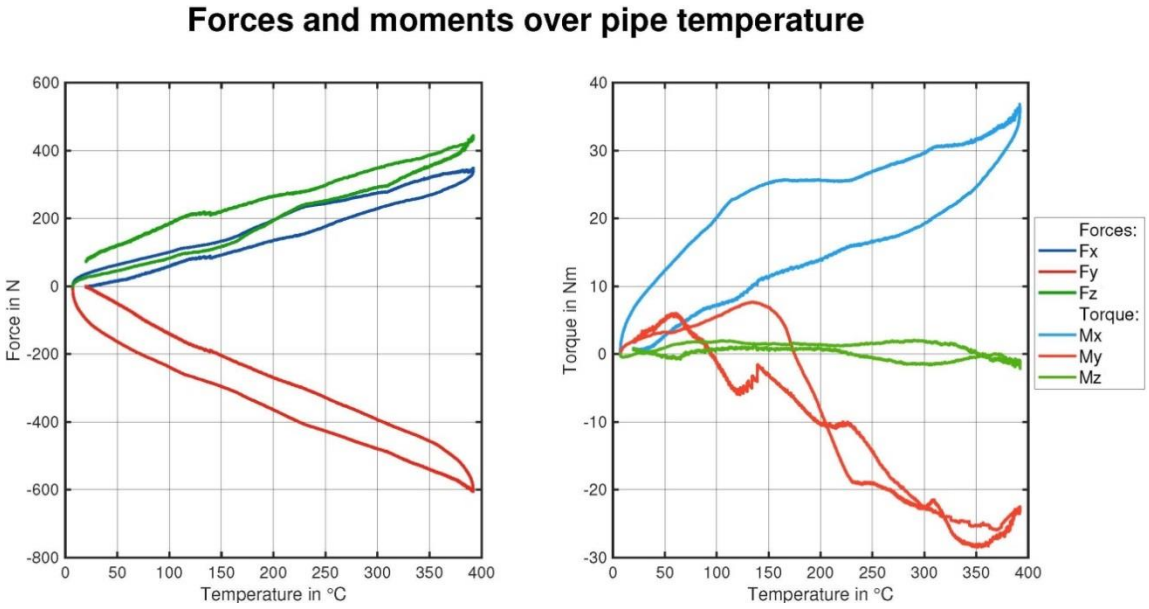

Figure 31: Forces and moments over mean pipe temperature during heat dilatation investigation

After avoidance of any flange contact till heating up the pipe section until 400 °C, the forces have a nearly smooth course as shown in **Figure 31.** In this figure, Fy is the biggest indicator for the correct function of the expansion joints. The heat dilatation leads to a negative Fy force, because the pipe section in the traverse expands from the central fixed bearing in the direction of the dynamometer. The location of bearings and compensators is depicted in **Figure 20** and the bending line of the traverse pipe section during heat dilatation with resulting forces in **Figure 32.** Fx and Fz are rising up very similar. The heat dilatation is also pushing the pipe section, which is mounted on the pipe support on top of the dynamometer head, away from the installed sensor housing (as force Fz shows). This is a reaction of the single hinged compensators during heat

expansion compensation. While a positive Fz force is the immediate reaction a positive force Fx is a side effect of the gimbal hinged compensator.

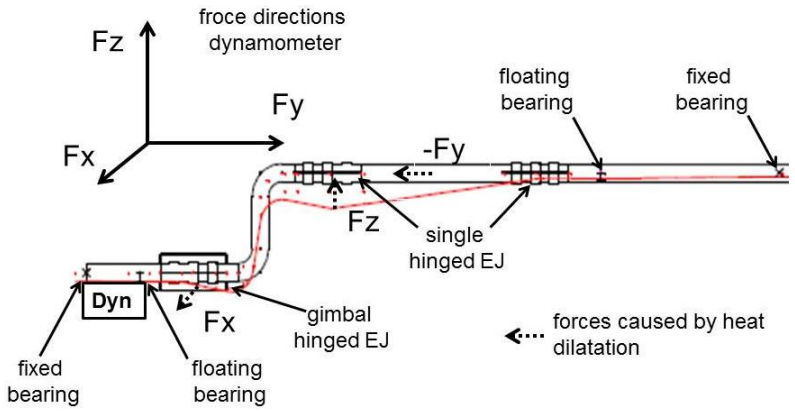

Figure 32: Extract of the traverse pipe section with direction of forces from heat dilatation measured by the dynamometer

It is noticeable, that only Mx and My are showing a bigger effect on the rising temperature of the pipe. The course of My is strongly fluctuating and a possible reason for this are the changing heater levels during operation. Fast temperature changes of the heater lead to a respond of My. Mx has comparatively smooth course and is resulting from the compensation in Fz direction. In conclusion, the forces have an influence on the dynamometer by heating up the pipe section until 400 °C. The compensation is not canceling out the forces and moments from the heat dilatation. The end values are too high to ignore them in the contemplation of the forces and moments resulting on the REPAs. They have to be considered as $F_{traverse}$ in the calculation **Eq. 2.4.**

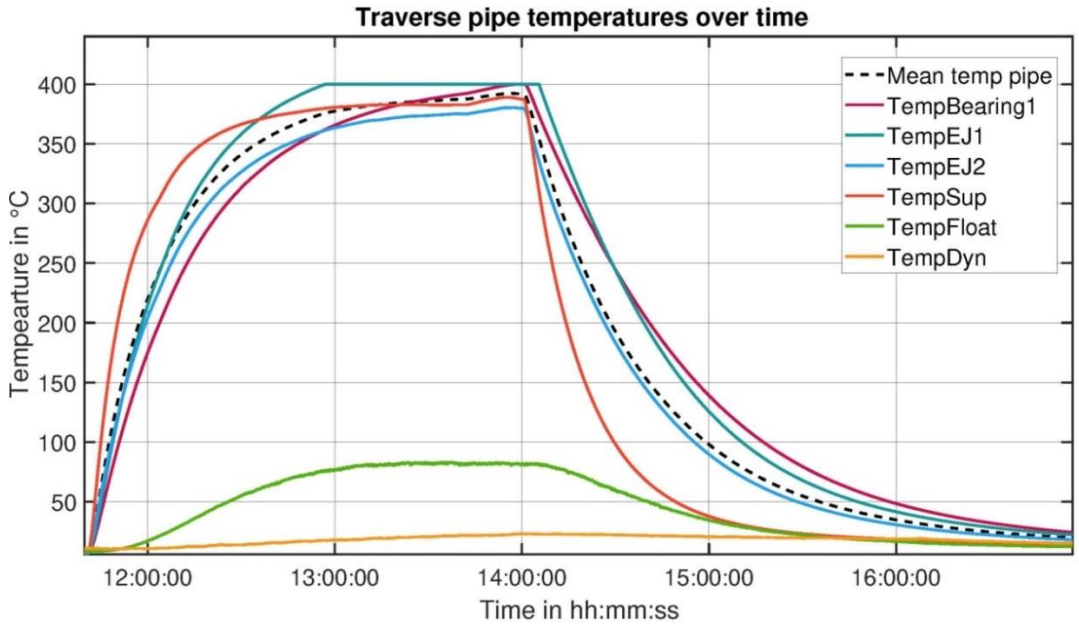

Figure 33: Traverse pipe temperatures during heat up and cool down phase of the section

Figure 33 shows the heat up process for the measurement results in **Figure 31**. The position of the installed temperature sensors starts from the central bearing in the middle of the traverse pipe section until the dynamometer pipe support. The detailed positions are shown in **Figure 19**. The four temperatures were measured by PT100 (TempBearing1, TempEJ1, TempEJ2, TempSup) form the average temperature of the pipe. During operation of the measurement setup different temperatures have been measured by a constant temperature of the heater. The measurement results show an unexpected order of the measured temperatures. Expected was an order of the sensors in correlation of the particular distance of the PT100 from the heat source. For example, the sensor TempBearing1 has the largest distance to the heater, but has measured the second hottest temperature during the heat up process. Because of bigger heat losses, this sensor should normally measure the highest temperature. Reasons for these deviations are different installation positions of the sensors and irregularities of the pipe insulation in these sections. The sensors are installed on the pipe surface and under the pipe insulation. Sections with less insulation lead to a faster heat transport to the environment and also a lower measured temperature. The cooling of the dynamometer works effective during the complete measurement, because the dynamometer temperature (TempDyn) is increasing negligible in contrast to the temperature measured at the floating bearing (TempFloat). An additional measurement has been done in **Appendix 7.5** with the focus on the permanent installed thermometers PT1000 in order to check the effectiveness of the installed fan for sensor cooling.

4.3.2 Rotation movement impact

In order to measure a reliable data set for the investigation of the rotation movement impact on forces and moments several tests have been done with the same test procedure (as described in chapter 4.1.2) to have a reliable data set for the evaluation. One test included seven rotation movements at seven different temperature points (200 °C – 400 °C). These single tests have been compared and the best results with a minimum of additional influences and deviations are presented in the evaluation. One single rotation movement is shown in **Figure 34** for ϑ_{Pipe} = 400 °C to represent the typical course of forces and moments resulting from the traverse pipe section without REPAs. Conspicuously are the deviations of each single force and moment for the movement in total from φ = -20° to φ = 180° and back. Expected was an idealistic course with the same graphs of the two partial movements {φ = -20° to φ = 180° and φ = 180° to φ = -20°) for each moment and force. That is not the case in this figure. Every measured graph of every measured output has deviations by a full motion of the traverse. One of the decisive uncertainties is the decreasing temperature after disconnecting the traverse pipe section from the heat source. The temperature losses are significant for one rotation movement at a specific temperature point. The heat losses are nearly as calculated in the heat loss estimation (**Appendix 7.2**). A full rotation takes an average of 5 minutes and leads to a drop in temperature of around

10 K per full rotation. Other impacts are the measurement uncertainties from the sensor itself. Fz is strongly affected by the rotation movement and shows the most impact of the weight force resulting from the traverse pipe section. A changing Fx force is also related to the weight transfer of the mounted pipe by rotating the traverse. Fx and Fy show nearly the same course, but transposed.

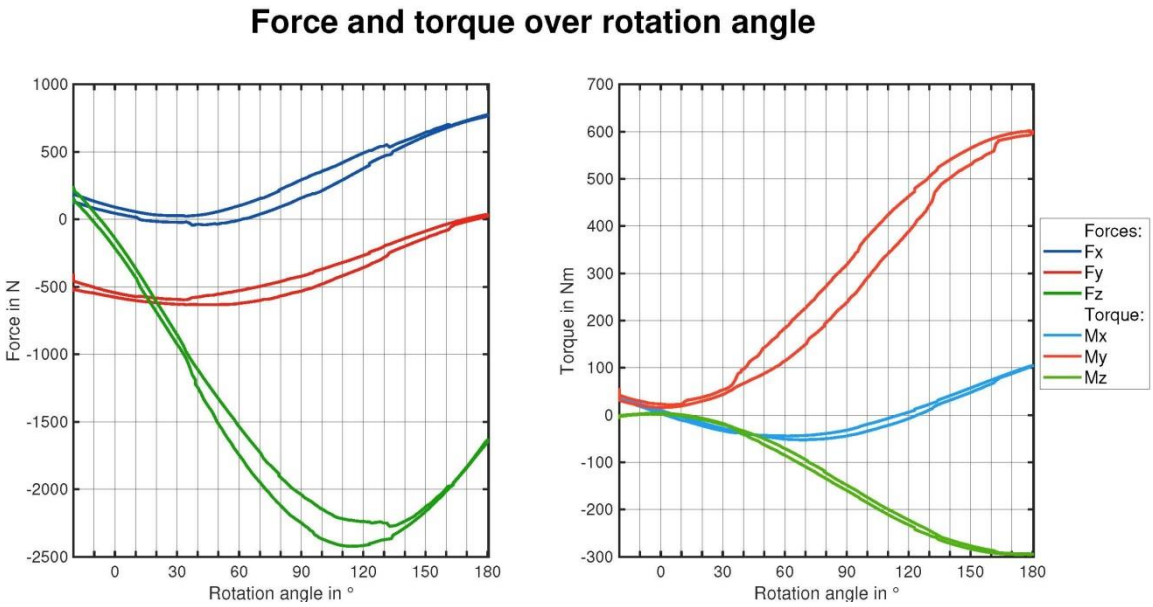

Figure 34: Rotation movement of the traverse without REPAs and air as HTF for ϑ_{Pipe} = 400 °C

4.3.3 Pipe temperature impact on rotation movements

All rotation movements shown in **Figure 35** and **Figure 36** are the result of one single measurement with one offset-compensation at the beginning. That means the temperature impact is measured during the complete operation time. The impact of the rising pipe temperature on the forces measured during rotation movements is slightly visible in the plot (**Figure 35)**. By comparing **Figure 35** with **Figure 31,** similarities in the course of the forces by an increasing temperature are visible. The end values for Fy decrease nearly to the same value (Fy = - 600 N by ϑ_{Pipe} = 400 °C) as in **Figure 31** until ϑ_{Pipe} = 400 °C. Fx and Fz increase by a rising temperature until ϑ_{Pipe} = 400 °C, but not in the same dimensions as shown in **Figure 31**. By considering the peak values of the rotation movements with the temperature impact on the forces, the influence is not negligible and has to find place in a calculation for the determination of $F_{traverse}$. The moments Mx and Mz in **Figure 36** show also the same course as depicted in **Figure 31**. Mx is increasing by a rising temperature and Mz has the same constant graph along the zero line. On the other hand My behaves differently to **Figure 31** and has a decreasing course. The temperature impact on the moments during the rotation movements is negligible compared to the peak values resulting from the traverse motion. In general, forces and moments show recurrent progression for the rotation motions with deviations on the end values. This fact makes a comparison possible.

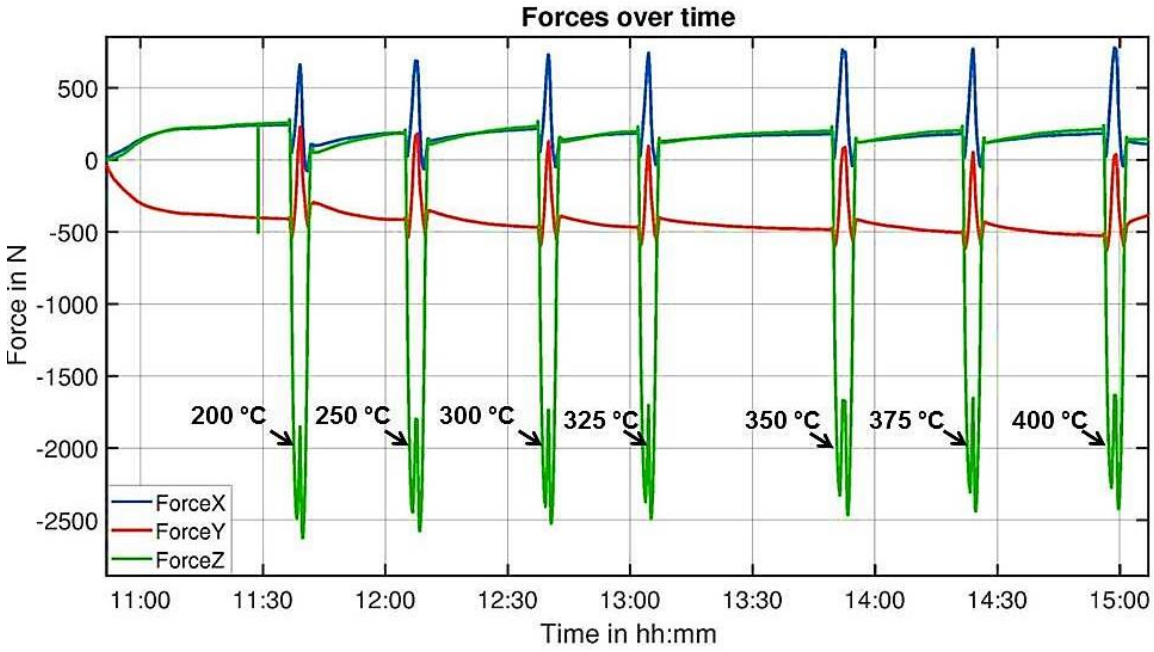

Figure 35: Forces for rotation movements for different temperature points of ϑ_{Pipe}

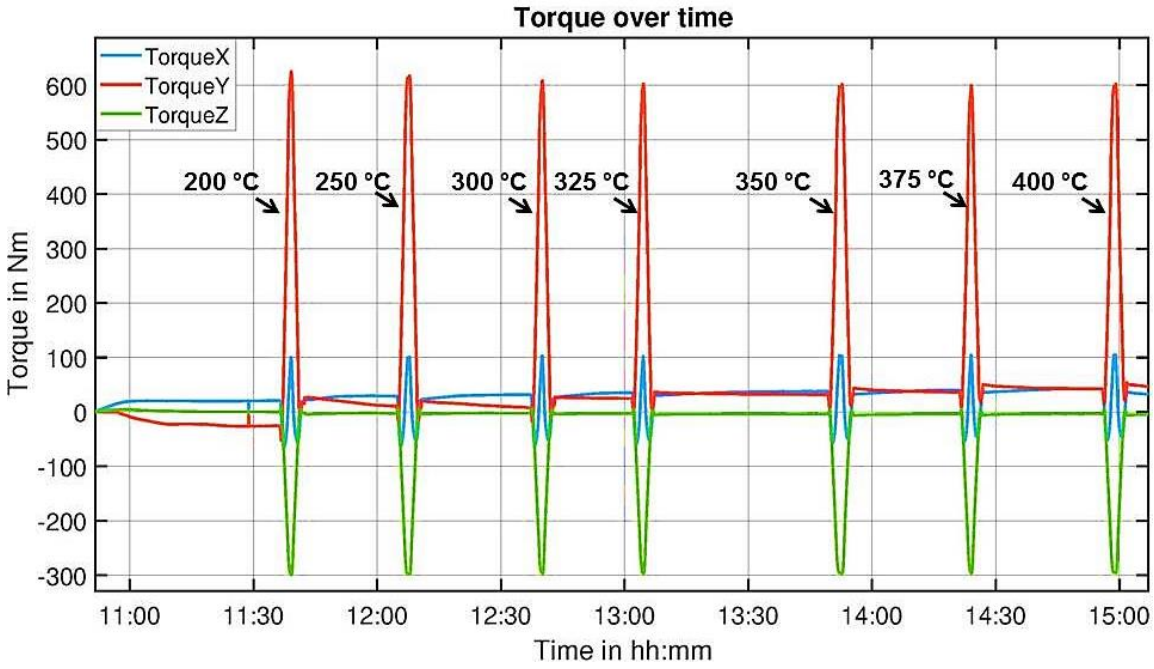

Figure 36: Torque for rotation movements for different temperature points of ϑ_{Pipe}

4.4 Comparison and validation of measurement results from tests without REPAs and air as HTF

4.4.1 Heat dilatation impact without REPAs and air as HTF

After the presentation and evaluation of the first results from tests without REPAs and air as HTF, a comparison to the ROHR2-model is done. The evaluated results from the traverse tests are used as references to check the accordance with the ROHR2-model simulation. **Figure 37** and **Figure 38** are showing the resulting forces and moments measured by the dynamometer for heating up the traverse pipe section until ϑ_{Pipe} = 400 °C by a position of φ = -20°. A similar course of forces occurs for Fy in both figures. A linear decrease as simulated in ROHR2 is existent for the results, but without same end values.

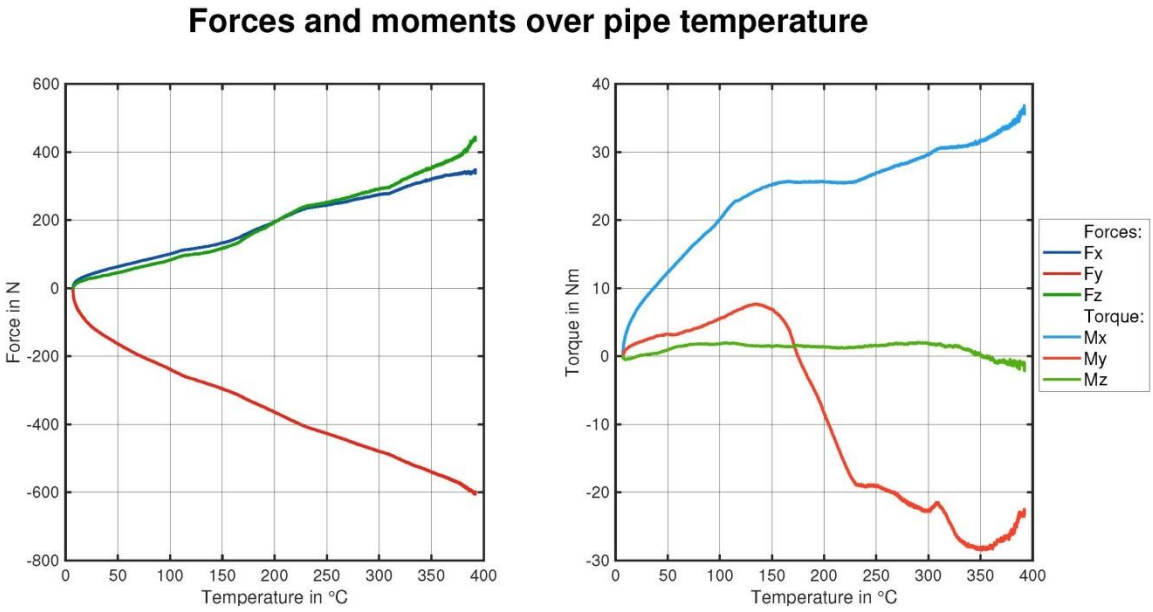

Figure 37: Forces and moments over mean pipe temperature during heat up of the traverse pipe section

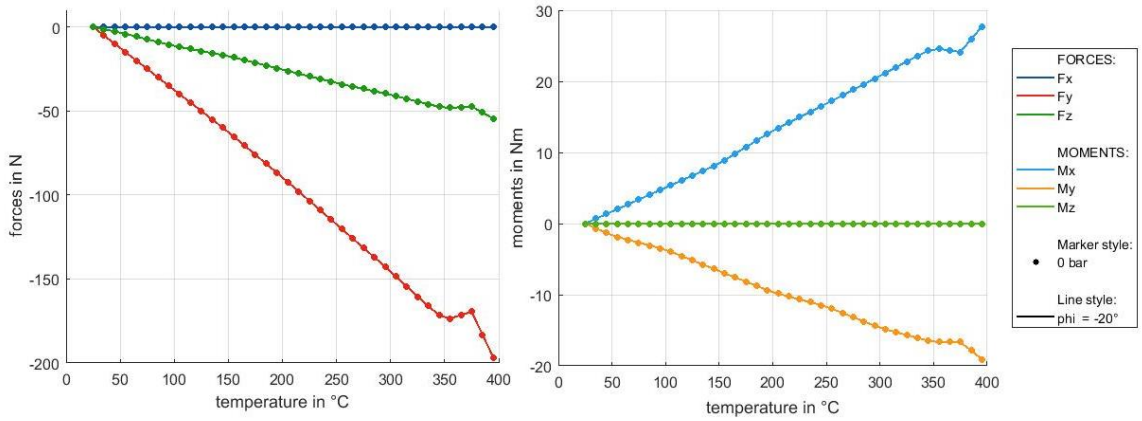

Figure 38: ROHR2 plot for the *Traverse_200* model, forces and moments over ϑ_{HTF}. Heat transfer medium is air and in this case the pressure is set to zero.

Under test conditions, the force Fy is three times higher than simulated. Fx and Fz increase by a rising temperature in the measurement results. The Fx force should be compensated completely by the gimbal hinged compensator as shown in the simulation. Fz is simulated in the opposite direction as a negative graph.

The moments are better simulated as the forces. The end values for My and Mx are nearly in the same dimensions, but the measurement results show unsteady graphs for My, Mx and Mz. Similarities to the simulated graphs prevail apart from deviations.

As shown in **Figure 31** the forces react in specific directions on the heat dilatation impact. The main reason for these deviations to the ROHR2-model is that the compensators do not work efficiently enough. The freedom of movement of the compensators has to be checked for further tests and investigations. Friction in the expansion joints is a possible reason for this deviation. Tests in the past have shown that the use of heat-resistant grease can lower the end values of the measured forces, but a full compensation is not possible. An improvement of the compensators is necessary to minimize the heat dilatation impact of the traverse pipe on the measurement of forces and moments. A change in the kind of compensators is possibly more efficient. The installation of a flexible hose directly before the dynamometer is a method to replace the current compensators. Another possibility is to subtract this known impact of the heat dilatation from the test results with REPAs and oil as HTF. Therefore, a representative measurement can be used as reference data set for each single force and moment for every temperature. By the help of linear regression, the results can be simplified as linear correlation. The resulting matrix can be integrated in the "Matlab" evaluation routine in order to plot only the forces and moments resulting from the REPAs in later life cycle tests.

4.4.2 Rotation movement impact without REPAs and air as HTF

By comparing **Figure 39** and **Figure 40**, significant differences between measurement and ROHR2-model are visible. In total, forces and moments are much more symmetrical in the simulation. The test results for Fy and Fx are nearly point symmetric and the mirror plane is present at φ = 90°. But in the ROHR2-model the graph for Fy is simulated axially symmetrical. Fz has the minimum at φ = 120°, thus the graph is staggered compared to the simulation. The end value for Fz has the doubled dimensions for the measured results. A reason for this can be a higher weight of the traverse pipe section for the finished installation as planed in the model. The insulation is considered in the ROHR2-model, but different materials have been used for the installation as planned. This leads to unexpected higher weight of the traverse pipe section and to higher end values for Fz.

My and Mz have point symmetric graphs in both figures and Mx shows an axially symmetrical course. One main difference between simulation and measured data is that in **Figure 39** all moments start near the zero line.

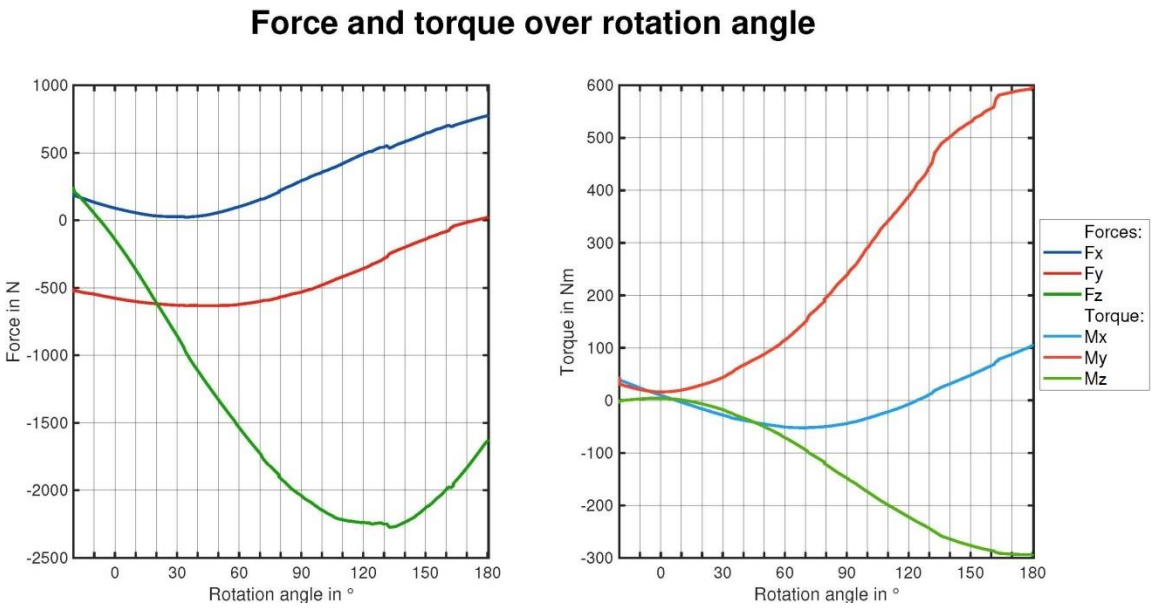

Figure 39: Rotation movement of the traverse without REPAs and air as HTF for ϑ_{Pipe} = 400 °C

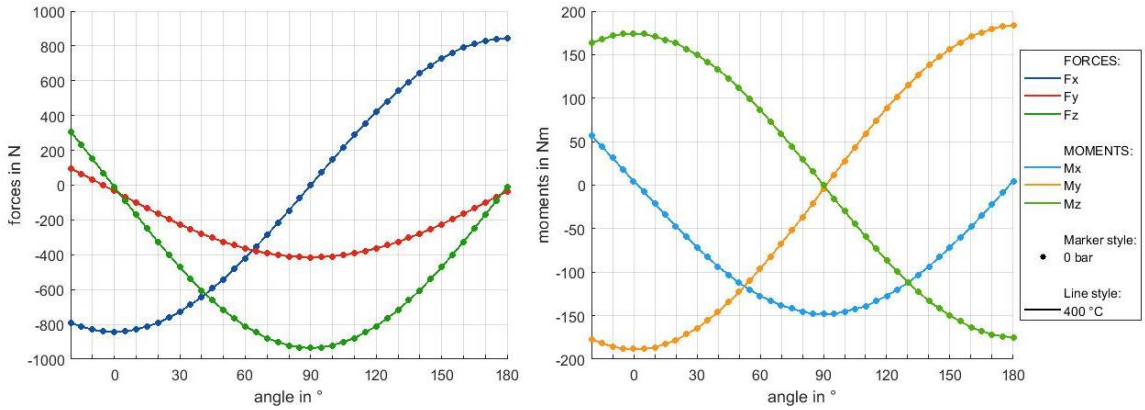

Figure 40: ROHR2 plot for the *Traverse_200* model, forces and moments over the rotation angle for ϑ_{HTF}= 400 °C

The rotation movement in the ROHR2-model begins with higher end values at the stow position φ = -20 for each moment. All graphs for the measured data show clear deviations for the end values of each moment during the complete rotation motion. The best simulated case is for Mx with matches in symmetry and nearly in the measurement range.

In conclusion, the ROHR2-model plot results for the rotation movement differ widely from the measured results. The plausibility of the model for the investigation of the rotation impact must be questioned. Sources of errors are that RHOHR2 allows no dynamic modelling and the used data base for each single angle is not representative for the REPA test rig. The simulation has to be checked for discrepancies to the real traverse pipe section weight. By considering the ROHR2-model as accurate enough reasons for the unsymmetrical course of forces and moments for the measurements have to be found.

4.5 Measurement uncertainties

The executed tests with the two described measurement setups are affected from different kinds of measurement uncertainties. The dynamometer is one of the used sensors with the highest influence on the accuracy of the measurements and can be considered as one source of deviations for both tests. Measurement uncertainties for the K6D175 dynamometer with effect on the forces and moments can be divided in:

- Measurement uncertainties with impact on the zero signal
- Measurement uncertainties that affect the characteristic
- Temperature based uncertainties

A detailed investigation of the dynamometer measurement uncertainties has been done in a previous thesis and also a calculation (Thesis Thore Müller, Chapter: 3 Dynamometer measurements and uncertainty [2]). This calculation is implemented in the evaluation routine in order to integrate it in the total contemplation.

Test results with installed REPAs and HELISOL© 5A as HTF:

In order to evaluate the measurement results more realistic, measurement uncertainties and improvements of the setup has to be considered. One influencing factor during the execution of the different test was a slightly unstable pressure and HTF temperature. This affects the forces and moments measured during rotation and translation movements. Another important affect is that the motion of the traverse during rotation movements suffers from switchover points of the kinematic unit. Those points lead to visible vibrations of the traverse and additional generated forces during each rotation. A further assessment was that the translation cylinder remains not in the exact position by a rotation of the traverse. A consequence of those unwanted motion of the pistons are additional forces for Fy. Reasons for this can be air in the hydraulic system of the drive unit. Different data sources like the PLC data and the dynamometer output have small deviations in time, because synchronization has been done manually on two computers. For life cycle tests after the commissioning, the integration of the dynamometer in the PLC is a necessary step to simplify the measurement and to reduce deviations. The precisions of the important sensors for the measurements have to be determined. The flow meter, rotation and translation position sensor, HTF temperature sensor and the pressure gauge have to be taken in to account in the measurement uncertainty calculation.

Test results without REPAs and air as HTF:

The most significant difference to the setup with HTF was the use of additional temperature sensors for the measurement. The installation outside on the surface of the traverse pipe and the heating from one side leads to large measurement uncertainties. Furthermore, the heat losses during each rotation movement had an impact on every measured test. Similar measurement uncertainties result from rotation position sensors and the dynamometer as by the setup with REPAs and HELISOL© 5A as HTF.

5 Conclusion and outlook

A safe, economic and ecological operation of Parabolic Trough Collector (PTC) power plant requires an indispensable durability of Rotation and Expansion Performing Assemblies (REPAs). These flexible pipe connections are a key component in the solar field and they have to work under harsh weather conditions for an operating period of 30 years. By simulating typical tracking motions of the collector and the linear expansion of the absorber tube, REPAs can be tested under near-operating conditions after finishing the commissioning of REPA test rig at the Plataforma Solar de Almería.

The content of this thesis provides an overview of the state of the art in parabolic trough collector power plants and the basic knowledge about the construction and function of the REPA test rig. Furthermore, the efforts are described to continue the commissioning of the sensor for the force-measurement and to evaluate the first measurement results from an integrated measurement setup and an additional test setup. Also a validation of the measurement results by the help of the simulation ROHR2-model has been done.

The commissioning of the test rig has been finished up to an important sub-step by operating the Heat Transfer Fluid (HTF) cycle with HELISOL® 5A under constant pressure and a HTF temperature of 400 °C. This important intermediate step until reaching the finished installation was crucial for the execution of the first tests with focus on the resulting forces and moments on the REPAs.

A measurement setup has been integrated in the existing test facility with improvements for an optimal sensor operation like an active cooling. The results from tests with two installed REPAs, a dynamometer in “top-west” position and HELISOL® 5A as HTF, provided insights about the measurement range during typical rotation and translation movements of the test rig to simulate the realistic motions of PTCs. One important finding is that the installed sensor operates at the range limit to detect all moments. The impact of different volume flows, rotation and translation movements at different HTF temperatures was measured and evaluated. Further tests have been made to investigate the influences of settling time and sensor drift.

Recurring results in form of typical graphs for forces and moments during rotation and translation movements lead to first conclusions about the impact of single components on the measurement results. Decisive influence on the forces and moments has the torque sword and the weight force of the installed REPAs at the end of traverse pipe section. The pipe section between the dynamometer support and the REPA connection has also a significant influence on the measured range of the moments.

Measurement uncertainties like a rising sensor temperature have been reduced at a minimum of a nearly ambient temperature. The fan as an active cooling device is upgradeable for the three planned dynamometers at the traverse and is a necessary component for a higher accuracy of the measurements. The test results from the dynamometer are plausible from the current point of view. But a more valid evaluation

can be given after separating the measured forces and moments from the traverse pipe section.

Another main objective was to plan and install a measurement setup and to perform a separate test to determine the forces and moments resulting from the traverse without REPAs and air as HTF. The impacts of heat dilatation, rotation movements and the temperature on the motions have been investigated. The determination of typical forces and moments during rotation movements and heat dilatation are used as reference values for the traverse pipe section. This defined influence can be subtracted from measurements with REPAs and for example HELISOL® 5A as HTF.

Moreover, the measurements results provide the evidence that the expansion joints are not compensating the complete heat dilatation of the traverse pipe section. Improvements of the compensators are required to reduce the impact of the thermal expansion. Replacing the compensators by a flexible hose is a possible solution. But a total compensation of all additional forces is not possible. In conclusion, the measurement of the forces and moments resulting from the traverse has to be integrated in a calculation. This can be done in the “Matlab” evaluation routine. The evaluation of the dynamometer results has been realized by this routine to combine the different data sources in order to plot the measured tests.

The ROHR2-model simulation for the traverse pipe section was more accurate for the heat dilatation of the pipe section, than the measured end values. Those differ significantly from the model results because of the temperature impact, which is clearly higher at the installed traverse. The installed compensators are not working as planned in the ROHR2-model. The simulation for the rotation movement impact shows significant deviations and has to be improved to use it for further tests.

The obtained findings from measurement results of both tests are described and evaluated in this thesis to understand the resulting forces and moments reacting on the first dynamometer and to contribute the start-up of the test facility. But the commissioning of the REPA test rig is a long-term process with many-sided tasks. **Figure 41** gives an overview of the necessary work steps until the first life cycle tests are possible.

In order to simulate the forces and moments of the traverse pipe section for the other three planned dynamometer, a revision of the current ROHR2-model for the “top-west” dynamometer is needed to have a more accurate estimation. Another important step is to improve the function of compensators and to integrate the heat dilation impact of the traverse pipe in the evaluation routine and also the rotation movement impact. After this, the subtraction of $F_{traverse}$ from the measurements with installed REPAs and HELISOL® 5A is possible and leads to unambiguous measurement results caused by the REPAs.

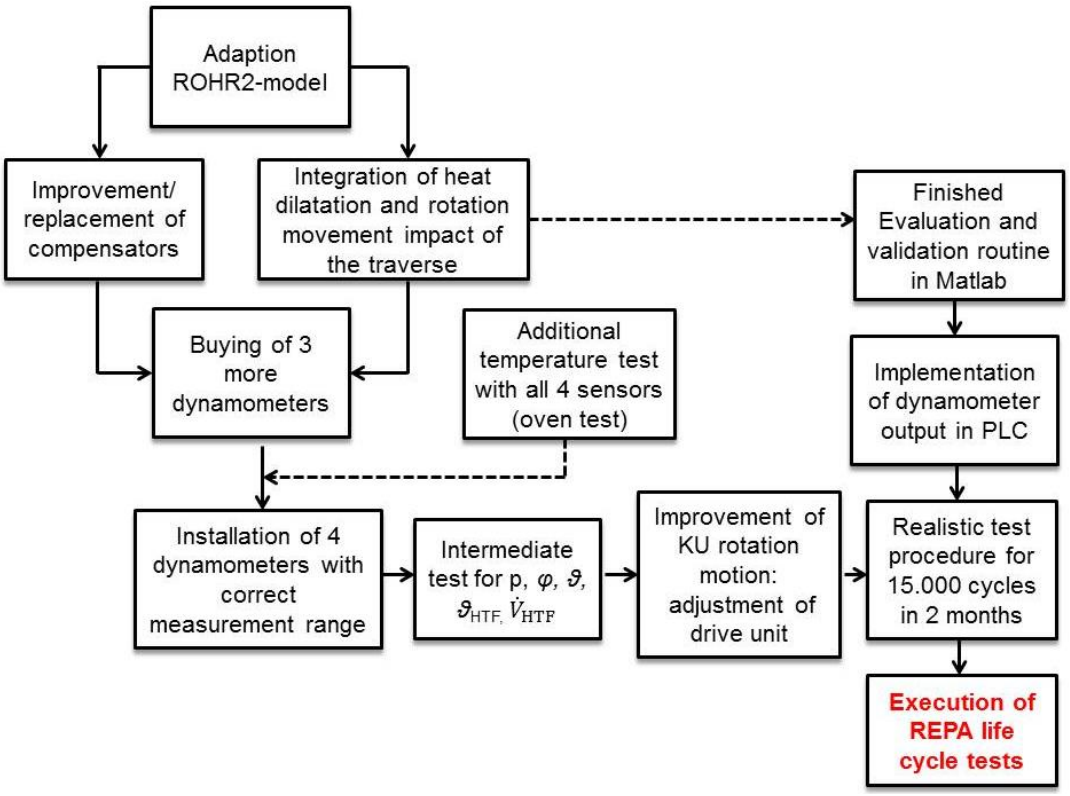

Figure 41: Work steps to finish the commissioning of the REPA test rig for the execution of first life cycle tests

Moreover, the next measurement range for the two dynamometers in “bottom-east” and “bottom-west” position has to be determined. This can be done by installing the first dynamometer under one of the swivel joints (replace dummy) and repeat the tests with REPAs and HELISOL® 5A as HTF. After the purchase of three dynamometers with correct range limits for the specific installation positions, a separate oven test with all four sensors can be done in order to know the temperature influence on the measured forces and moments.

Not every impact has been investigated successfully by the tests with REPAs and HELISOL® 5A as HTF. Repetitions of sub-tests for the impact of pressure and HTF temperature on the rotation movements are necessary to get a more detailed knowledge about all variable parameters of the test rig. This test was also affected by mechanical influences. Interferences resulting from switchover points lead to unsymmetrical rotation movements and require adjustments of the drive unit. Furthermore, a counterweight has to be installed to compensate the traverse and to ensure smooth rotation motions.

The first measurement results show that the commissioning of the test rig is progressing steadily and partial successes are available. By finishing the described work steps, a more reliable evaluation of the dynamometer measurements will be possible and REPA life cycle test can be executed under authentic operation conditions.

6 References

[1] Science universe, Physics articles (2012): **available**: http://scienceuniverse101.blogspot.com.es/2012/02/coefficient-of-linear-expansion.html#.Wm4GU02WzIU, **accessed**: 28.01.2018

[2] Müller, Thore (2017): Commissioning and validation of the underlying model of a test rig analyzing rotation and expansion performing assemblies in parabolic trough collector power plants, Master's Thesis RWTH University, Aachen, Germany

[3] European Commission (2018): Climate Action, **available**: https://ec.europa.eu/clima/policies/international/negotiations/paris_de, **accessed**: 27.01.2018

[4] Quaschning, Volker (2010): Renewable Energy and Climate Change, John Wiley & Sons, Ltd

[5] Dr Heller, Peter (2015.): The Performance of Concentrated Solar Power (CSP) Systems, Duxford: Woodhead Publishing

[6] Elsevier B.V. (2017): Progress in concentrated solar power technology with parabolic trough collector system, **available**: https://ars.els-cdn.com/content/image/1-s2.0-S1364032117308122-gr2.jpg, **accessed**: 27.12.2017

[7] C. Márquez Salazar (2008): CSP today - An Overview of CSP in Europe, North Africa and the Middle East

[8] Solargis, Direct Normal Irradiation (DNI) (2016), **available**: https://solargis.com/products/maps-and-gis-data/free/download/world, **accessed**: 27.12.2017

[9] Trieb, Franz (2009): SolarPaces Conference Berlin, Global Potential of Concentrating Solar Power

[10] Ragheb , M. (2014): Solar Thermal Power and Energy Storage Historical Perspective, **available**: http://www.google.de/url?sa=t&rct=j&q=&esrc=s&source=web&cd=4&ved0ahUKEwisgurYnNLYAhVJOJoKHQgLBAoQFghNMAM&url=http%3A%2F%2Fwww.solarthermalworld.org%2Fsites%2Fgstec%2Ffiles%2Fstory%2F2015-04-18%2Fsolar_thermal_power_and_energy_storage_historical_perspective.pdf&usg=AOvVaw1G7Pujlk5fxVjKKDCEwks6, **accessed**: 12.01.2018

[11] Barcia Lourdes A, Menéndez Rogelio Peón, Esteban Juan Á. Martínez, Prieto Miguel A. José, Ramos Juan A. Martín, de Cos Juez F. Javier, Reviriego Antonio Nevado, (2015): Dynamic Modeling of the Solar Field in Parabolic Trough Solar Power Plants, **available**: http://www.mdpi.com/19961073/8/12/12373, **accessed**: 14.01.2018

[12] Schweitzer Axel, Meese Ludwig, Birkle Manuel, Schiel Wolfgang, Balz Markus (2012): Pioneer again -EuroTrough goes India 50 MW CSP plant Godavari in Rajasthan, **available**: https://www.researchgate.net/figure/Components-of-collector-structure-of-the-EuroTrough_282859630, **accessed**: 14.01.2018

[13] Quaschning, Volker (2013): Regenerative Energiesysteme Technologie – Berechnung – Simulation, Auflage 8, Hanser Verlag München

[14] Prof. Dr Pitz-Paal, Hennecke Klaus, Dr Heller, Peter, Dr Buck Reiner (2013): Solar Thermal power plants, Utilising concentarted sunlight for generating energy

[15] Buehler Reuben, Yang Sam, Ordonez Juan C. (2016): Heat Transfer Fluids for Parabolic Trough Solar Collectors – A Comparative Study, **available**: http://ieeexplore.ieee.org/stamp/stamp.jsp?arnumber=7897145 **accessed**: 14.03.2018

[16] Schaffer Erich, Wacker Chemie AG, Dr. Dersch, Dr. Dorrich, Herr Hilgert, Dr. Jung (2016): HELISOL® - ein Siliconöl basierter Wärmeträger für CSP Kraftwerke, **available:** https://www.linguee.de/deutsch-englisch/search?source=auto&query=cite, **accessed**: 14.03.2018

[17] Dr.-Ing. Wittmann, Michael: Molten Salt Systems - Higher thermal efficiencies by using salt instead of oil, **available:** http://www.dlr.de/sf/en/desktopdefault.aspx/tabid-10647/18795_read-44147/ **accessed:** 05.03.2018

[18] Hoffschmidt B.: University Lecture "Solar Components". Institute of Solar Research, RWTH Aachen University

[19] Plumpe, Andreas (2016): Design of a Test Rig and its Testing Methods for Rotation and Expansion Performing Assemblies in Parabolic Trough Collector Power Plants, Master's Thesis RWTH University, Aachen, Germany

[20] Wagner, Walter (2012): Rohrleitungstechnik, Vogel Industrie Medien

7 Appendix

7.1 CAD Drawings for heater framework, fan, connection of REPA and heater

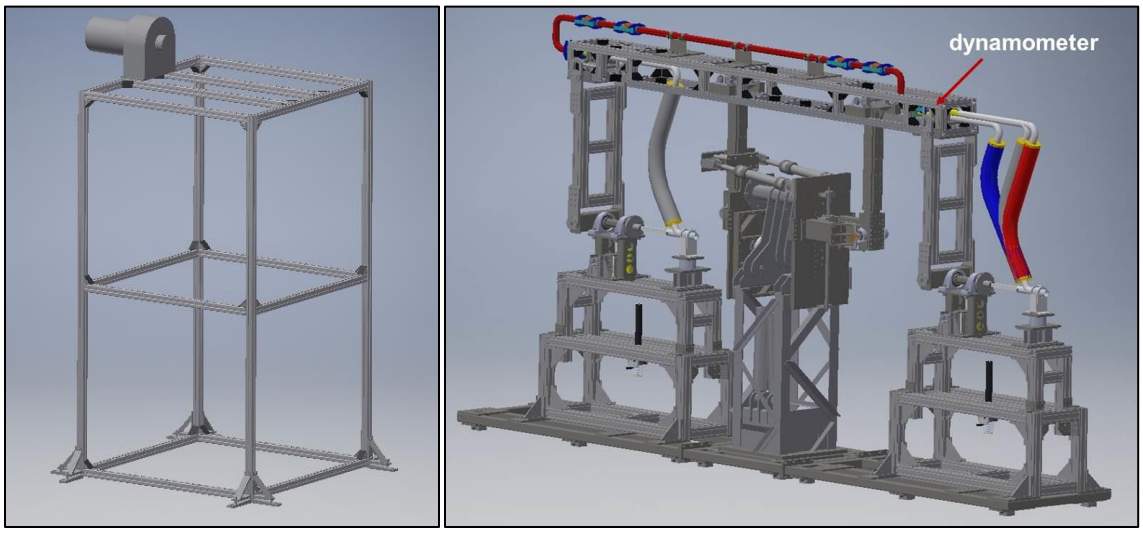

Figure 42: Left: "Autodesk Inventor" drawing of the "Item" structure for the traverse heating, Right: Autodesk Inventor drawing of the traverse, kinematic unit and both tables

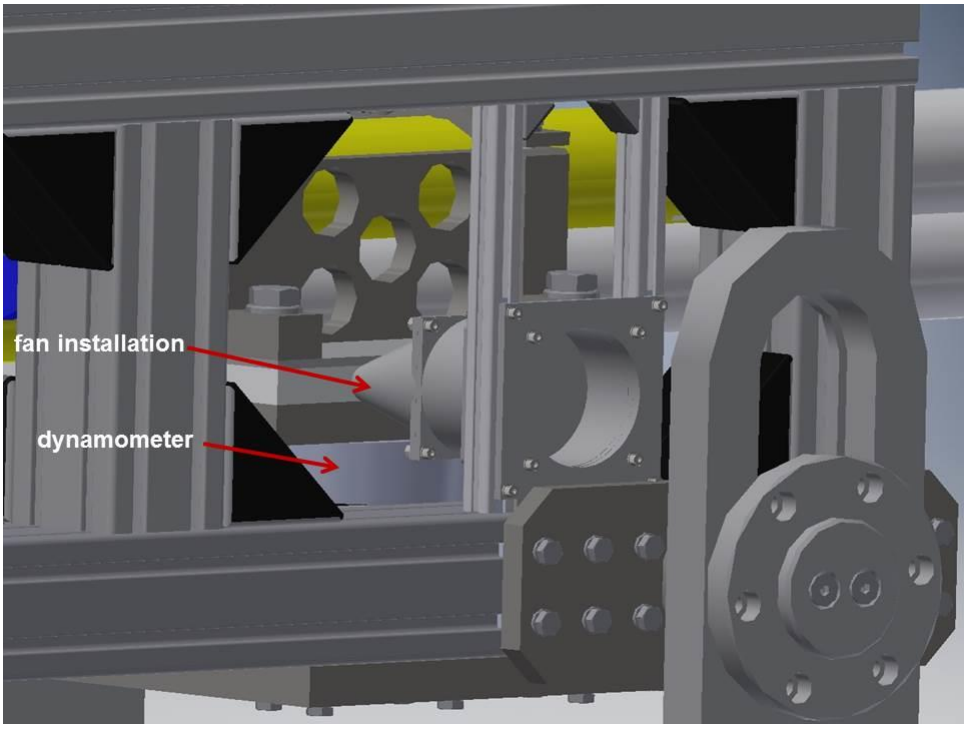

Figure 43: "Autodesk Inventor" drawing of the fan installation

7.2 Estimation of heat losses for test without REPAs and air as HTF

Table 6: Used pipe sizes in the traverse

Used pipe sizes in the traverse [mm]					
Nominal diameter	**Outer diameter**	**Wall thickness**	**Inner diameter**	**Outer radius**	**Inner radius**
DN 50	60.3	5.54	49.22	30.15	24.61
DN 65	73	7.01	58.98	36.5	29.49
DN 80	88.9	7.62	73.66	44.45	36.83
DN100	114.3	8.56	97.18	57.15	48.59
DN150	168.3	10.97	146.36	84.15	73.18

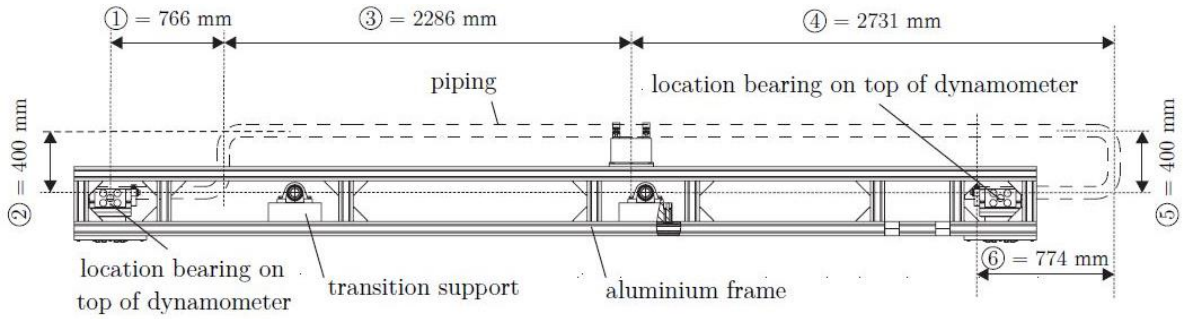

Figure 44: Technical drawing of the traverse pipe section with dimensions for pipe segments [19]

Table 7: Lengths of pipe sections

Traverse section	Length Traverse [m]
1	0.766
2	0.4
3	2.286
4	2.731
5	0.4
6	0.774
Straight pipe length	7.357
L_{Elbow}	0.3
Total length	7.66

$$L_{\mathrm{Elbow}} = 4 \cdot \frac{\pi * r}{4} \qquad \text{(Eq. A.1)}$$

Table 8: Elbow radius of the pipe section

Elbow radius in the pipe section [mm]	
REPA	Radius
DN50	76.2
DN65	95.3
DN80	114.3
DN100	152.4

Table 9: Main parameters heat loss estimation

description	symbol	value	unit
Tube inner diameter	d_i	58.98	mm
Tube outer diameter	$d_{a,w}$	73	mm
Insulation thickness	$t_{a,d}$	120	mm
Total tube length	L	7.7	m
Insulated length (idealized)	L_i	7.7	m
Radiation coefficient of a black body	C_S	$5{,}67*10^{-8}$	W/(m² K)
Emissions ratio: aluminum sheet rolled	ε	0.05	
Outer diameter with insulation	D_a, $d_{a,d}$	313	mm
Wind velocity	w	2	m
Thermal conductivity of Insulation	λ_i	0.151	W/(m K)
Heat transfer coefficient at iso-outside	α_a	18.99	W/(m² K)
Radiation component	$\alpha_{a,rad}$	0,34	W/(m² K)
Convective component	$\alpha_{a,conv}$	18,65	W/(m² K)
Temperatures			
Air temperature	ϑ_m	400	°C
Ambient temperature	ϑ_a	25	°C
Temperature difference	ΔV	375	°C
Permitted surface temperature	$\vartheta_{D,a}$	50	°C
Teat losses			
Per m insulated tube	$\dot{q}_L$	236,2	W/m
Heat loss insulated tube total	$\dot{Q}$	2061	W
Heat loss insulated tube	k_L	0.63	W/(m K)

Heat transfer coefficient: $\alpha_a = \alpha_{a,rad} + \alpha_{a,conv}$ (Eq. A2)

Radiation component: $\alpha_{a,rad} = \varepsilon \cdot C_s \cdot \frac{(\vartheta_{D,a} + 273.15 \cdot K)^4 - (\vartheta_a + 273.15)^4}{\vartheta_{D,a} - \vartheta_a}$ (Eq. A3)

Calculation conditions: $w \cdot D_a > 0{,}00855 \frac{m^2}{s}$ $w \cdot D_a \leq 0{,}00855 \frac{m^2}{s}$ (Eq. A4)

Convective component for $w \cdot D_a = 0{,}626 \frac{m^2}{s}$: $\alpha_{a,conv} = 8{,}9 \cdot \frac{w^{0,9}}{D_a^{0,1}}$ (Eq. A5)

Calculation for thermal transmission coefficient:

$$k_L = \frac{\pi}{\frac{1}{2\lambda_i} \cdot \ln\frac{d_{a,d}}{d_{a,w}} + \frac{1}{\alpha_a \cdot d_{a,d}}}$$ (Eq. A6)

Table 10: Layer material specifications

Layer	Value	Unit
Volume		
Steal	0.011	m³
Isolation	0.557	m³
Air	0.021	m³
Mass of layer		
Steal	86.01	kg
Isolation	77.99	kg
Air	0.01	kg
Density		
Steal	7730	kg/m³
Isolation	140	kg/m³
Air	0.49	kg/m³
Specific heat capacity		
Steal	470	J/Kg*k
Isolation	1030	J/Kg*k
Air	1000	J/Kg*k

Heat loss: (Eq. A7)

$$\dot{q_{\mathrm{L}}} = k_{\mathrm{L}} \cdot \Delta\vartheta$$

Layer volume: (Eq. A8)

$$V = \pi \cdot (r_{\mathrm{a}} - r_{\mathrm{i}})^2 \cdot L$$

Heat loss per second: (Eq. A9)

$$\frac{d}{dt} \sum_i (m_i \cdot cp_i \cdot T_i) = \sum \dot{Q}_i$$

Heat loss outside: $\frac{dT}{dt} = \frac{\sum \dot{Q}_i}{\sum m_i \cdot cp_i}$ (Eq. A10)

Heat loss outside without safety factor: $\frac{T}{t} = 0{,}017 \frac{K}{s} = \mathbf{1.02} \frac{\boldsymbol{k}}{\boldsymbol{min}}$

Heat loss outside with safety factor: $\frac{T}{t} = 0{,}034 \frac{K}{s} = \mathbf{2.04} \frac{\boldsymbol{k}}{\boldsymbol{min}}$

The implementation of a safety factor is needed, because heat losses like the open pipe ends are not considered in the calculation. Another impact is that the expansion joints have a thinner insulation as the rest of the traverse pipe section. An aluminum metal sheet as cover has been omitted in order to ensure the compensator motions. Anyway this value of $2.04 \frac{k}{min}$ is adequate for a sufficient assessment [20].

7.3 Additional information

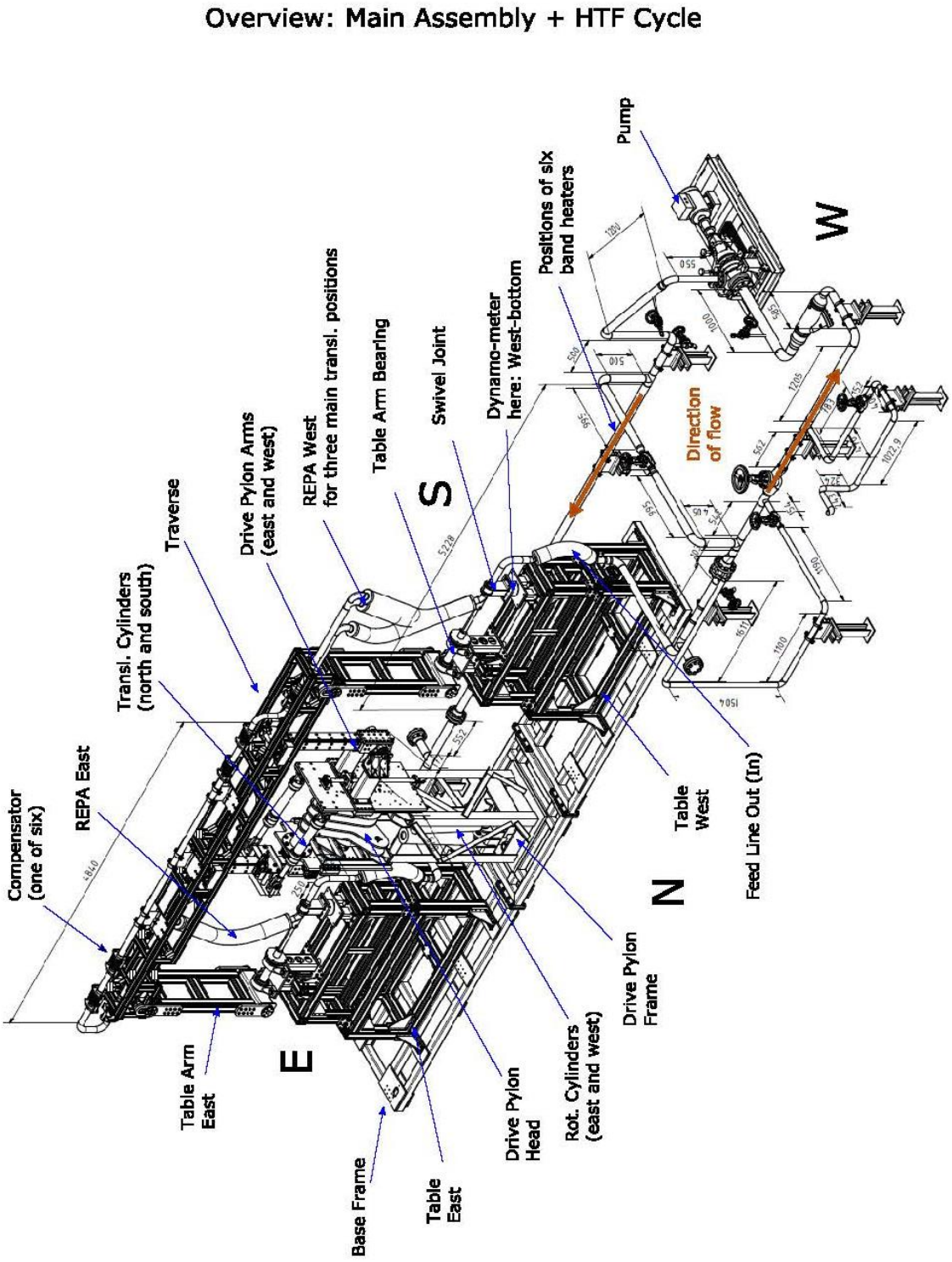

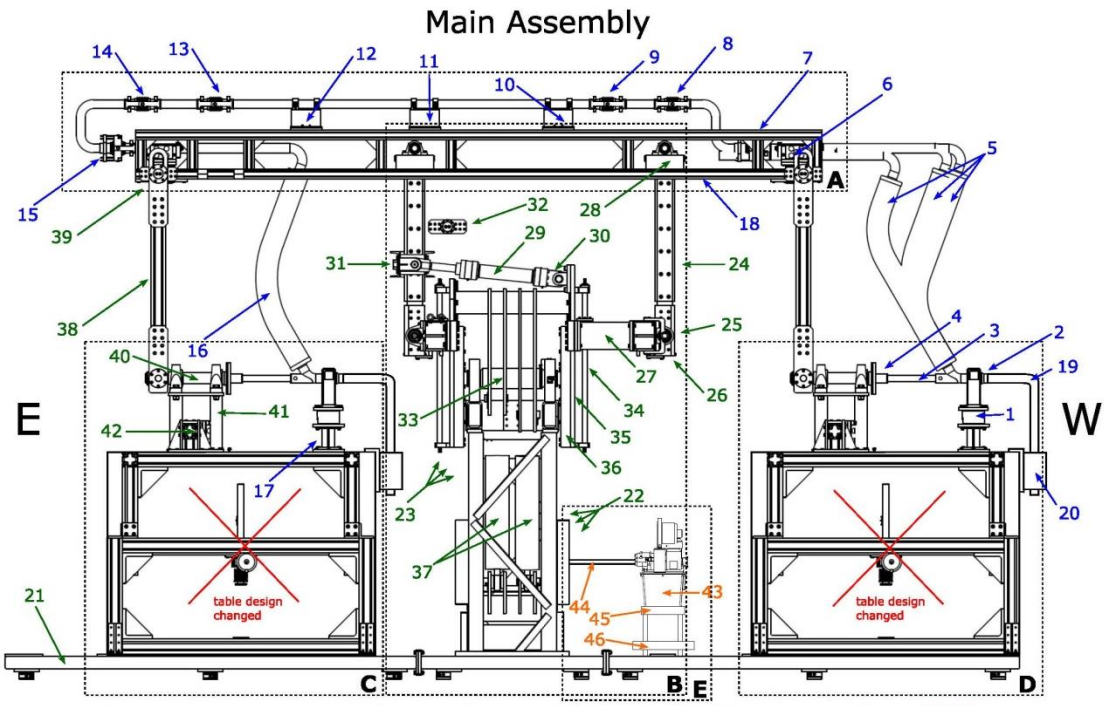

Main Parts

- **A.** Traverse
- **B.** Drive Pylon
- **C.** Table East
- **D.** Table West
- **E.** Hydraulic System

HTF-Cycle

1. Dynamo-meter (two per REPA: bottom and top)
2. Swivel Joint
3. Torsion Sword
4. Torsion Sword Flange
5. REPA West (depicted for three typical transl. angles)
6. Sensor Bearing (fix bearing, including dynamo-meter top position)
7. Compensator West-Outer (gimbal hinged angular expansion joint)
8. Compensator West-Center (single hinged angular expansion joint)
9. Compensator West-Inner (single hinged angular expansion joint)
10. Red Steel Bearing West (sliding bearing)
11. Red Steel Bearing Center (fix bearing)
12. Red Steel Bearing East (sliding bearing)
13. Compensator East-Inner (single hinged angular expansion joint)
14. Compensator East-Center (single hinged angular expansion joint)
15. Compensator East-Outer (hinged angular expansion joint)
16. REPA East (only one transl. angle)
17. Swivel Joint Bearing
18. ITEM-Profile
19. Intermediate Pipe Knee
20. Table Pipe Bearing (fix bearing, east and west)

Kinematic

21. Base Frame
22. Drive Pylon Base Frame
23. Drive Head Assembly
24. Drive Pylon Arm
25. Drive Pylon Arm Bearing
26. Drive Pylon Arm Support Bracket
27. Drive Pylon Arm Support Intake
28. Drive Pylon Arm Connection
29. Translation Cylinder (north and south)
30. Translation Cylinder End Plate Bearing
31. Translation Cylinder Arm Bearing
32. Translation Cylinder Traverse Connection
33. Drive Pylon Head Lever
34. Spindle Drive
35. End Plate (east and west)
36. End Plate Frame
37. Rotation Cylinders (east and west)
38. Swivel Drive Arm
39. Swivel Drive Arm Traverse Connection
40. Swivel Drive
41. Swivel Drive Support
42. Swivel Drive Support for small REPAs (currently not used)

Hydraulic System:

43. Hydraulic Unit
44. Hydraulic Tubing
45. Hydraulic Unit Support
46. Hydraulic Unit Oil Tray

Instrumentation

1. HTF Pump
2. PT Pump discharge / Vent valve discharge
3. Shut-off Pump discharge
4. Drain valve discharge
5. Bypass shut off valve
6. Band heaters
7. Volume flow orifice
8. Feed Line – In Flexible Hose
9. Feed Line – Out Flexible Hose
10. PT Kinematic out / Vent Valve Kinematic - Out
11. Drain Valve (Check Valve)
12. Check Valve
13. Shut-off Expansion Vessel In
14. Shut-off Expansion Vessel Bypass
15. Shut-off Expansion Vessel Out
16. Strainer
17. Shut-off Pump suction
18. PT Pump suction / Vent valve suction

Pipe Sections and Connections

30. Kinematic Unit - In
31. Kinematic Unit – Out
32. Bypass
33. Expansion Vessel Inlet
34. Expansion Vessel Outlet
35. Expansion Vessel Bypass
36. Feed Line

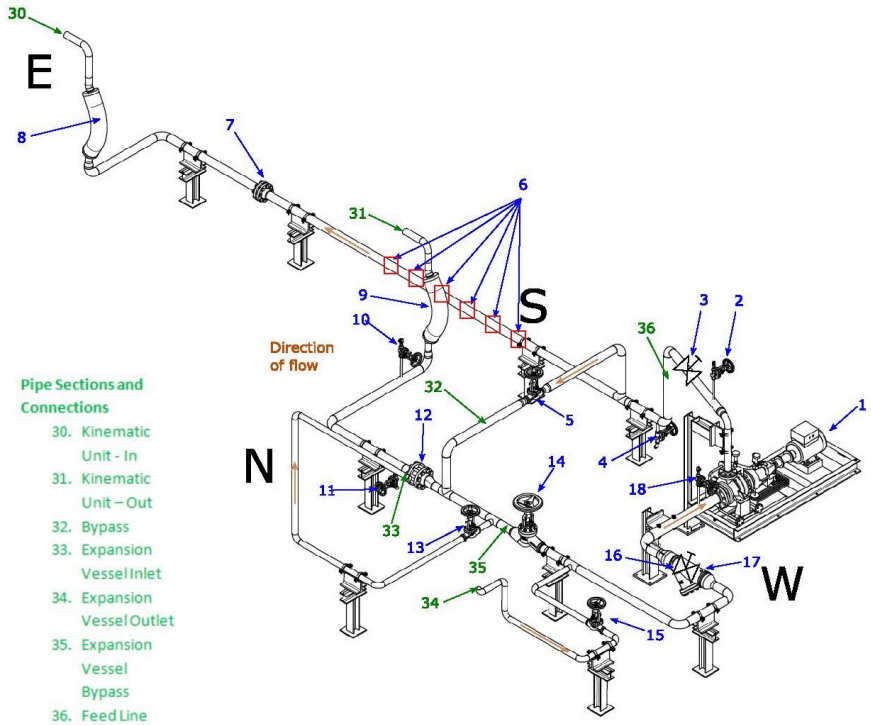

HTF-Cycle without expansion vessel and piping inside kinematic unit

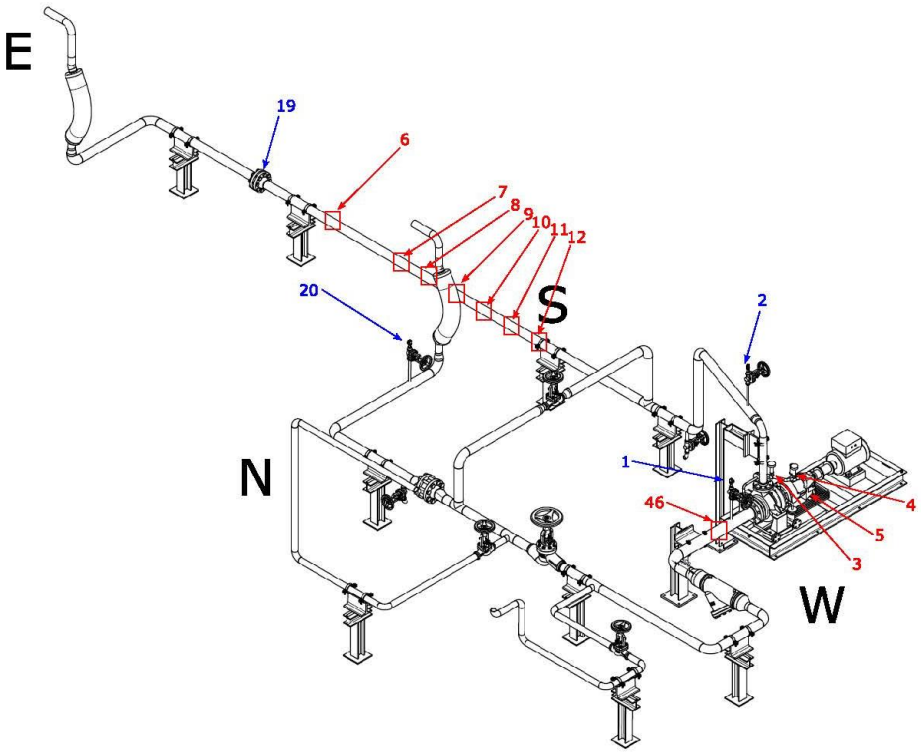

Sensors (part 1)

Sensors (part 2)

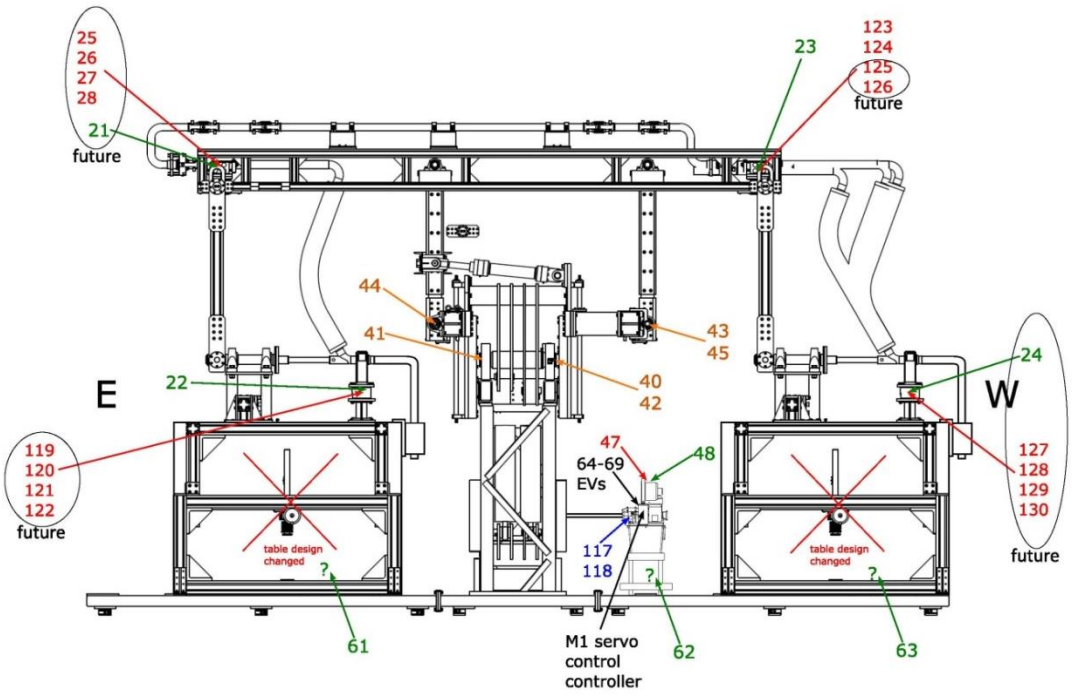

Sensors (part 3)

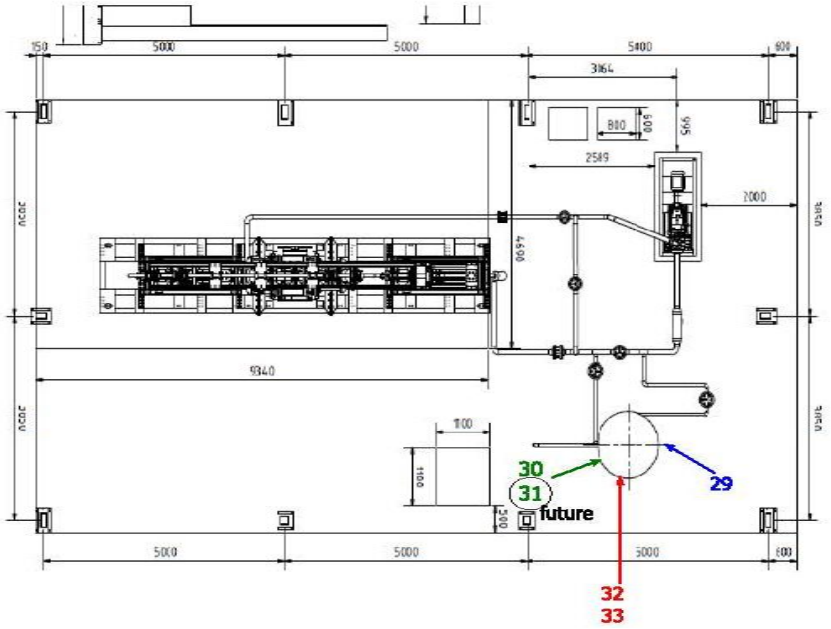

Table 1: Sensor descriptions: taken from signal list (02. Dec 2016)

No.	Ch.-Type	Description	Sensor-Type	PSA-nom.
1	absolute pressure	suction side absolute	S-20	PE-HTF-01-W
2	absolute pressure	pressure side absolute	S-20	PE-HTF-02-W
3	temperature	motor, HTF pump	Pt100_T1, 4 wire	TT-HTF-01-W
4	temperature	Bearing, HTF pump	Pt100_T2, 4 wire	TT-HTF-02-W
5	temperature	lubricating oil, HTF pump	Pt100_T3, 4 wire	TT-HTF-03-W
6	temperature	fluid temp. heater outlet	Thermocouple Type K TC-15	TT-HTF-04-W
7	temperature	tube surface temp. heater 1	Thermocouple Type K	TT-HTF-05-W
8	temperature	tube surface temp. heater 2	Thermocouple Type K	TT-HTF-06-W
9	temperature	tube surface temp. heater 3	Thermocouple Type K	TT-HTF-07-W
10	temperature	tube surface temp. heater 4	Thermocouple Type K	TT-HTF-08-W
11	temperature	tube surface temp. heater 5	Thermocouple Type K	TT-HTF-09-W
12	temperature	tube surface temp. heater 6	Thermocouple Type K	TT-HTF-10-W
19	differential pressure	orifice plate differential pressure	DTP-10	PE-HTF-03-W
20	absolute pressure	absolute pressure test facility outlet	S-20	PE-HTF-04-W
21	multi axis load cell	force/torque REPA No. 1 east top	K6D175	
22	multi axis load cell	force/torque REPA No. 2 est bottom	K6D175	
23	multi axis load cell	force/torque REPA No. 3 west top	K6D175	
24	multi axis load cell	force/torque REPA No. 4 west bottom	K6D175	
25	temperature	temperature multi force east top 1.1	Pt1000	
26	temperature	temperature multi force east top 1.2	Pt1000	
27	temperature	temperature multi force east top 1.3	Pt1000	
28	temperature	temperature multi force east top 1.4	Pt1000	
29	absolute pressure	absolute pressure, N2 tubing	S-20	PE-HTF-05-W
30	level switch	level switch expansion vessel (top)	2 x SPDT	FA-HTF-01-W
31	level switch	level switch expansion vessel (bottom)	2 x SPDT	FA-HTF-03-W
32	temperature	temperature expansion vessel 1 (liquid)	Thermocouple Type K TC-10	TT-HTF-15-W
33	temperature	temperature expansion vessel 2 (gas)	Thermocouple Type K TC-10	TT-HTF-16-W

Table 2: Sensor descriptions: continued

No.	Ch.-Type	Description	Sensor-Type	PSA-nom.
40	limit switch	inductive sensor rotation negative	Balluf BES M12MI-POC40B-S04G	ZS-CI-01-W
41	limit switch	inductive sensor rotation positive	Balluf BES M12MI-POC40B-S04G	ZS-CI-02-W
42	inclination	magnetic tape sensor rotation	ASM PMIS3-50-50-20Khz-HTL-21-7M-S	ZT-CI-11-W
43	limit switch	inductive sensor translation negative	Balluf BES M12MI-POC40B-S04G	ZS-CI-04-W
44	limit switch	inductive sensor translation positive	Balluf BES M12MI-POC40B-S04G	ZS-CI-05-W
45	rotary encoder	rotary encoder -translation	MH64-1023MU multiturn FSG	ZS-CI-06-W
46	temperature	HTF temperature pump inlet	Thermocouple Type K TC-15	TT-HTF-17-W
47	temperature	hydraulic oil temperature	SSM.1.B4.150.54.S1 level switch with PT100	TT-CI-13-W
48	level switch	hydraulic oil level	SSM.1.B4.150.54.S1 level switch with PT100	LA-CI-03-W
61	leakage sensor	leakage / swim sensor		FA-HTF-02-W
62	leakage sensor	conrad leakage sensor		FA-HTF-02-W
63	leakage sensor	conrad leakage sensor		FA-HTF-02-W
117	relative preasure	pressure transmitter hydraulic unit rotation (150)	MODS-250-G1/4-A-M12	PE-CI-01-W
118	relative preasure	pressure transmitter hydraulic unit translation (151)	MODS-250-G1/4-A-M12	PE-CI-02-W
119	temperature	temperature multi force east bottom 2.1	Pt1000	
120	temperature	temperature multi force east bottom 2.2	Pt1000	
121	temperature	temperature multi force east bottom 2.3	Pt1000	
122	temperature	temperature multi force east bottom 2.4	Pt1000	
123	temperature	temperature multi force west top 3.1	Pt1000	TT-HTF-11-W
124	temperature	temperature multi force west top 3.2	Pt1000	TT-HTF-12-W
125	temperature	temperature multi force west top 3.3	Pt1000	TT-HTF-13-W
126	temperature	temperature multi force west top 3.4	Pt1000	TT-HTF-14-W
127	temperature	temperature multi force west bottom 4.1	Pt1000	
128	temperature	temperature multi force west bottom 4.2	Pt1000	
129	temperature	temperature multi force west bottom 4.3	Pt1000	
130	temperature	temperature multi force west bottom 4.4	Pt1000	
64-69			EVs	
M1			servo control controller	

7.4 Data sheets and certificates

Mehrachsen-Kraft-Momentensensor K6D175

Messbereiche	Fx /kN	Fy /kN	Fz /kN	Mx /kNm	My /kNm	Mz /kNm
K6D175 10kN/1kNm	10	10	20	1	1	2
K6D175 20kN/2kNm	20	20	50	2	2	5
K6D175 50kN/5kNm	50	50	100	5	5	10

Beschreibung

Der Mehrachsen Sensor K6D eignet sich für die Kraft- und Drehmomentmessung in drei zueinander senkrechten Achsen.

Die Messbereiche für die Kräfte und Momente lassen sich werksseitig in einem weiten Bereich anpassen. Der K6D175 wurde speziell für folgende Anwendungen entwickelt:

1. Robotik
2. Messungen in der Automatisierungstechnik

Die Auswertung der Kraft- und Momentenbelastung erfolgt z.B. mit einem Messverstärker GSV-1A8USB..Die Berechnung der 6 Lastgrößen ist z.B. über eine Windows-DLL oder über Labview möglich mit Hilfe eines bereitgestellten digitalen Kalibrierdokuments. Das Kalibrierdokument enthält die individuellen Kalibrierfaktoren und Fehlerkorrekturen des Sensors.

ME-Meßsysteme GmbH, Neuendorfstr. 18a, DE-16761 Hennigsdorf
Tel +49 (0)3302 78620 60, Fax +49 (0)3302 78620 69, info@me-systeme.de, www.me-systeme.de

Abmessungen

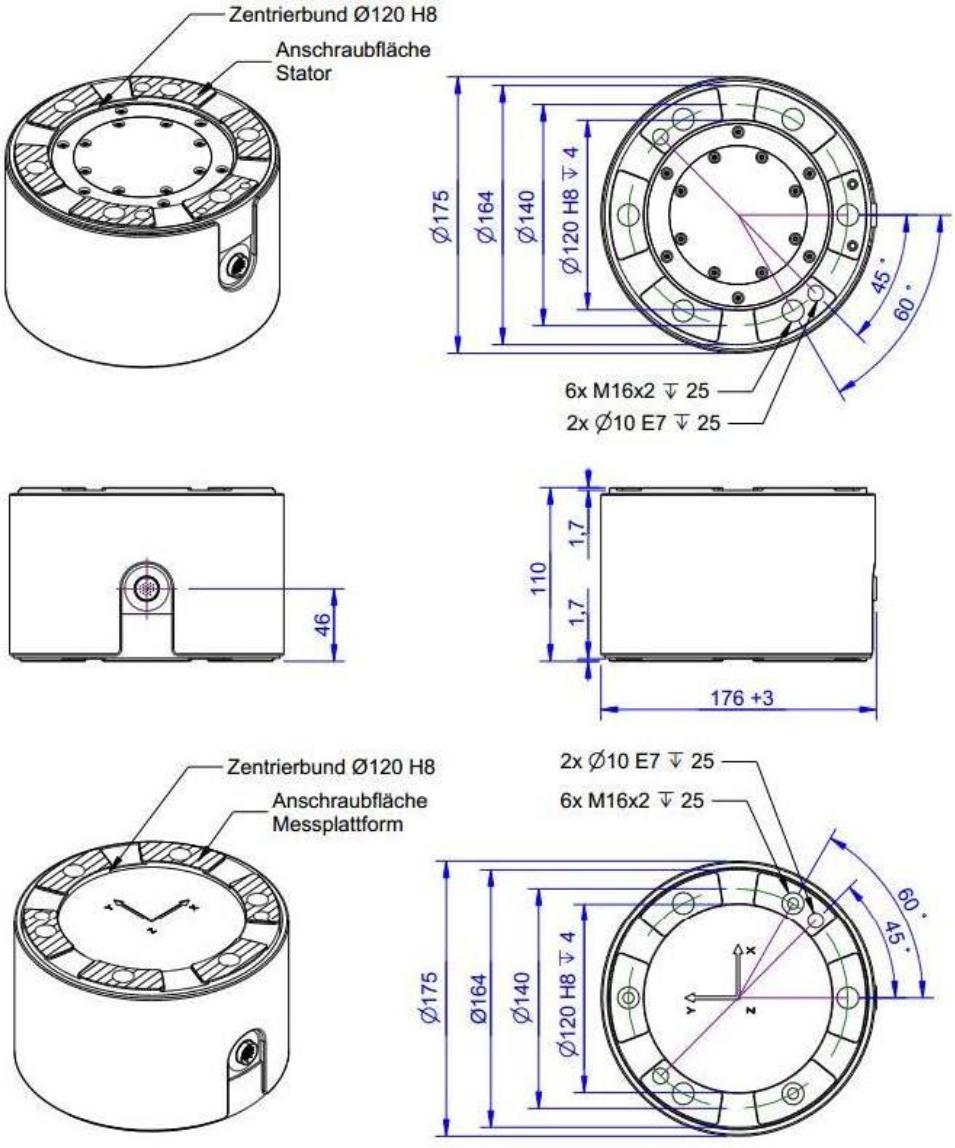

Technische Daten

Maße / Material		
Bauform		Messplattform
Material		Edelstahl 1.4542
Abmessungen	mm x mm	Ø175 x 110
Krafteinleitung		6x M16
mechanische Daten		
Nennkräfte (FS) Fx, Fy, Fz	kN	10, 20, 50
Nennmomente (FS) Mx, My, Mz	kNm	1, 2, 5
Gebrauchslast	%FS	150
Bruchlast	%FS	300
Messweg bei FS 1)	mm	ca. 0,1
Verdrillung bei FS 1)	rad	ca. 0,01
elektrische Daten		
Nennkennwert 2)	mV/V @ FS	ca. 0,5
Nullsignal	mV/V	<2
max. Speisespannung	V	5
Eingangswiderstand	Ohm	350 ±10
Ausgangswiderstand	Ohm	350 ±10
Isolationswiderstand	Ohm	>2 10^9
Steckverbinder, 24-polig, M16, Serie 723		09-0497-00-24
Genauigkeit		
rel. Spannweite 3)	%FS	0,5
rel. Linearitätsabweichung	%FS	<0,1
rel. Umkehrspanne	%FS	<0,1
Temperatureinfluss auf das Nullsignal	%FS/K	<0,1
Temperatureinfluss auf den Kennwert	%RD/K	<0,05
rel. Kriechen (30 min)	%FS	<0,1
Temperatur / Umwelt		
Nenntemperaturbereich	°C	-10… +70
Gebrauchstemperaturbereich	°C	-10 … +85
Lagertemperaturbereich	°C	-10 … +85
Schutzart		IP67

Abkürzungen: RD: Istwert („Reading“); FS: Endwert („Full Scale“);

1) Messweg bei einachsiger Belastung Fx oder Fy oder Fz;
2) Vergleichswert bei einachsiger Belastung Fz;
3) Wiederholbarkeit bei gleicher Einbaulage und mehrachsiger Belastung;

Die Kalibrierung der einzelnen Achsen sowie das Übersprechen werden für den Sensor individuell ermittelt und in einer Kalibriermatrix dokumentiert.

Steifigkeitsmatrix

K6D175 10kN/1kNm

178,1 kN/mm	0,0	0,0	0,0	10331 kN	0,0
0,0	178,1 kN/mm	0,0	-10331 kN	0,0	0,0
0,0	0,0	786,7 kN/mm	0,0	0,0	0,0
0,0	-10331 kN	0,0	2149,7 kNm	0,0	0,0
10331 kN	0,0	0,0	0,0	2149,7 kNm	0,0
0,0	0,0	0,0	0,0	0,0	1404,3 kNm

K6D175 20kN/2kNm

375,5 kN/mm	0,0	0,0	0,0	21800 kN	0,0
0,0	375,5 kN/mm	0,0	-21800 kN	0,0	0,0
0,0	0,0	1658,3 kN/mm	0,0	0,0	0,0
0,0	-21800 kN	0,0	4531,7 kNm	0,0	0,0
21800 kN	0,0	0,0	0,0	4531,7 kNm	0,0
0,0	0,0	0,0	0,0	0,0	2960,2 kNm

K6D175 50kN/5kNm

614,4 kN/mm	0,0	0,0	0,0	35600 kN	0,0
0,0	614,4 kN/mm	0,0	-35600 kN	0,0	0,0
0,0	0,0	2713,6 kN/mm	0,0	0,0	0,0
0,0	-35600 kN	0,0	7415,4 kNm	0,0	0,0
35600 kN	0,0	0,0	0,0	7415,4 kNm	0,0
0,0	0,0	0,0	0,0	0,0	4844,0 kNm

Anschlussbelegung

Kanal	Signal	Bezeichnung	PIN	Aderfarbe
1	+Us1	positive Brückenspeisung	1	weiß
	-Us1	negative Brückenspeisung	2	braun
	+Ud1	positiver Brückenausgang	3	grün
	-Ud1	negativer Brückenausgang	4	gelb
2	+Us2	positive Brückenspeisung	5	grau
	-Us2	negative Brückenspeisung	6	rosa
	+Ud2	positiver Brückenausgang	7	blau
	-Ud2	negativer Brückenausgang	8	rot
3	+Us3	positive Brückenspeisung	9	schwarz
	-Us3	negative Brückenspeisung	10	violett
	+Ud3	positiver Brückenausgang	11	grau-rosa
	-Ud3	negativer Brückenausgang	12	rot-blau
4	+Us4	positive Brückenspeisung	13	weiß-grün
	-Us4	negative Brückenspeisung	14	braun-grün
	+Ud4	positiver Brückenausgang	15	weiß-gelb
	-Ud4	negativer Brückenausgang	16	gelb-braun
5	+Us5	positive Brückenspeisung	17	weiß-grau
	-Us5	negative Brückenspeisung	18	grau-braun
	+Ud5	positiver Brückenausgang	19	weiß-rosa
	-Ud5	negativer Brückenausgang	20	rosa-braun
6	+Us6	positive Brückenspeisung	21	weiß-blau
	-Us6	negative Brückenspeisung	22	braun-blau
	+Ud6	positiver Brückenausgang	23	weiß-rot
	-Ud6	negativer Brückenausgang	24	braun-rot

Zubehör

Messverstärker

Der Messverstärker GSV-1A8/K6D ist mit einem 24-poligen Steckverbinder zum Anschluss eines 6-Achsen Sensors vorbereitet. Mit der Software GSVmulti werden die mechanischen Kräfte und Momente werden aus den 6 Ausgangsspannungen der einzelnen Messkanäle mit der Kalibriermatrix verrechnet.

Kalibriermatrix

Die Kalibriermatrix enthält 36 Kalibrierfaktoren zur Berechnung der Kräfte und Momente aus den 6 Ausgangssignalen des Kraftsensors. Eine Labview vi steht zur Verarbeitung der Kalibriermatrix zur Verfügung.

Software

Die Software GSVmulti ist im Lieferumfang mit Messverstärkern GSV-1A8USB/K6D enthalten. Die Software gestattet die Anwendung der Kalibriermatrix und die VVerschiebung des Kordinatensystems zur Darstellung der Momente um einen frei wählbaren Bezugspunkt.

Zur Erstellung eigener Software steht ein Labview VI zur Verfügung.

Montagehinweis

Die Krafteinleitung erfolgt auf einem Kreisring /auf 6 Kreissegmenten Ø155 – Ø140mm auf den Stirnseiten des Sensors. Die Fläche innerhalb des Kreisrings Ø140mm bleibt unbelastet.

Der Aussenumfang der Kreissegmente kann zur Zentrierung verwendet werden. Eine Zentrierbohrung dient zur Sicherung der Winkellage.

Stand: 29.06.2015

20547788-1
ME
2017-1

K6D-CalibrationMatrix HL

Kalibriergegenstand:	System bestehend aus: 6-Achsen Kraft-Momentensensor und Messverstärker
Hersteller:	ME-Meßsysteme GmbH Neuendorfstr. 18a 16761 Hennigsdorf
Typ:	Sensor: K6D175 10kN/1kNm SN:15401935 Messverstärker: GSV-1A8USB K6D/M16 SN:15156211
Auftraggeber:	Deutsches Zentrum für Luft und Raumfahrt Geb. Plataforma Solar de Almeria (DLR-PSA), Raum 1 Ctra. de Senés s/n ES-04200 Tabernas/Almeria
Auftragsnummer:	20547788
Anzahl der Seiten des Kalibrierscheins	4

Die Kalibrierung erfolgte unter Berücksichtigung der Anforderungen der DIN EN ISO/IEC 17025 mit Messmitteln die im Sinne der DIN EN ISO 9001 und DIN EN ISO 10012 auf Nationale Normale rückführbar sind. Die regelmäßige Überprüfung durch die zertifizierten und akkreditierten Institutionen sichert, dass die Rückführbarkeit aufrecht erhalten wird.

Prüfer:	T.Künstner
Datum:	03.01.2017

20547788-1
ME
2017-1

Kalibriereinrichtung / Prüfnormale

1	Referenzgewicht	Gewichtssatz von 2,5 g – 10 kg, Klasse M1, SN:4840416, 73118-D-K-15192-01-00-2016-4 Gewichtssatz von 2,5 g – 10 kg, Klasse M1, SN:4840416, 73119-D-K-15192-01-00-2016-4 Gewichtssatz 100g – 10 kg, Klasse M1, SN: 4900416, 73120-D-K-15192-01-00-2016-04 Gewichtssatz 100g – 10 kg, Klasse M1, SN: 4910416, 73121-D-K-15192-01-00-2016-04
2	Werkstoffprüfmaschine	ZD20EDC, SN:04/M06, 5759-D-K-17452-01-01, 2016-10

Angaben zur Kalibrierung

Umgebungstemperatur 21 °C± 1,5 °C

Kalibrierverfahren /Messbedingungen

Der 6-Achsen Kraft-Momentensensor Typ K6D175 wurde in Reihe mit einem Referenzgewicht sowie mit einer Werkstoffprüfmaschine belastet. Die Richtung der Referenzkräfte und Referenzmomente auf den Sensor wurde durch unterschiedliche Montagepositionen des Mehrkomponenten-Sensors in der Kalibriervorrichtung sichergestellt.

Als Anzeige wurde der Messverstärker GSV-1A8USB K6D/M16 (15156211) verwendet.

Zur Ermittlung der Kalibriermatrix wurden aus 48 Messreihen 6 linear unabhängige Lastvektoren mit Hilfe des Kalibriervorrichtung aufgebracht.

Vor jeder Belastung mit einem Lastvektor wird ein Nullabgleich durchgeführt.

Zustand der Kalibriergegenstände

Gegenstand	Typ	S/N	Zustand
6-Achsen Kraft-Momentensensor	K6D175 10kN/1kNm	15401935	Gebraucht/Rekalibrierung
Messverstärker	GSV-1A8USB K6D/M16	15156211	Gebraucht/Rekalibrierung

20547788-1
ME
2017-1

Nullpunkterfassung

Kanal	1	2	3	4	5	6
mV/V	0,0075	0,0160	0,0146	0,0037	0,0141	0,0063

Kalibriermatrix

Die Kalibriermatrix beschreibt den Zusammenhang zwischen den angezeigten Spannungen des Messverstärkers an den Kanälen 1 bis 6 (Bezeichner „ai0“ bis „ai5“) und den Komponenten 1 bis 6 (Fx, Fy, Fz, Mx, My, Mz) des Lastvektors.

	Kanal					
	1	2	3	4	5	6
Referenz						
Fx in N/V	6,10	1988,56	-1971,82	8,49	1954,07	-2055,73
Fy in N/V	-2161,41	1223,06	1196,94	-2338,29	1204,39	1231,05
Fz in N/V	-3175,05	-3057,37	-3257,57	-3212,60	-3216,90	-3174,84
Mx in Nm/V	-115,66	-115,22	-123,88	-124,54	226,16	222,88
My in Nm/V	-194,49	-193,88	200,39	199,22	5,30	8,36
Mz in Nm/V	128,81	-136,12	131,60	-137,26	131,52	-138,73

Abbildung 1: Kalibriermatrix in N/V und Nm/V

	Kanal					
	1	2	3	4	5	6
Referenz						
Fx in N / mV/V	15,24	4971,41	-4929,54	21,22	4885,18	-5139,34
Fy in N / mV/V	-5403,52	3057,65	2992,35	-5845,72	3010,98	3077,63
Fz in N / mV/V	-7937,62	-7643,42	-8143,92	-8031,49	-8042,25	-7937,10
Mx in Nm / mV/V	-289,14	-288,05	-309,71	-311,34	565,39	557,21
My in Nm / mV/V	-486,21	-484,71	500,96	498,05	13,25	20,90
Mz in Nm / mV/V	322,03	-340,30	329,00	-343,15	328,81	-346,83

Abbildung 2: Kalibriermatrix in N/mV/V und Nm/mV/V

20547788-1
ME
2017-1

Koordinatenursprung

Der Ursprung des Koordinatensystems befindet sich im Zentrum des Sensors auf der Oberfläche der oberen Seite. An der Stelle des Ursprungs ist eine Gravierung vorhanden.

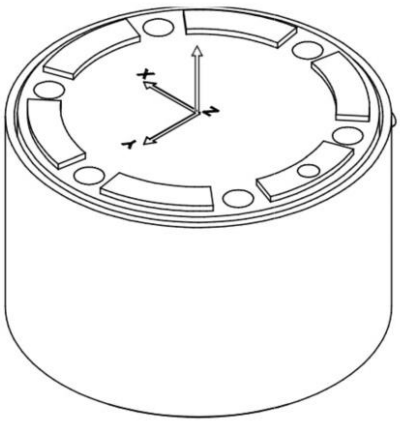

Abbildung 3: Ursprung des Koordinatensystems

Messunsicherheit

Mit einer Wahrscheinlichkeit von 95% besitzen die Messergebnisse folgende Unsicherheit.

	Fx	Fy	Fz	Mx	My	Mz
Nennlast	2350 N	800 N	2050 N	400 Nm	400 Nm	300 Nm
Messunsicherheit	±6N	±12N	±40N	±3,0Nm	±1,5Nm	±2,0Nm

Temperaturtest

	Nullpunktsignal in mV/V					
Temperatur	**Kanal 1**	**Kanal 2**	**Kanal 3**	**Kanal 4**	**Kanal 5**	**Kanal 6**
20 °C	0,0000	0,0000	0,0000	0,0000	0,0000	0,0000
80 °C	-0,0072	-0,0108	0,0077	-0,0109	-0,0085	-0,0256
20 °C	-0,0001	-0,0012	0,0003	-0,0036	-0,0021	0,0013

Counter Rotating Fan

80 mm sq. San Ace 80

General Specifications

- Material ····· Frame: Plastics (Flammability: UL94V-0),
  Impeller: Plastics (Flammability: UL94V-0)
- Expected Life ····· Refer to specifications (L10:Survival rate:90% at 60℃, rated voltage, and continuously run in a free air state)
- Lead Wire ····· Inlet ⊕red ⊖black Sensor yellow Control brown
  Outlet ⊕orange ⊖gray Sensor purple Control white
- Storage Temperature ···· −30℃ to +70℃ (Non-condensing)

80×80×80mm (Mass : 450g) 9CRA type

Specifications

The following nos. **have PWM controls and pulse sensors.**

Model No.	Rated Voltage [V]	Operating Voltage Range [V]	PWM duty cycle※ [%]	Rated Current [A]	Rated Input [W]	Rated Speed [min⁻¹] Inlet	Rated Speed [min⁻¹] Outlet	Max. Airflow [m³/min]	Max. Airflow [CFM]	Max. Static Pressure [Pa]	Max. Static Pressure [inchH₂O]	SPL [dB(A)]	Operating Temperature [℃]	Expected Life [h]
9CRA0812P8G001	12	10.8 to 13.2	100	5.3	63.6	12,000	11,300	4.5	158.9	1,150	4.62	76	−20 to +70	40,000(60℃ (70,000(40℃)
			0	0.2	2.4	2,000	1,900	0.74	26.1	31.9	0.13	30		
9CRA0824P8G001	24	21.6 to 26.4	100	2.65	63.6	12,000	11,300	4.5	158.9	1,150	4.62	76		
			0	0.09	2.16	2,000	1,900	0.74	26.1	31.9	0.13	30		
9CRA0848P8G001	48	40.8 to 55.2	100	1.32	63.4	12,000	11,300	4.5	158.9	1,150	4.62	76		
			0	0.29	13.9	5,000	4,700	1.88	66.2	200	0.80	52		

※PWM Frequency : 25kHz

Other sensor specifications are available as options. Please refer to the index (p. 501).

Dimensions (unit: mm)

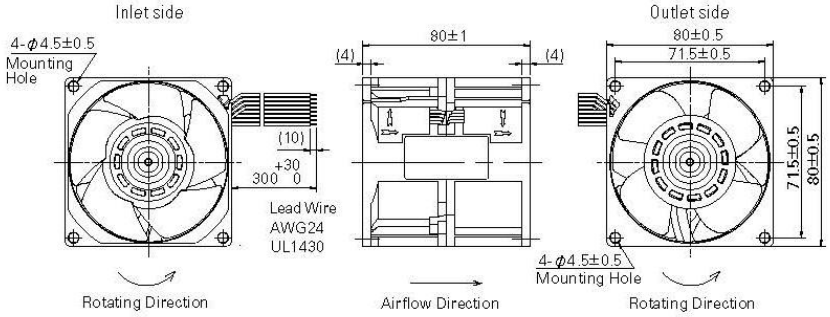

Reference Dimensions of Mounting Holes and Vent Opening (unit: mm)

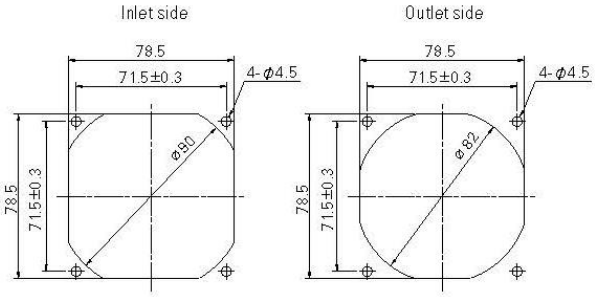

Options (unit: mm)

Finger Guards

Color
Model : 109-049E Surface treatment : Nickel-chrome plating (silver)
: 109-049H : Cation electropainting (black)

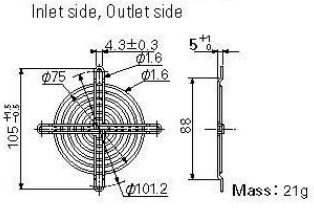

Options (unit: mm)

Resin Finger Guards

Model : 109-1002G

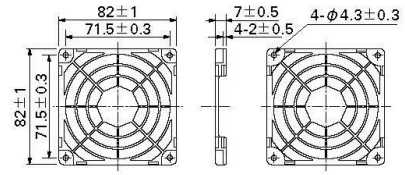

Mass : 10g

Resin Filter Kits

Model : 109-1002F13 (13PPI), 109-1002F20 (20PPI)
: 109-1002F30 (30PPI), 109-1002F40 (40PPI)

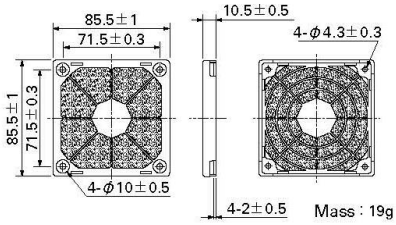

Mass : 19g

Airflow - Static Pressure Characteristics

PWM Duty Cycle

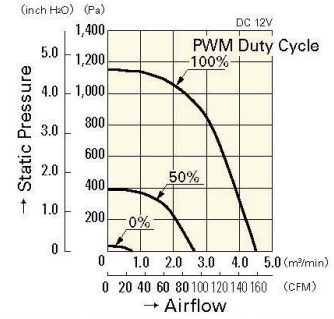

9CRA0812P8G001

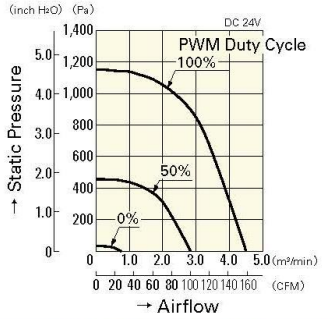

9CRA0824P8G001

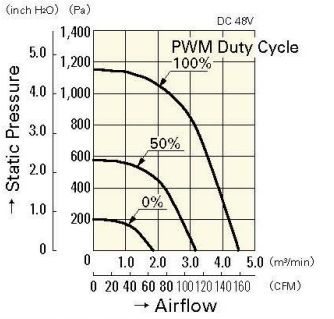

9CRA0848P8G001

Operating Voltage Range

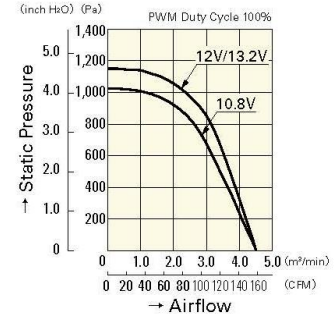

9CRA0812P8G001

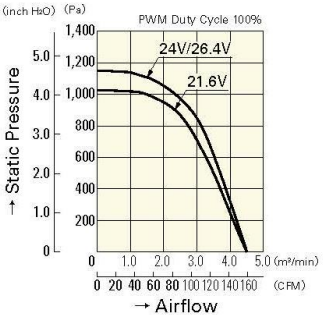

9CRA0824P8G001

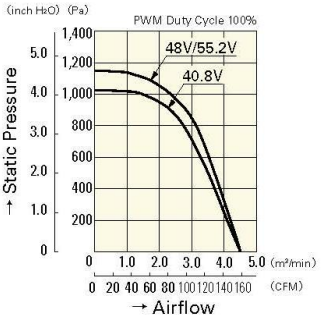

9CRA0848P8G001

PWM Duty - Speed Characteristics Example

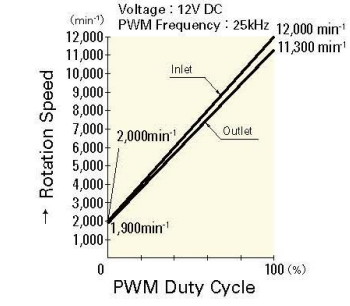

9CRA0812P8G001

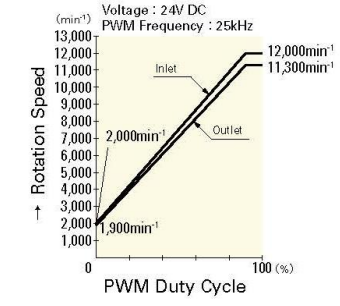

9CRA0824P8G001

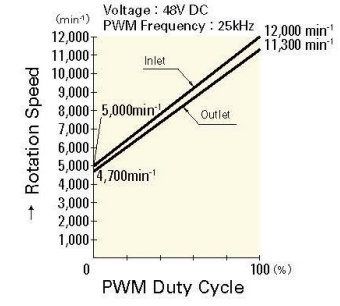

9CRA0848P8G001

7.5 Sensor cooling for K6D175 dynamometer

Another impact has been detected in pervious tests. Without an active cooling, the metal plate with the two PT1000 sensors heats up to nearly ϑ_{PT1000} = 50~60 °C depending on the duration of operation and the HTF temperature. Improvements of the sensor insulation have been integrated in the past in form of ceramic plates between the bolts and the metal plates. Two ceramic plates have been installed with an air gap between them to reduce thermal conduction through the traverse pipe support and the metal structure on top of the sensor as shown in **Figure 45**.

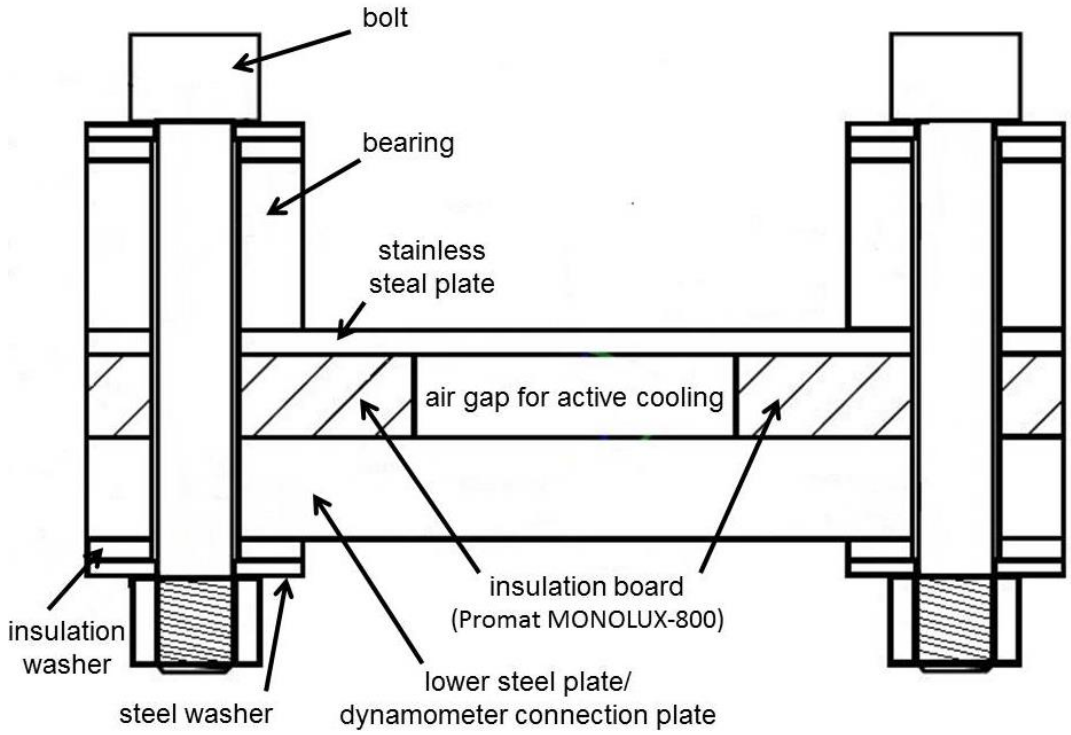

Figure 45: Technical drawing of the dynamometer support with integrated insulation [2]

The designed insulation for the sensor is not adequate to reduce the sensor temperature ϑ_{Dyn} to a nearly ambient temperature ϑ_{amb}. In order to measure this important influence, two PT1000 thermocouples have been integrated in the metal plate on top of the dynamometer, as depicted on the left picture in **Figure 17** To ensure a minimum measurement uncertainty, the insulation has been upgraded by a counter rotating fan San Ace 80 to blow an airstream between the described air gap. A data sheet of the fan can be found in **Appendix 7.4** and an “Autodesk” drawing extract for the installed cooling in **Appendix 7.1**.

The environmental impacts on the dynamometer are limited in order to prevent damages to electronical parts and strain gauges. To obtain the most accurate measurement, it is indispensable to minimize the influence of temperature to the sensor. This has been a problem during tests in the past for heating up the traverse without REPAs. The sensor takes on a temperature between 60 ~ 70 °C by a mean pipe

temperature of around 350 °C without a direct cooling [2]. The nominal temperature range for the sensor is -10…70 °C and the service temperature range amounts -10…85 °C (**Appendix 7.4**). Only the operation in the nominal temperature range ensures acceptable measurement uncertainties. The service temperature range is a limit for an operation without damages but with high uncertainties. In later tests, the facility operates by ϑ_{HTF} = 450 °C and this will lead to higher temperatures than 70 °C. An active cooling is necessary to ensure a minimum of measurement inaccuracies for the dynamometers in top position.

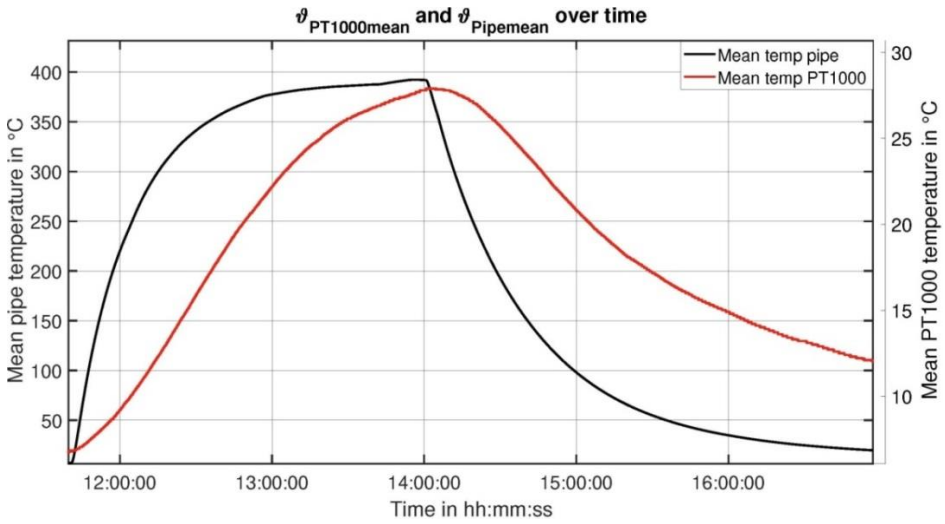

Figure 46: Mean PT1000 temperature and mean pipe temperature over time during heat up and cool down phase of the measurement set up.

Figure 46 depicts the effect of the temporary installed fan. The temperature ϑ_{PT1000} measured by two PT1000 sensors is the only representative value for ϑ_{dyn}. But the real dynamometer temperature must have a lower value, because it has a further distance away from the hot pipe section. Various measurements show that the cooling works effective. ϑ_{PT1000} can be reduced until 30 °C by starting the fan at the beginning of every heating process. The influence of the temperature on forces and moments measured by the dynamometer can be reduced significantly by this installation. This is a necessary additional cooling for the two sensors in the traverse. The influence of the temperature on the bottom sensor has to be investigated, because of the different mounting position.

7.6 Structure of "Matlab" evaluation routine

An evaluating routine is programmed with Matlab to execute a measurement data processing. This routine forms the basis for all graphics of both tests. The following **Figure 47** shows the main structure of the routine.

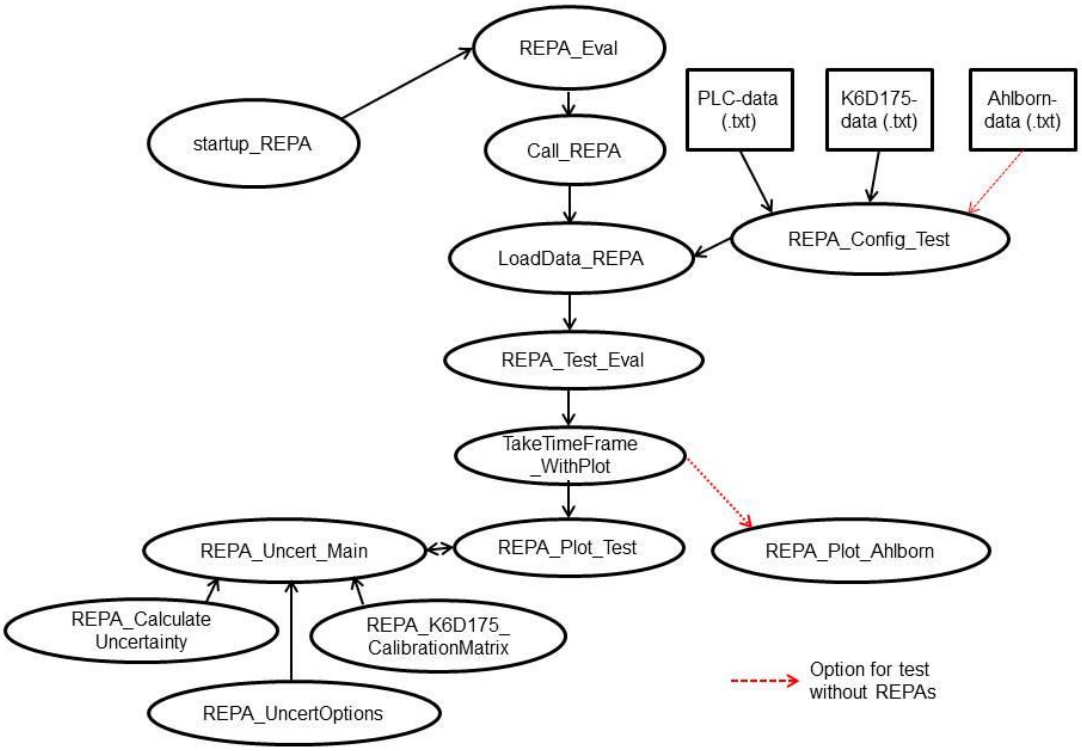

Figure 47: Structure of the Matlab evaluation routine

In general, the routine is currently defined only for the test case in order to read in three different data sources. The data of the PLC and dynamometer are the basic measurements sets for the REPA life cycle tests after a successful commissioning. In addition, the Ahlborn temperature data of the traverse test without REPAs can be read in. Measurement uncertainties of the dynamometer are calculated for each single data set. The specific graphics for the test without REPAs and air as HTF are outsourced in a separate function, because this test will be irrelevant by a finished installation. All data sources are matched to each other by cutting the time length of the larger ones to the length of the shorter ones. Gaps and doubles in data are also removed automatically. All mat. files are stored in a structure called handles to transport them as a package to the different functions and to use them later for other implementations.